NAVAL POSTGRADUATE SCHOOL
MONTEREY, CALIFORNIA

THESIS

ANALYSIS AND SIMULATION OF THE ADVANCED AMPHIBIOUS ASSAULT VEHICLE (AAAV) ELECTRICAL SYSTEM ARCHITECTURE

by

Gabriel Beltran

June 2000

Thesis Advisor: John G. Ciezki

Approved for public release; distribution is unlimited.

REPORT DOCUMENTATION PAGE

Form Approved OMB No. 0704-0188

1. AGENCY USE ONLY *(Leave blank)*	2. REPORT DATE June 2000	3. REPORT TYPE AND DATES COVERED Master's Thesis

4. TITLE AND SUBTITLE ANALYSIS AND SIMULATION OF THE ADVANCED AMPHIBIOUS ASSAULT VEHICLE (AAAV) ELECTRICAL SYSTEM ARCHITECTURE

5. FUNDING NUMBERS

6. AUTHOR(S) Gabriel Beltran

7. PERFORMING ORGANIZATION NAME(S) AND ADDRESS(ES)
Naval Postgraduate School
Monterey CA 93943-5000

8. PERFORMING ORGANIZATION REPORT NUMBER

9. SPONSORING/MONITORING AGENCY NAME(S) AND ADDRESS(ES)

10. SPONSORING/MONITORING AGENCY REPORT NUMBER

11. SUPPLEMENTARY NOTES The views expressed in this thesis are those of the author and do not reflect the official policy or position of the Department of Defense or the U.S. Government.

12a. DISTRIBUTION/AVAILABILITY STATEMENT
Approved for public release; distribution is unlimited.

12b. DISTRIBUTION CODE

13. ABSTRACT *(maximum 200 words)*

The Advanced Amphibious Assault Vehicle (AAAV) is a high water speed amphibious armored personnel carrier that will replace the current family of Marine Corps amphibious assault vehicles. The AAAV is currently in Phase I of the DOD Acquisition Process. During this phase-extensive development, testing is being conducted and prototypes are being constructed. Ongoing tests of the current electrical system architecture are revealing problems and issues that need to be addressed. Present testing is also revealing the need for a troubleshooting tool that can be used to simulate and test proposed solutions.

A distributive computing effort is being conducted with Purdue University in order to provide the Marine Corps a tool where by it can test and evaluate the entire AAAV electrical system architecture. This document provides a general system description of the AAAV, an electrical system architecture overview, and a candidate electrical system description. Testing, modeling, and computer simulation efforts applied to the NBC (Nuclear, Biological, and Chemical) fan/filter motor drive and battery banks are described and the resulting data analyzed. Current research is investigating an issue regarding energy being forced back into the high power distribution bus due to regeneration from sudden impacts on the vehicle turret. An ultra capacitor bank may be incorporated in the AAAV electrical system in an effort to mitigate the effect of this regenerative energy. Therefore, testing, modeling, and computer simulation of an ultra capacitor is also reported.

14. SUBJECT TERMS Advanced Amphibious Assault Vehicle (AAAV) ACSL, simulation, brushless DC machine, distributed computing, ultra-capacitor

15. NUMBER OF PAGES 136

16. PRICE CODE

17. SECURITY CLASSIFICATION OF REPORT	18. SECURITY CLASSIFICATION OF THIS PAGE	19. SECURITY CLASSIFICATION OF ABSTRACT	20. LIMITATION OF ABSTRACT
Unclassified	Unclassified	Unclassified	UL

NSN 7540-01-280-5500

Standard Form 298 (Rev. 2-89)
Prescribed by ANSI Std. 239-18 298-102

Approved for public release; distribution is unlimited.

ANALYSIS AND SIMULATION OF THE ADVANCED AMPHIBIOUS ASSAULT VEHICLE (AAAV) ELECTRICAL SYSTEM ARCHITECTURE

Gabriel Beltran
Captain, United States Marine Corps
B.S.M.E., Texas Tech University, 1993

Submitted in partial fulfillment
of the requirements for the degree of

MASTER OF SCIENCE IN ELECTRICAL ENGINEERING

from the

NAVAL POSTGRADUATE SCHOOL
June 2000

Author: Gabriel Beltran

Approved by:

John G. Ciezki, Thesis Advisor

Robert W. Ashton, Second Reader

Jeffrey B. Knorr, Chairman
Department of Electrical and Computer Engineering

ABSTRACT

The Advanced Amphibious Assault Vehicle (AAAV) is a high water speed amphibious armored personnel carrier that will replace the current family of Marine Corps amphibious assault vehicles. The AAAV is currently in Phase I of the DOD Acquisition Process. During this phase-extensive development, testing is being conducted and prototypes are being constructed. Ongoing tests of the current electrical system architecture are revealing problems and issues that need to be addressed. Present testing is also revealing the need for a troubleshooting tool that can be used to simulate and test proposed solutions.

A distributive computing effort is being conducted with Purdue University in order to provide the Marine Corps a tool where by it can test and evaluate the entire AAAV electrical system architecture. This document provides a general system description of the AAAV, an electrical system architecture overview, and a candidate electrical system description. Testing, modeling, and computer simulation efforts applied to the NBC (Nuclear, Biological, and Chemical) fan/filter motor drive and battery banks are described and the resulting data analyzed. Current research is investigating an issue regarding energy being forced back into the high power distribution bus due to regeneration from sudden impacts on the vehicle turret. An ultra capacitor bank may be incorporated in the AAAV electrical system in an effort to mitigate the effect of this regenerative energy. Therefore, testing, modeling, and computer simulation of an ultra capacitor is also reported.

TABLE OF CONTENTS

I. INTRODUCTION

A. AAAV Program

The AAAV (Advanced Amphibious Assault Vehicle) will provide the Marine Corps a weapons system fully capable of implementing ship-to-objective maneuver as an integral part of the amphibious triad (AAAV, V-22, LCAC) to execute the concepts of Operational Maneuver From The Sea (OMFTS) and Ship to Objective Maneuver (STOM). Battlespace dominance by Marine forces will be significantly enhanced as a result of the AAAV's high water speed and superior land mobility which have historically limited the rapid maneuver of armored combat vehicles. The AAAV will travel as fast as 29 miles-per-hour (mph) on water as opposed to the 10 mph the current AAV can travel. The AAAV is designed to allow immediate, high-speed maneuver of Marine infantry units as they emerge from attack positions aboard ships located beyond the visual horizon -- 25 miles and beyond. Projection of these forces will be conducted as a single, seamless stroke that capitalizes on the intervening sea and land terrain to achieve surprise and rapidly exploit weak points in enemy littoral defenses. In short, the AAAV is faster, can travel greater distances before refueling, is navigationally smarter and more maneuverable than its predecessor.

The AAAV is currently in Phase I (Program Definition and Risk Reduction) of the Department of Defense (DoD) Acquisition Process. Phase II (Engineering and Manufacturing Development) is scheduled to begin Fiscal Year 2001 (FY01). The final phase, Phase III (Production, Fielding/Deployment and Organizational Support), is

scheduled to begin FY06. The total cost of the program is expected to be $7.5B with each unit costing $6.6M. The Marine Corps is scheduled to receive 1013 units. [Ref.1]

B. Research Focus

A distributive computing effort is being conducted with Purdue University in order to provide the Marine Corps a tool where by it can test and evaluate the entire AAAV electrical system architecture. Reporting in this thesis includes a general system description of the AAAV, an electrical system architecture overview, and a candidate electrical system description. Efforts are then applied to documenting the testing, modeling, and computer simulation of the NBC (Nuclear, Biological, and Chemical) fan/filter motor drive and battery banks. Furthermore, research will also address the requirement to capture energy being forced back into the high power distribution unit due to regeneration from sudden impacts on the vehicle turret. An ultra capacitor bank may be incorporated in the AAAV electrical system in an effort to capture regenerative energy. Therefore, testing, modeling, and computer simulation of an ultra capacitor is also reported.

C. Chapter Overview

Chapter I of this thesis provides an introduction to the AAAV program. It also identifies the research focus and provides a chapter overview. Chapter II contains a comprehensive system description of the AAAV. It details a general system description and introduces the four modes of operation. In addition the discussion within Chapter II addresses the electrical system architecture, beginning with a topology overview and

ending with a primary components description. Chapter III contains an introduction to distributed computing and background information on the programming language ACSL (Advanced Continuous Simulation Language), which will be used in this thesis to develop an NBC fan drive model. Further, the Automated State Model Generation Algorithm used by P. C. Krause & Associates (PCK&A), and Purdue University, to develop their NBC fan drive model is described and referenced in Chapter III. Chapter IV includes a description of the selected candidate electrical system architecture. In addition it provides background on the major components of the selected architecture, specifically the NBC fan, ultra capacitor, and batteries. Chapter V provides discussion regarding the modeling efforts applied to the NBC fan drive, ultra capacitor, and battery unit. It also provides results and conclusions for each model. Chapter VI is the conclusion. It summarizes the research while documenting results of the work. It also identifies Department of Defense relevance of the work and ideas for future work.

THIS PAGE INTENTIONALLY LEFT BLANK

II. AAAV SYSTEM DESCRIPTION

A. Introduction

This chapter provides a comprehensive system description of the AAAV. It details a general system description and introduces the four modes of operation. In addition the chapter addresses the electrical system architecture, beginning with a topology overview and ending with a brief description of the primary components.

B. System Description

The Advanced Amphibious Assault Vehicle (AAAV) is a high water speed amphibious armored personnel carrier that will replace the current family of Marine Corps amphibious assault vehicles, the AAV7A1 series. Operationally configured, the AAAV will weigh about 37 tons, be able to carry 17 combat-equipped Marines and a crew of three over 3 foot high waves in excess of 20 knots, and travel over land at 45 mph. Armed with a 7.62 mm machine gun and a 30 mm cannon, the AAAV will use Global Positioning System, forward-looking infrared, and a night vision system for navigation, targeting, and intelligence gathering. [Ref. 1]

The AAAV force is designed to provide a tactical assault and sustainment capability for Marines of the Marine Air-Ground Task Force. From amphibious ships standing well offshore, even over the horizon from the objective, the AAAV rapidly transports the landing force over the beachhead to an objective ashore, using maneuver and speed, plus on-board firepower to achieve superiority over enemy forces. Once ashore, the AAAV will serve as an armored personnel carrier, providing transportation,

protection, direct fire support and command, control and communications (C3I) for the Marines.

High water speed requires minimal hydrodynamic drag; to accomplish this, the AAAV will retract its tracks and suspension system and deploy cover plates on its underside to present a smooth surface. Thus, while in the water and traveling at high speed, the AAAV will be a planing hull craft. When the AAAV approaches 15 to 20 feet of water depth at the shore, it will reduce speed to come off plane, retract the cover plates, lower the suspension and tracks, and travel the remaining distance to the shore at a speed of approximately 8 to 10 knots.

Once ashore, the Marine Corps will use the AAAV (P) as a tracked armored personnel carrier to accomplish ***dominant maneuver*** and ***precision engagement***; in that mode, the 17 infantrymen carried inside will typically dismount to fight. The crew will use the AAAV (P)'s primary and secondary weapon (predicted to be a 25-35 mm cannon and 7.62 mm coaxial mounted machine-gun, respectively, with fully stabilized turret and forward looking infrared optics) to support the infantry and armor combat elements.

The AAAV's land mobility characteristics must be comparable to the Marine Corps's M1A1 Abrams main battle tank. This requires a top speed of approximately 45 mph, the capability to traverse the same terrain as the tank during cross-country operations, and the capability to cross the same obstacles and terrain features (for example, trenches, hills, walls, and soft soils) as the tank.

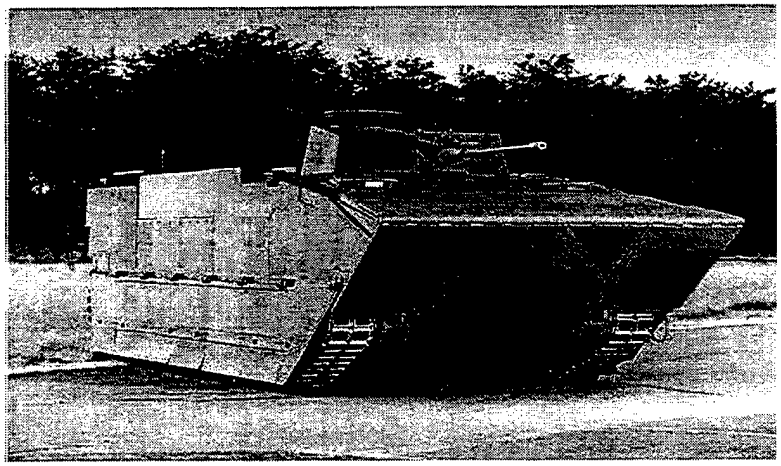

Figure 2-1, Advanced Amphibious Assault Vehicle. [Ref. 1]

1. System Operating Modes

a. High Speed Water Mode

An exploded view of the AAAV in high speed water mode is provided in Figure 2-2. The AAAV will operate in this mode during waterborne operations and will possess the following attributes.

- Top Speed: 20-25 knots in 3 feet significant wave height
- Maintains a heading in 10 feet significant wave height
- Self-righting (100 degrees)
- High water speed turning diameter <170 meters
- Stops forward motion within 75 meters
- Water range: 65 nautical miles

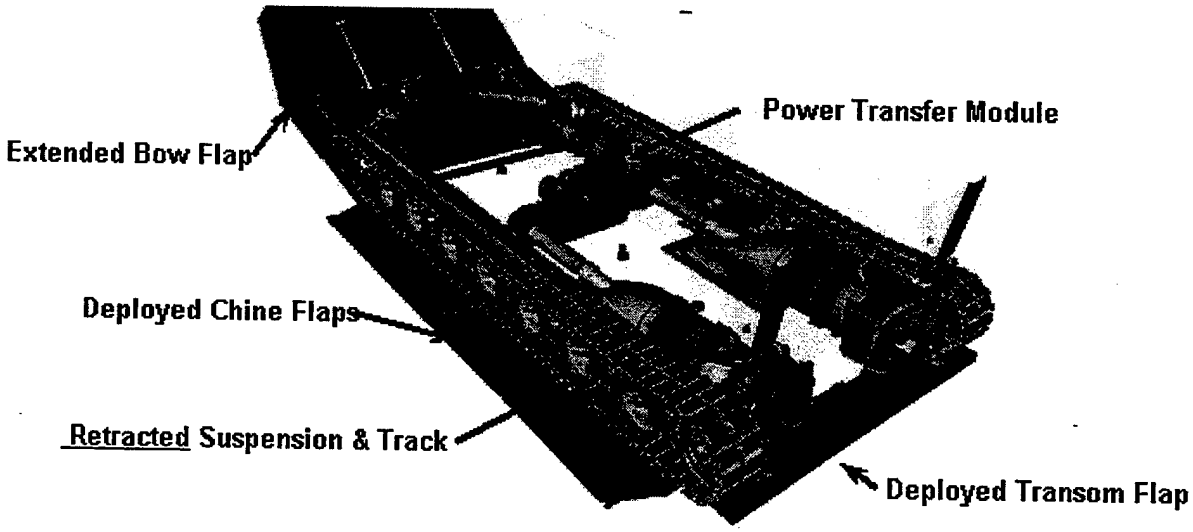

Figure 2-2, AAAV High Speed Water Mode. [Ref. 1]

b. Transition Mode

A view of the vehicle in transition mode is documented in Figure 2-3. The AAAV will operate in this mode while entering and exiting the water (from ship to land). Additional details include

- Used to enter and exit the water (from ship to land)
- Slow waterspeed operations
  - Top speed: 9 knots (4.5 knots reverse)
  - Surf transit: 8-foot plunging surf
  - Survivability: 360° rollover, 180° pitch-poling
  - Fully submersible for 5 seconds
- Also used for riverine and coastal operations

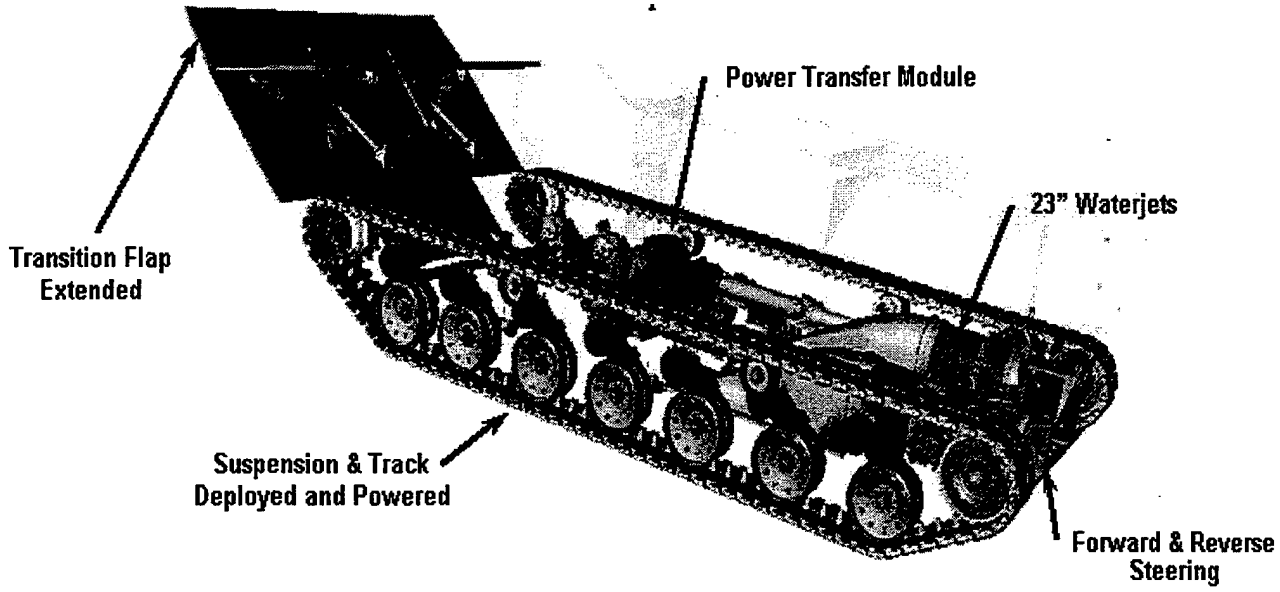

Figure 2-3, AAAV Transition Mode. [Ref. 1]

c. Land Mode

The vehicle in land mode is pictured in Figure 2-4. The AAAV will operate in this mode on land and possess the following attributes.

- Cross country mobility: > = M1A1 Abrams tank
- Top speed: 45 mph (0-20 mph in 7 seconds)
- Range: 400 miles (land only) or 250 miles after 1-hour (25 nautical miles) high water speed transit
- Obstacle crossing
  - 8-foot trench span, 3-foot vertical wall

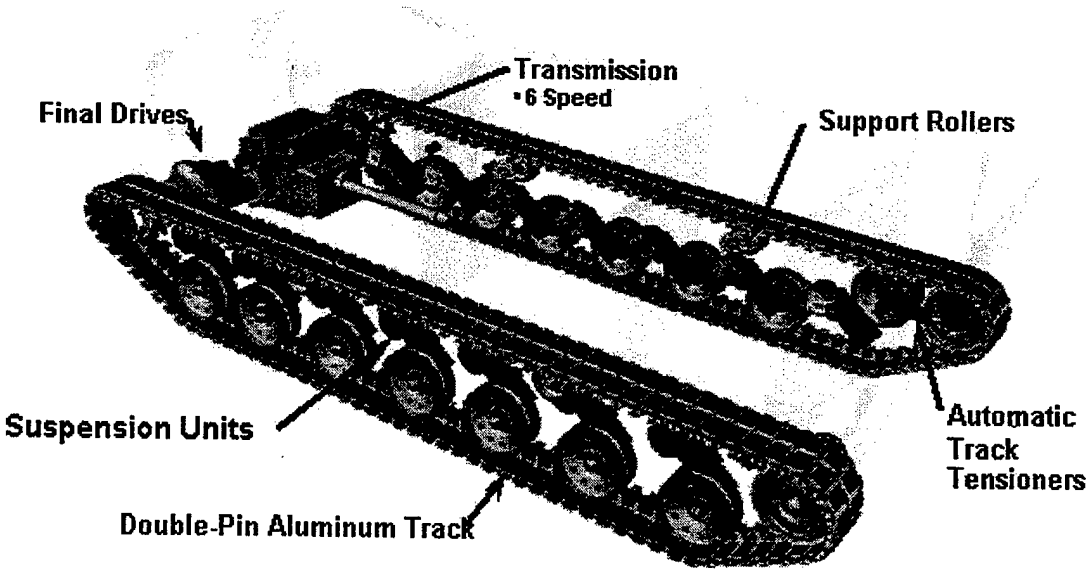

Figure 2-4, AAAV Land Mode. [Ref. 1]

d. Silent Watch Mode

A number of the key system components associated with the silent watch mode are illustrated in Figure 2-5. The AAAV will operate in this mode while stationary on land. In this mode, the following attributes hold.

- Used for stationary vehicle to reduce acoustic and thermal signature
- Fully combat ready
- One or more crewman on watch

- All com/nav/fire control/vision subsystems fully operational

- Achieve full land mode capability within 60 seconds

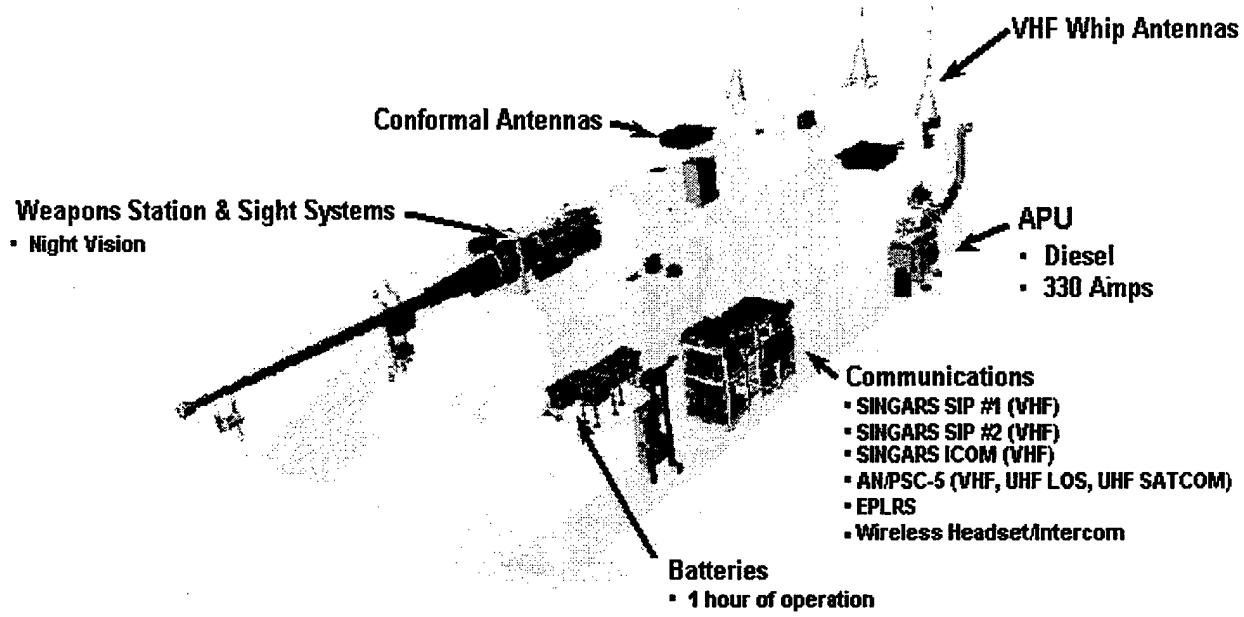

Figure 2-5, AAAV Silent Watch Mode. [Ref. 1]

C. Electrical System Architecture

1. Topology Overview

A block diagram of the electrical system is shown in Figure 2-6. This architecture schematic is of a level of detail greater than will be initially modeled by P.C. Krause & Associates or addressed in this thesis. The candidate electrical system for modeling and

simulation can be found in Chapter IV, Figure 4-1. While a detailed description of the entire electrical architecture is outside the scope of this thesis, the primary components are identified below.

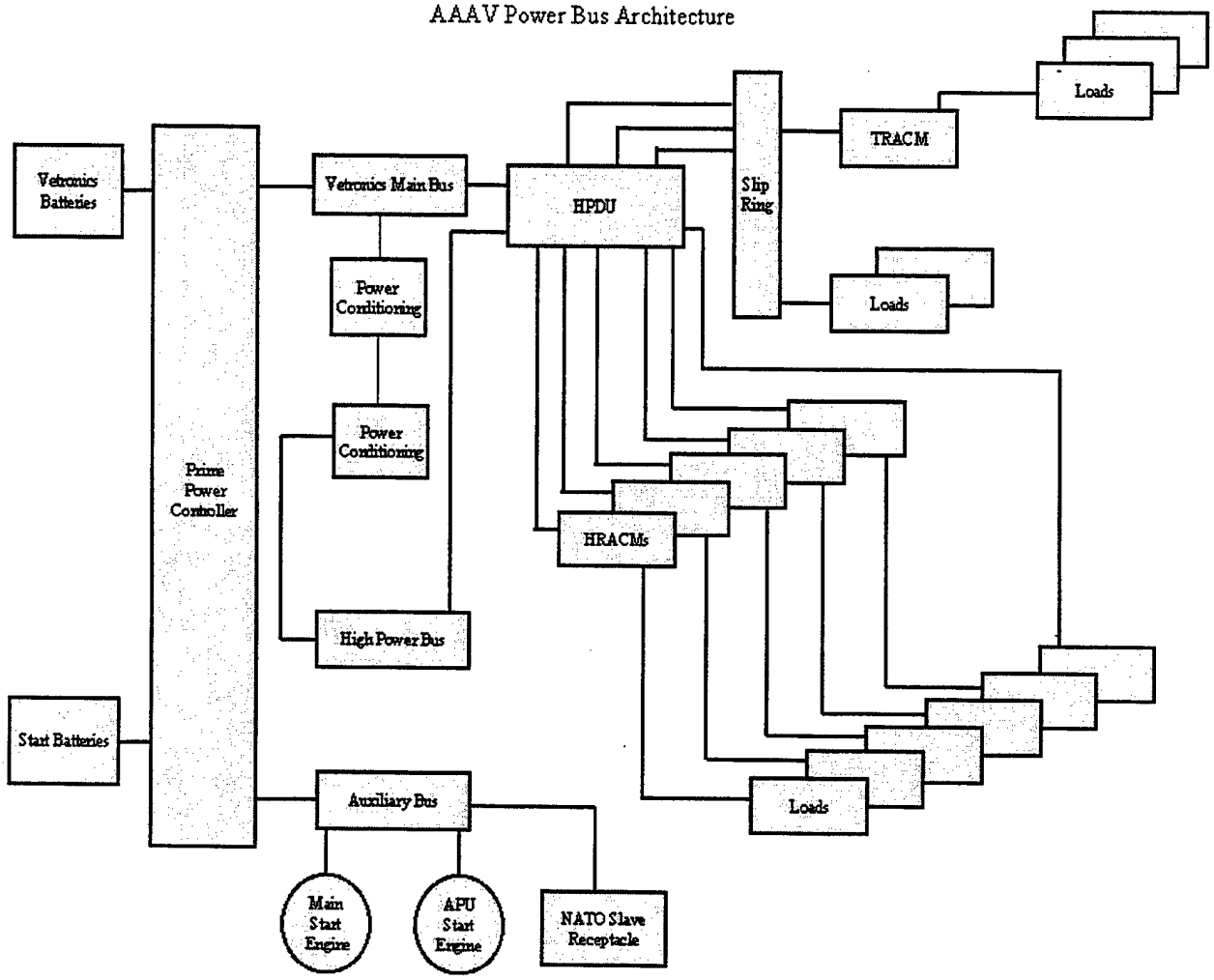

Figure 2-6, Electrical System Architecture. [Ref. 2]

2. Primary Components

a. Batteries

- Eight (8), 12 volt, manufactured by Optima
  - Three series pairs dedicated for starting.
  - One series pair dedicated to the Vetronics Bus during starting

b. Generators

- Main generator – 800 Amp, six-phase wound-rotor synchronous generator connected to two six-pulse diode bridge rectifiers whose dc outputs are connected in parallel. The field windings are connected to an exciter that is a three-phase machine whose armature voltages are rectified using a rotating six-pulse diode bridge rectifier.
  - Auxiliary Generator – 330 Amp, connected to the Vetronics Bus

c. Ultra Capacitor

- 100 Volt, 1F, 5000J capacitor manufactured by Pinnacle Research Institute. Not shown in Figure 2-6. See Figure 4-1.

d. Hull Power Distribution Unit (HPDU)

- Provides main power distribution to the Vetronics bus and high power bus.

e. **Remote Acquisition and Control Modules (RACMs)**

- Five (5-HRACM) hull and one (1-TRACM) turret
- Provide Secondary power distribution, Sensor Data Collection, Sensor Power, and Communications through Utility Data Bus

f. **Sealed Slip Rings**

- Provides power and data signal path to electrical systems located in the turret.

g. **NBC Fan Drive**

- 3.5 Hp, Wye wound, permanent magnet, brushless DC motor manufactured by Invincible Airflow Systems. Powered using a 120-degree voltage source inverter with sensorless control.

III. COMPUTER SIMULATION

A. Introduction

Chapter III contains an introduction to the theory behind the application of distributed computing to power system simulations. It also provides an overview of the programming language ACSL (Advanced Continuous Simulation Language), which will be used in this thesis to develop an NBC fan drive model. Further, it will introduce the Automated State Model Generation Algorithm used by PCK&A, and Purdue University, to develop their NBC fan drive model.

B. Distributed Computing

The consulting firm, P.C. Krause and Associates (PCK&A), has developed a technique that will aid in the simulation of complex systems in general and power electronic based systems in particular. This technique has been termed distributed computing. Distributed computing is a heterogeneous simulation environment that makes it possible to divide the simulation of power electronic based systems into any number of synchronized personal computers (PC). Moreover, subsystems can be implemented using different languages (i.e., Simulink, Saber, and ACSL) making it possible to have the advantage of a very large computer by paralleling inexpensive PC's.

In addition to the gain in computational speed, another advantage of this simulation environment is the ability to decouple the user interface and the simulation that is controlled by the interface. In particular, the user interface can be executed on any computer that is connected to the Internet allowing users at remote locations to "exercise"

the simulation and retrieve data. Also vendors who develop proprietary simulations can link the model as executable and not divulge the model inner workings.

C. ACSL Background

The acronym ACSL (pronounced "axel") stands for the Advanced Continuous Simulation Language. It has been developed expressly for the purpose of modeling dynamic systems described by time dependent, nonlinear differential equations, and/or transfer functions [Ref. 3]. Simulation of physical systems is a standard analysis tool used in the evaluation of hardware design prior to and in concert with actual construction. An accurate simulation model may provide invaluable insight into design flaws or system limitations before extensive capital investment is made on hardware. For instance in analyzing the AAAV electrical power system, the engineers of General Dynamics uncovered an instability in the electrical system during low power operation when the batteries are disconnected. Discovering the instability early will allow the General Dynamics team to troubleshoot the instability. Knowing this up front, the proposed design could then be modified without costly retrofits or adhoc solutions.

For the power engineer, ACSL facilitates the analysis and control of complex electromechanical networks. Variable speed electric drives are popularly used in pumping applications (fans, blowers, and compressors), large machinery actuation (elevators, hoists, cranes, conveyors, and crushers), remote servoing (robotics and precision machine tools), electric vehicle propulsion (cars, busses, trains, and ships), and as an alternative to hydraulic and pneumatic actuation systems. In addition to the electromechanical device, all of these systems are characterized by nonlinearities which

make application of linear system theory difficult (if not impossible). After designing comprehensive electric drives containing power electronic converters, electric machines, multi-loop analog and digital controls, and various protection and sensing devices, it is advantageous for the engineer to develop computer-based models which predict as accurately as possible the operational modes of the interconnected system. As the hardware becomes available, the models are validated and refined as necessary. Thus, modeling and simulation are integral parts of the design and analysis process.

The ACSL program is intended to provide a simple method of representing these mathematical models on a digital computer. Working from an equation description of the problem (with logical conditions conveniently handled), the user writes ACSL statements to describe the system under investigation. Run-time commands exercise the model; these statements can be submitted for solution in command files or entered interactively. Simulation studies may be conducted, variables plotted, and the system re-evaluated for changes in parameters and operating conditions.

D. Automated State Model Generation Algorithm

P. C. Krause and Associates (PCK&A) are using a new approach of automatically generating state space models in their simulation, and study, of the candidate electrical system for the AAAV. This new approach is termed the Automated State Model Generation Algorithm [Ref. 4]. As the software is proprietary and not widely available, this method will *not* be used in the simulation and study conducted by this thesis. This background is included to ensure a complete and thorough understanding of the methods employed by PCK&A in their development and study of the candidate electrical system.

background is included to ensure a complete and thorough understanding of the methods employed by PCK&A in their development and study of the candidate electrical system.

In the Automated State Model Generation Algorithm the candidate electrical system is described by the standard node incidence matrix and elementary branch data (e.g. resistances inductances, and back emf's) [Ref. 4]. The standard node incidence matrix is established by numbering the nodes and branches of the circuit. For example in Figure 3-1 below, the node incidence matrix would be of the form shown in Figure 3-2. The nodes are labeled vertically on the right while the branch elements are specified horizontally across the top.

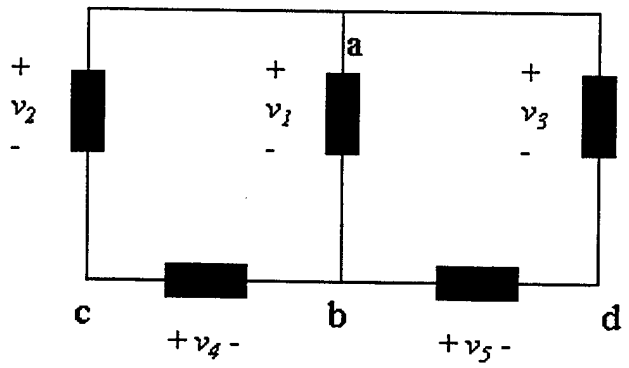

Figure 3-1, Example Circuit. [Ref. 4]

$$A_a = \begin{array}{c} \begin{matrix} 1 & 2 & 3 & 4 & 5 \end{matrix} \\ \begin{bmatrix} 1 & 1 & 1 & 0 & 0 \\ -1 & 0 & 0 & -1 & -1 \\ 0 & -1 & 0 & 1 & 0 \\ 0 & 0 & -1 & 0 & 1 \end{bmatrix} \end{array} \begin{matrix} a \\ b \\ c \\ d \end{matrix}$$

Figure 3-2, Node Incidence Matrix. [Ref. 4]

The elementary branch that PCK & A employs to model portions of systems ranging from thyristor switches to machine phases is illustrated in Figure 3-3. If the switch is closed (state=1), the branch is active. If the switch is open (state=0), the branch is inactive.

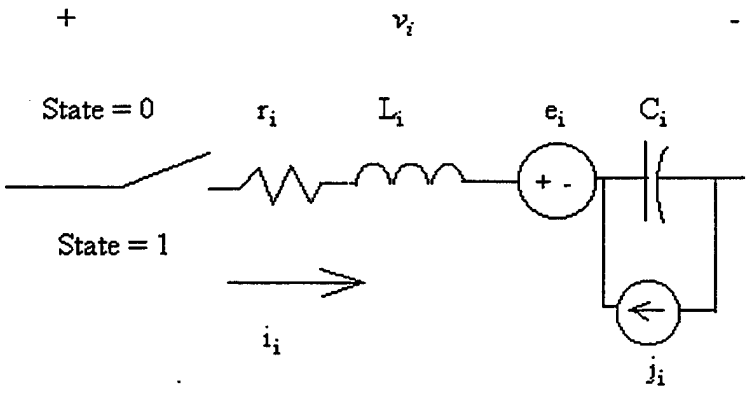

Figure 3-3, Branch Model. [Ref. 4]

From this input data the Automated State Model Generation Algorithm will automatically establish the composite system state equations, thus relieving the analyst from establishing the

differential equations by more tedious conventional means [Ref. 4]. Since the state equations are now available, linearization and eigenvalue analysis can be performed at the system level. Further, the state equations can then be solved numerically using one of a number of well-established numerical algorithms (i.e., ones available in ACSL: Runge-Kutta, Gears-Stiff, etc.).

IV. ELECTRICAL SYSTEM COMPONENT BACKGROUND

A. Introduction

This Chapter includes a description of the selected candidate electrical system architecture. In addition it provides background on the major components of the selected architecture, specifically the NBC fan drive, ultra capacitor, and batteries.

B. Candidate Electrical System Description

Figure 2-6, illustrates a general electrical system architecture for the AAAV. From this system architecture PCK&A selected a candidate system, Figure 4-1, for initial modeling purposes and to demonstrate the principle of distributed computing.

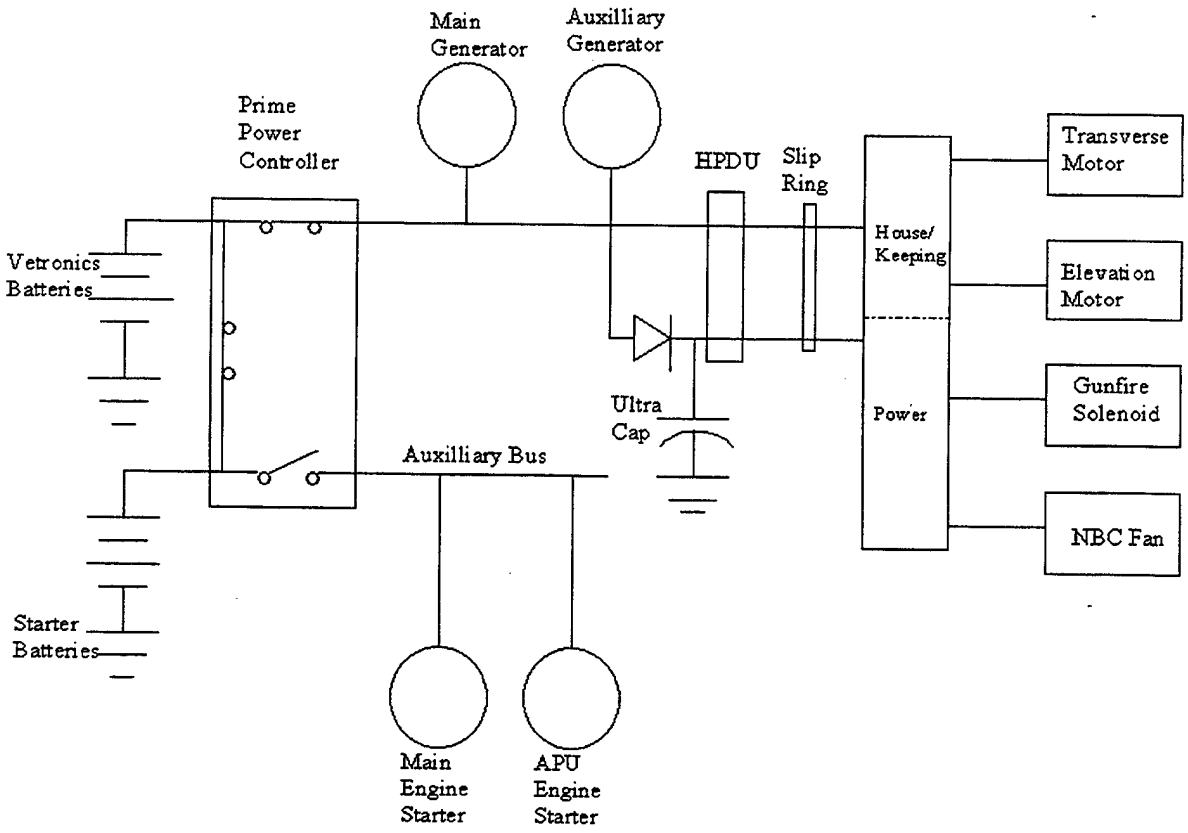

Figure 4-1, AAAV Candidate Electrical System Description. [Ref. 2]

C. NBC Fan Drive Background

1. Introduction

The brushless dc motor is becoming widely used as a small-horsepower control motor. The brushless dc motor, however, is really not a dc motor at all; in fact it is a permanent-magnet synchronous machine. Nevertheless, when it is supplied from a source with frequency equal to the electrical angular speed of its rotor, it becomes a brushless dc motor. The nomenclature is adopted not because it looks like a dc motor, but

because its torque speed characteristics can be made to resemble those of a dc shunt motor with a constant field current. If the permanent-magnet synchronous machine is to be supplied from a source of frequency that always corresponds to the electrical angular speed of its rotor, it is necessary that the rotor position be identified. This can be done in several ways, such as with a light beam and a toothed gear, or indirectly by using the back emf voltages found by sensing the open-circuit phase voltages, or by using Hall-effect sensors which magnetically sense the position of the rotor poles. The stator voltage source and rotor electrical angular speed are self-synchronized using a dc-to-ac inverter, wherein the transistors are switched on and off based on rotor position. There are numerous types of inverters. This thesis will explore the 180° and the 120° voltage source inverters.

In this section a description of the permanent-magnet synchronous machine is set forth. Next, the 180° inverter operation is explained. The operation of the 180° inverter is then used as a basis for the explanation of the operation of the 120° inverter. This explanation is completed by defining a sensorless control method for the 120° inverter.

2. Description of the Brushless DC Machine

The term "brushless dc" is somewhat of a misnomer since the brushless dc machine is actually a permanent-magnet synchronous motor such as the one depicted in Figure 4-2. In fact, the only difference between the common notion of a permanent-magnet synchronous machine and the brushless dc machine is in the form of the applied voltages.

In this chapter a background on the brushless dc machine is provided beginning with a description of the permanent-magnet synchronous machine in machine variables. The machine equations are then transformed into the rotor reference frame. Finally, in the context of the rotor reference frame, the form of the applied voltages is specified. Additional background is available in references [5] and [6].

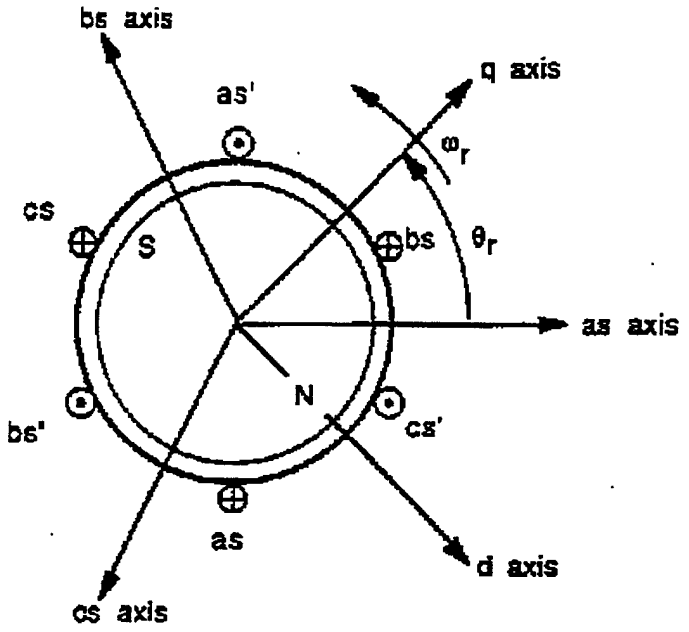

Figure 4-2, Three-Phase Permanent-Magnet Synchronous Machine.

a. Machine Equations

The purpose of this section is to set forth the machine equations for the permanent-magnet synchronous machine. The equations presented here are subject to the following assumptions: (1) the machine is non-salient, (2) the back emf is sinusoidal, and

(3) the machine is wye connected. The stator phase voltage equations describing the permanent-magnet synchronous machine are given in vector form by (4.1)

$$\vec{v}_{abcs} = r_s \vec{i}_{abcs} + \rho \vec{\lambda}_{abcs} \tag{4.1}$$

where ρ is the Heaviside operator d/dt. The flux linkage equations are similarly given by (4.2)

$$\vec{\lambda}_{abcs} = \begin{bmatrix} L & -M & -M \\ -M & L & -M \\ -M & -M & L \end{bmatrix} \vec{i}_{abcs} + \lambda_m' \begin{bmatrix} \sin(\theta_r) \\ \sin\left(\theta_r - \frac{2\pi}{3}\right) \\ \sin\left(\theta_r + \frac{2\pi}{3}\right) \end{bmatrix} \tag{4.2}$$

where λ_m' is a machine parameter dependent on the strength of the permanent magnet.

Since the machine is wye connected (the three stator currents must sum to zero), (4.2) may be rewritten as (4.3) where L_s is defined by (4.4). This representation is convenient since the three stator equations become uncoupled.

$$\vec{\lambda}_{abcs} = L_s \vec{i}_{abcs} + \lambda_m' \begin{bmatrix} \sin(\theta_r) \\ \sin\left(\theta_r - \frac{2\pi}{3}\right) \\ \sin\left(\theta_r + \frac{2\pi}{3}\right) \end{bmatrix} \tag{4.3}$$

$$L_s = L + M \tag{4.4}$$

The electromagnetic torque (T_e) is established by expressing the co-energy, taking the derivative of the co-energy with respect to θ_r, and multiplying the result by the number of pole pairs [Ref. 5].

$$T_e = \left(\frac{P}{2}\right)\lambda'_m\left(\frac{3}{2}i_{as}\cos(\theta_r) + \frac{\sqrt{3}}{2}(i_{bs} - i_{cs})\sin(\theta_r)\right) \tag{4.5}$$

b. Machine Equations in the Rotor Reference Frame

Considerable insight and simplification may be gained by making a change of variables which transforms all machine variables (abcs) to rotor reference frame variables (qd0s). The transformation from abcs variables to qd0s variables is given by (4.6) and (4.7) where $\vec{f}$ may represent voltage, current, or flux linkage.

$$\vec{f}_{qd0s} = K_s^r \vec{f}_{abcs} \tag{4.6}$$

$$K_s^r = \frac{2}{3}\begin{bmatrix} \cos(\theta_r) & \cos\left(\theta_r - \frac{2\pi}{3}\right) & \cos\left(\theta_r + \frac{2\pi}{3}\right) \\ \sin(\theta_r) & \sin\left(\theta_r - \frac{2\pi}{3}\right) & \sin\left(\theta_r + \frac{2\pi}{3}\right) \\ \frac{1}{2} & \frac{1}{2} & \frac{1}{2} \end{bmatrix} \tag{4.7}$$

The angle θ_r is the rotor electrical angle that necessarily varies at the rotor electrical angular velocity. The inverse transformation is

$$\left(K_s^r\right)^{-1} = \begin{bmatrix} \cos(\theta_r) & \sin(\theta_r) & 1 \\ \cos\left(\theta_r - \frac{2\pi}{3}\right) & \sin\left(\theta_r - \frac{2\pi}{3}\right) & 1 \\ \cos\left(\theta_r + \frac{2\pi}{3}\right) & \sin\left(\theta_r + \frac{2\pi}{3}\right) & 1 \end{bmatrix} \tag{4.8}$$

Applying the transformation to the machine equations and expanding those equations yields

$$v_{qs}^r = \left(r_s + \rho L_s\right) i_{qs}^r + \omega_r L_s i_{ds}^r + \omega_r \lambda_m' \tag{4.9}$$

$$v_{ds}^r = \left(r_s + \rho L_s\right) i_{ds}^r - \omega_r L_s i_{qs}^r \tag{4.10}$$

$$T_e = \left(\frac{3}{2}\right)\left(\frac{P}{2}\right)\lambda_m' i_{qs}^r \tag{4.11}$$

It can be seen from (4.11) that if torque is to be constant, then i_{qs}^r must be constant. Hence from (4.9) and (4.10), steady-state operation requires that v_{qs}^r and v_{ds}^r are constant as well. The steady-state line-to-neutral voltages may be given by

$$\vec{v}_{abcs} = \begin{bmatrix} V_s \cos(\theta_r + \alpha) \\ V_s \cos\left(\theta_r - \frac{2\pi}{3} + \alpha\right) \\ V_s \cos\left(\theta_r + \frac{2\pi}{3} + \alpha\right) \end{bmatrix} \tag{4.12}$$

where α is some arbitrary phase angle. Note, to achieve brushless dc operation, the stator voltages must vary at the rotor electrical angular velocity. Then, for any rotor speed, (4.13) and (4.14) apply. If the amplitude V_s is constant, then so are v_{qs}^r and v_{ds}^r .

$$v_{qs}^r = V_s \cos(\alpha) \tag{4.13}$$

$$v_{ds}^r = -V_s \sin(\alpha) \tag{4.14}$$

For steady-state conditions, with $\alpha = 0$ and $\omega_r L_s << r_s$, (4.13), (4.14), (4.9)-(4.11) may be manipulated to yield (4.15) which is identical in form to the steady-state torque equation of an armature-controlled dc machine.

$$T_e = \left(\frac{3}{2}\right)\left(\frac{P}{2}\right)\frac{\lambda_m'}{r_s}\left(V_s - \lambda_m'\omega_r\right) \tag{4.15}$$

Now that the basic features of brushless dc operation have been set forth, the problem of actually obtaining the voltages described by (4.12) is addressed. One device used to obtain these voltages in practice is known as an inverter. The inverter is the subject of the next section.

3. Inverter Operation

There are several methods of achieving stator voltages of the form given by (4.12), where the frequency of the voltages is variable. One method is to use a device known as an inverter. A typical three-phase inverter is depicted in Figure 4-3. Assuming ideal components, the inverter operates without loss and thus a conducting device is modeled as a short circuit and a blocking device is modeled as an open circuit. The tradeoff in using an inverter is that the voltages produced contain harmonics that increase loss in the stator circuits and can introduce torque pulsations.

There are two types of inverters, the 120° and the 180°. In the 120° case, each transistor is on 120° out of a 360° cycle. Likewise, in the 180° case, each transistor is on 180° out of 360°. Although the 120° inverter-driven brushless dc machine is more difficult to handle analytically, it has a practical advantage in that it can be operated without any rotor position sensors. In this case, position information is derived indirectly from measurement of the open-circuit phase voltages.

a. Basic Inverter Operation

A schematic depiction of the brushless DC inverter system appears in Fig 4-3. The inverter consists of six transistors, T1-T6, which are used to convert DC power to AC power and six free-wheeling diodes, D1-D6, which are necessary to protect the transistors from the inductive nature of the load.

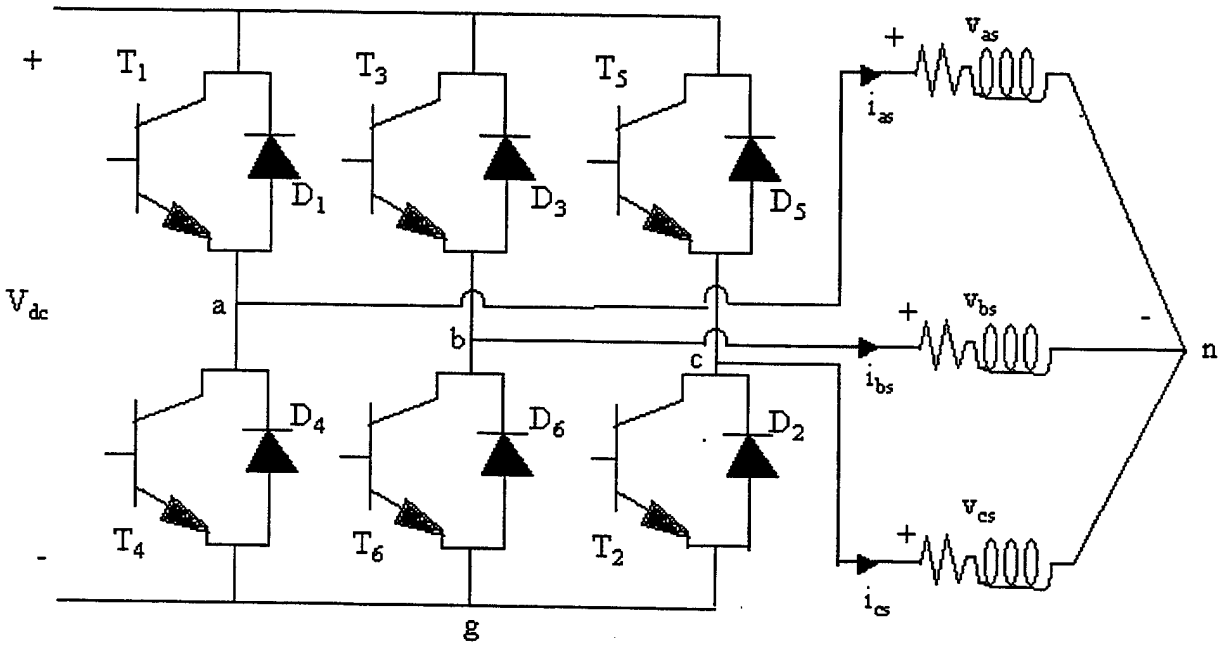

Figure 4-3, Inverter and Machine.

The first step toward the analysis of the inverter is to apply Kirchhoff's Voltage Law (KVL) starting at the negative dc rail (g), proceeding across the lower transistor and across the machine phase, and returning to the negative dc rail via the neutral point (n). Applying this path for each machine phase yields

$$v_{ag} = v_{as} + v_{ng} \tag{4.16}$$

$$v_{bg} = v_{bs} + v_{ng} \tag{4.17}$$

$$v_{cg} = v_{cs} + v_{ng} \tag{4.18}$$

Kirchhoff's Current Law (KCL) dictates for a wye connection that

$$i_{as} + i_{bs} + i_{cs} = 0 \tag{4.19}$$

Equations (4.19) and (4.3) may be used to show that the sum of the stator flux linkages, namely $\lambda_{as} + \lambda_{bs} + \lambda_{cs}$, is zero. Since the sum of the stator currents is zero, and the sum of the stator flux linkages is zero, (4.1) shows that

$$v_{as} + v_{bs} + v_{cs} = 0 \tag{4.20}$$

The neutral to ground (where ground is the lower rail of the dc supply) voltage, v_{ng}, is obtained by adding (4.16), (4.17), and (4.18), and then subtracting (4.20) which results in

$$v_{ng} = \frac{1}{3}\left(v_{ag} + v_{bg} + v_{cg}\right) \tag{4.21}$$

Substituting (4.21) into (4.16), (4.17), and (4.18) yields the following expressions for the phase voltages.

$$v_{as} = \frac{2}{3}v_{ag} - \frac{1}{3}v_{bg} - \frac{1}{3}v_{cg} \tag{4.22}$$

$$v_{bs} = \frac{2}{3}v_{bg} - \frac{1}{3}v_{ag} - \frac{1}{3}v_{cg} \tag{4.23}$$

$$v_{cs} = \frac{2}{3}v_{cg} - \frac{1}{3}v_{ag} - \frac{1}{3}v_{bg} \tag{4.24}$$

b. Six-Step 180° Continuous-Current Inverter

The logical signals for the switching (commutation) of the transistors are shown in Figure 4.4. T_1 is turned on at $\theta_r = -90°$ and turned off at $\theta_r = +90°$, at the same time T_4 is turned on. Note, in practice some delay must be present to avoid short-circuiting the dc input supply. The gating signals for the top transistors associated with the remaining two phases (T_3 and T_5) are each phase displaced from the T_1 signal by 120° so that a balanced set of voltages is produced across the load. It is assumed that the turn-off time of the transistors is negligible whereupon the transistors become ideal switches. At the instant T_1 is turned off, and T_4 is gated on, the current T_1 was carrying is diverted to the diode D_4. The diode continues to conduct until the current decreases to zero. Once

the current i_{as} reverses direction it is carried by T_4. This mode of inverter operation is generally referred to as the continuous-voltage or continuous-current mode. [Ref. 7]

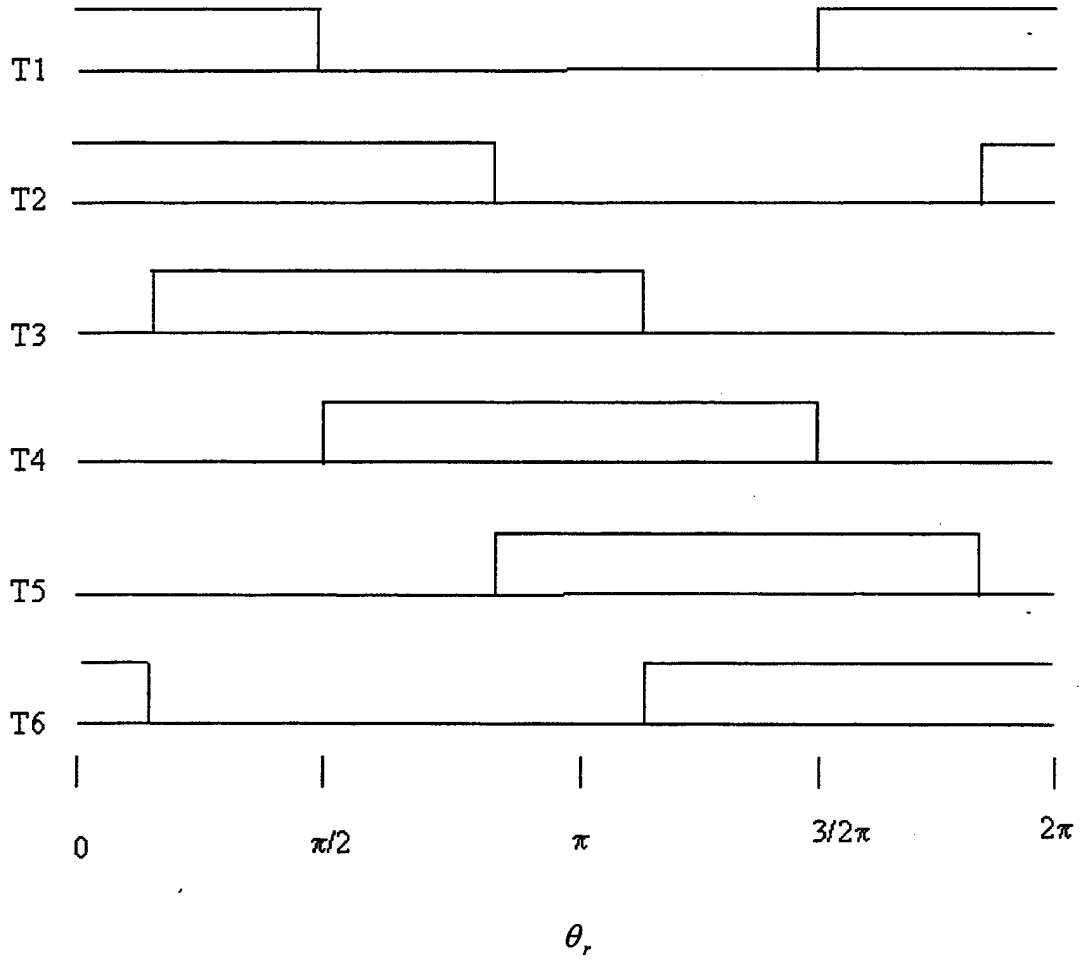

Figure 4-4, Transistor Switching Logic for the 180° Continuous-Current Inverter.

The operation of the 180° inverter is set forth in Table 4.1. In the table electrical rotor position is divided into six 60° segments known as Basic Switching Intervals (BSI). The second column specifies the center of each switching interval in terms of $\theta_r + \phi$. The angle ϕ is known as the advance-firing angle, which allows the shifting of the transistor firing sequence relative to the position of the rotor. The third column of Table 4.1 defines the transistor firing sequence by indicating which transistors are gated on in a given BSI. The transistor firing pattern results in pole (abcg) and phase (abcs) voltages which are specified in Table 4.1 [Ref. 7]. Note that once the switching pattern is assigned, the phase voltages are completely determined. This fact makes programming the 180° inverter rather straightforward in ACSL.

BSI	$\theta_r + \phi$	Transistors On	v_{ag}	v_{bg}	v_{cg}	v_{as}	v_{bs}	v_{cs}
I	0°	1,2,6	V_{dc}	0	0	$\frac{2}{3}V_{dc}$	$-\frac{1}{3}V_{dc}$	$-\frac{1}{3}V_{dc}$
II	60°	1,2,3	V_{dc}	V_{dc}	0	$\frac{1}{3}V_{dc}$	$\frac{1}{3}V_{dc}$	$-\frac{2}{3}V_{dc}$
III	120°	2,3,4	0	V_{dc}	0	$-\frac{1}{3}V_{dc}$	$\frac{2}{3}V_{dc}$	$-\frac{1}{3}V_{dc}$
IV	180°	3,4,5	0	V_{dc}	V_{dc}	$-\frac{2}{3}V_{dc}$	$\frac{1}{3}V_{dc}$	$\frac{1}{3}V_{dc}$
V	240°	4,5,6	0	0	V_{dc}	$-\frac{1}{3}V_{dc}$	$-\frac{1}{3}V_{dc}$	$\frac{2}{3}V_{dc}$
VI	300°	1,5,6	V_{dc}	0	V_{dc}	$\frac{1}{3}V_{dc}$	$-\frac{2}{3}V_{dc}$	$\frac{1}{3}V_{dc}$

Table 4.1, 180° Inverter Operation.

Expressing the phase voltages given in Table 4.1 as a Fourier series in electrical rotor position, neglecting all harmonics, and incorporating the transformation to the rotor reference frame yields

$$v_{qs}^{r} = \frac{2V_{dc}}{\pi}\cos(\phi) \tag{4.25}$$

$$v_{ds}^{r} = -\frac{2V_{dc}}{\pi}\sin(\phi) \tag{4.26}$$

Comparing (4.24) and (4.25) to (4.13) and (4.14), it is apparent that the 180° inverter α and ϕ are equivalent.

c. 120° Discontinuous-Current Inverter

The logical signals for the switching (commutation) of the transistors are shown in Figure 4-5. T_1 is turned on at $\theta_r = 0°$ and turned off at $\theta_r = +120°$; however, T_4 is not turned on until 60° later at $\theta_r = 180°$ Hence, the diode in parallel with T_4 begins conducting when T_1 is turned off and continues to conduct until the current i_{as} becomes zero. At this point the *as* winding of the machine becomes open- circuited. The 60°-delay in turning T_4 on is done primarily for the purpose of lessening the possibility of a short circuit occurring through T_1 and T_4 and to provide an open-circuit period for indirectly sensing the rotor position. The voltage v_{ag} in Figure 4-3 is equal to the source voltage

v_{dc} if T_1 is turned on or if the diode in parallel with T_1 is conducting. When T_4 is turned on or when the diode in parallel with T_4 is conducting, v_{ag} is zero.

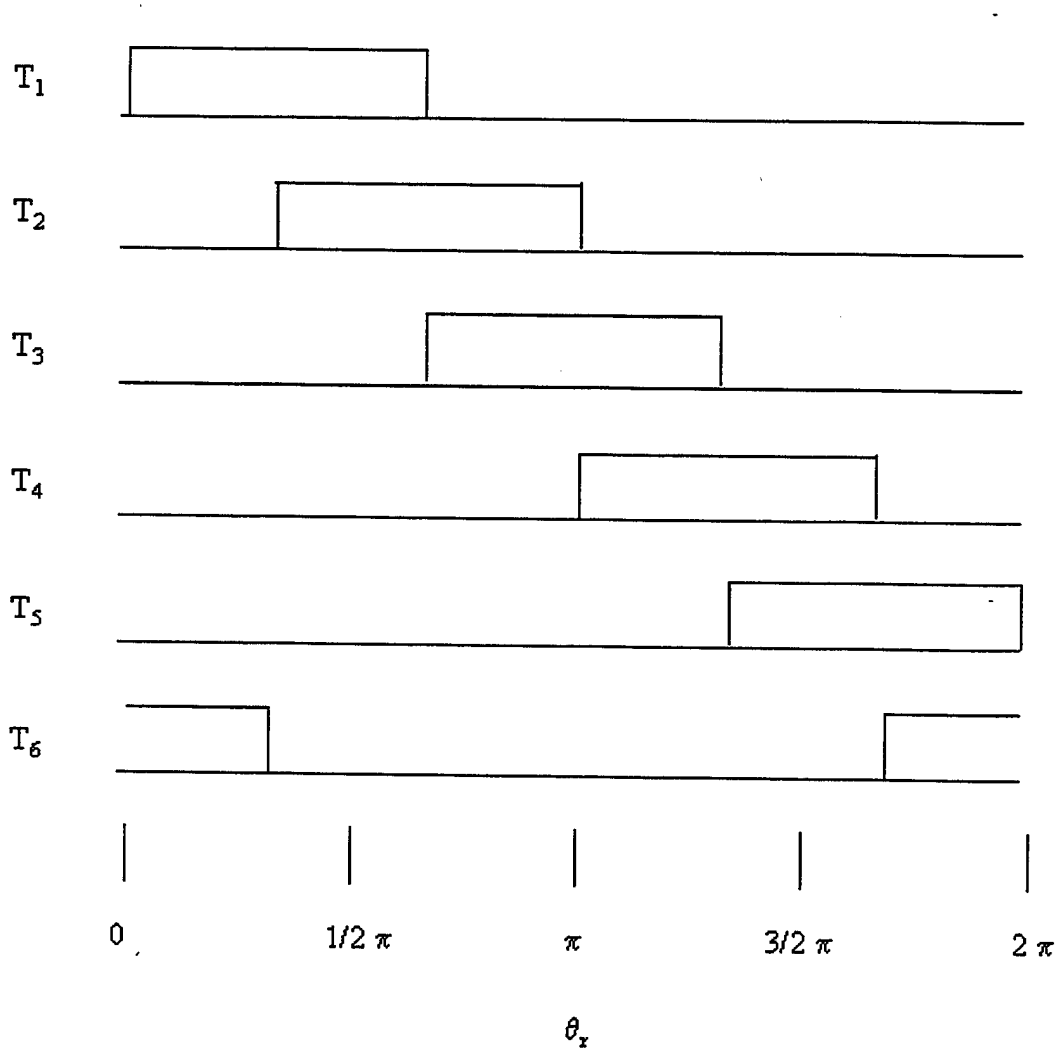

Figure 4-5. Transistor Switching Logic for the 120° Discontinuous-Current Inverter.

The operation of a 120° inverter is summarized in Table 4.2, which is much the same as Table 4.1 except for two important differences. The first is that only two transistors are gated on at any given instant of time. Secondly, question marks

appear periodically in the last three columns to indicate that the instantaneous current determines the voltages in the corresponding phase. [Ref. 7]

BSI	$\Theta_r + \phi$	Transistors On	V_{ag}	V_{bg}	V_{cg}
I	0°	1,6	V_{dc}	0	?
II	60°	1,2	V_{dc}	?	0
III	120°	2,3	?	V_{dc}	0
IV	180°	3,4	0	V_{dc}	?
V	240°	4,5	0	?	V_{dc}
VI	300°	5,6	?	0	V_{dc}

Table 4.2, 120° Inverter Operation.

The dependence of the phase voltages on the current in the open-circuited phase is best illustrated by examining one specific BSI. In BSI II if $i_{bs} < 0$, then current will flow through D3 and thus $v_{bg} = V_{dc}$. Conversely, if $i_{bs} > 0$ then current flows through D6 which causes $v_{bg} = 0$. Finally, if $i_{bs} = 0$, then v_{bs} is the open-circuit voltage as derived from (4.1) and (4.3) and given by

$$v_{bs} = \lambda'_m \omega_r \cos\left(\theta_r - \frac{2\pi}{3}\right) \tag{4.27}$$

If (4.17) is substituted into (4.21), then the neutral to ground voltage is given by

$$v_{ng} = \frac{1}{2}\left(v_{ag} + v_{bs} + v_{cg}\right) \tag{4.28}$$

Upon using (4.27) for v_{bs} in (4.28) and then using (4.28) to replace v_{ng} in (4.17), the voltage across the lower transistor in leg B (T_6) is

$$v_{bg} = \frac{1}{2}V_{dc} + \frac{3}{2}\lambda'_m\omega_r \cos\left(\theta_r - \frac{2\pi}{3}\right) \tag{4.29}$$

Similarly, (4.28) can be used to find v_{as} and v_{cs} from (4.16) and (4.18).

$$v_{as} = \frac{1}{2}V_{dc} - \frac{1}{2}\lambda'_m\omega_r \cos\left(\theta_r - \frac{2\pi}{3}\right) \tag{4.30}$$

$$v_{cs} = -\frac{1}{2}V_{dc} - \frac{1}{2}\lambda'_m\omega_r \cos\left(\theta_r - \frac{2\pi}{3}\right) \tag{4.31}$$

This analysis can be repeated and adapted for each basic switching interval (BSI). Table 4.3 reflects the pole voltages, v_{abcg}, when each phase current, i_{abcs}, is exactly equal to zero. For each phase current, i_{abcs}, greater than zero, each pole voltage, v_{abcg}, is equal to V_{dc}. For each phase current, i_{abcs}, less than zero, each pole voltage, v_{abcg}, is equal to zero. Table 4.4 similarly reflects the stator phase voltages, v_{abcs}, when the phase currents, i_{abcs}, are equal to zero.

BSI	$\theta_r + \phi$	Trans On	V_{ag}	V_{bg}	V_{cg}
I	0°	1,6	V_{dc}	0	$\frac{1}{2}V_{dc} + \frac{3}{2}\lambda_m' \omega_r \cos\left(\theta_r + \frac{2\pi}{3}\right)$
II	60°	1,2	V_{dc}	$\frac{1}{2}V_{dc} + \frac{3}{2}\lambda_m' \omega_r \cos\left(\theta_r - \frac{2\pi}{3}\right)$	0
III	120°	2,3	$\frac{1}{2}V_{dc} + \frac{3}{2}\lambda_m' \omega_r \cos(\theta_r)$	V_{dc}	0
IV	180°	3,4	0	V_{dc}	$\frac{1}{2}V_{dc} + \frac{3}{2}\lambda_m' \omega_r \cos\left(\theta_r + \frac{2\pi}{3}\right)$
V	240°	4,5	0	$\frac{1}{2}V_{dc} + \frac{3}{2}\lambda_m' \omega_r \cos\left(\theta_r - \frac{2\pi}{3}\right)$	V_{dc}
VI	300°	5,6	$\frac{1}{2}V_{dc} + \frac{3}{2}\lambda_m' \omega_r \cos(\theta_r)$	0	V_{dc}

Table 4.3, Pole Voltages for BSI I through VI with Non-Conducting Phase Open Circuited.

BSI	$\theta_r + \phi$	Trans On	V_{as}	V_{bs}	V_{cs}
I	0°	1,6	$\frac{1}{2}V_{dc} - \frac{1}{2}\lambda_m' \omega_r \cos\left(\theta_r + \frac{2\pi}{3}\right)$	$-\frac{1}{2}V_{dc} - \frac{1}{2}\lambda_m' \omega_r \cos\left(\theta_r + \frac{2\pi}{3}\right)$	$\lambda_m' \omega_r \cos\left(\theta_r + \frac{2\pi}{3}\right)$
II	60°	1,2	$\frac{1}{2}V_{dc} - \frac{1}{2}\lambda_m' \omega_r \cos\left(\theta_r - \frac{2\pi}{3}\right)$	$\lambda_m' \omega_r \cos\left(\theta_r - \frac{2\pi}{3}\right)$	$-\frac{1}{2}V_{dc} - \frac{1}{2}\lambda_m' \omega_r \cos\left(\theta_r - \frac{2\pi}{3}\right)$
III	120°	2,3	$\lambda_m' \omega_r \cos(\theta_r)$	$\frac{1}{2}V_{dc} - \frac{1}{2}\lambda_m' \omega_r \cos(\theta_r)$	$-\frac{1}{2}V_{dc} - \frac{1}{2}\lambda_m' \omega_r \cos(\theta_r)$
IV	180°	3,4	$-\frac{1}{2}V_{dc} - \frac{1}{2}\lambda_m' \omega_r \cos\left(\theta_r + \frac{2\pi}{3}\right)$	$\frac{1}{2}V_{dc} - \frac{1}{2}\lambda_m' \omega_r \cos\left(\theta_r + \frac{2\pi}{3}\right)$	$\lambda_m' \omega_r \cos\left(\theta_r + \frac{2\pi}{3}\right)$
V	240°	4,5	$-\frac{1}{2}V_{dc} - \frac{1}{2}\lambda_m' \omega_r \cos\left(\theta_r - \frac{2\pi}{3}\right)$	$\lambda_m' \omega_r \cos\left(\theta_r - \frac{2\pi}{3}\right)$	$\frac{1}{2}V_{dc} - \frac{1}{2}\lambda_m' \omega_r \cos\left(\theta_r - \frac{2\pi}{3}\right)$
VI	300°	5,6	$\lambda_m' \omega_r \cos(\theta_r)$	$-\frac{1}{2}V_{dc} - \frac{1}{2}\lambda_m' \omega_r \cos(\theta_r)$	$\frac{1}{2}V_{dc} - \frac{1}{2}\lambda_m' \omega_r \cos(\theta_r)$

Table 4.4 Stator Phase Voltages for BSI I through VI with Non-Conducting Phase Open Circuited.

d. Sensorless Control

Brushless dc motors are usually controlled using dc-ac inverters as previously discussed. The motor requires a rotor position sensor for starting and for providing the proper commutation sequence to turn on the power devices in the inverter. Hall effect sensors can be used; however, they must be specially mounted in the interior of the stator. Further these sensors are temperature sensitive, limiting the operation of the motor to below about 75 °C. Due to these limitations of the motor operation with Hall devices, sensorless operation of the PM brushless motor is receiving more attention.

Several schemes for position sensorless operation of PM motors have been reported and reviewed. They are based on the following techniques. [Ref. 8]

1. *Position sensing using the back emf of the motor.*
2. *Position information using the stator third harmonic component.*
3. *Position information based on detection of the conducting interval of free-wheeling diodes connected in anti-parallel with the power devices.*
4. *Position information using the motor parameters, and the measured terminal voltages and currents.*

Position sensing using the back emf of the motor is being utilized for control of the NBC fan motor. The sensed back emf can be used in several ways to obtain the proper switching sequence for the inverter power devices. Some or these methods are:

- The zero-crossing approach based on detecting the instant at which the back emf in the unexcited phase crosses zero or reaches a predetermined level.
- Phase-lock-loop (PLL) technique to lock on to the back emf waveform in the unexcited phase winding during each 60 degree excitation interval.
- Back emf integration approach, which provides a commutation pulse when the integrated rectified back emf waveform reaches a preset threshold value.

The zero-crossing approach method is utilized in the NBC fan drive and therefore is discussed. In a 120° inverter-driven permanent-magnet brushless dc machine only two of the three phases are excited at any one time. The back emf voltage in the unexcited phase can be measured to establish a switching sequence for commutation of the power devices in the inverter. Based on the rotor position, the power devices are commutated sequentially every 60 degrees to continually synchronize the phase excitation with the rotating rotor magnetic field.

The pole voltages v_{ag}, v_{bg}, v_{cg}, and the neutral voltage v_{ng} are measured. At the instants of the zero crossing of the back emf waveform, the pole voltage is equal to the neutral voltage. When the back emf of phase A crosses zero, then $v_{ag} = v_{ng} \approx \frac{V_{dc}}{2}$. In order to use this zero-crossing point to derive the switching sequence, this point has to be phase shifted by 90 degrees [Ref. 8].

D. Ultra Capacitor Background

As shown in the candidate electrical system description, an ultra capacitor bank will be modeled and validated. This ultra capacitor may be incorporated in the AAAV electrical system in an effort to capture regenerative energy. Regenerative energy could be produced as a result of a sudden impact on the vehicle's main gun turret. This energy could be forced back into the high power distribution bus thus potentially damaging the system. Theoretically, the ultra capacitor bank will absorb this energy and prevent any damage.

Ultra capacitors are being considered over conventional capacitors due to their high capacitance relative to their small compact size. Since the technology is new, a short discussion on ultra capacitors will follow.

Conventional capacitors store energy in the form of separated electric charge. The greater the area for storing charge and the closer the separated charges results in greater capacitance. A conventional capacitor achieves its cross-sectional area from plates of flat, conductive material. To realize high capacitance, this material can be wound in great lengths to increase its surface area. A conventional capacitor separates its charged plates with a dielectric material, sometimes plastic or paper film, or even a ceramic. These dielectrics can be made only as thin as the available films or other applied material.

An ultra capacitor gets its surface area from a porous carbon-based electrode material. The porous structure of this material allows its surface area to approach 2000 square meters per gram, much greater than can be accomplished using flat or textured films and plates. An ultra capacitor's charge separation distance is determined by the size

of the ions in the electrolyte, which are attracted to the charged electrode. This charge separation is much smaller than can be accomplished using conventional dielectric materials.

The combination of enormous surface area and extremely small charge separation gives the ultra capacitor its outstanding capacitance (1 Farad, 100Volts) relative to conventional capacitors.

E. Battery Background

As shown in the candidate electrical system description, two battery banks, one connected to the Vetronics bus and the other to the auxiliary bus (see Figure 4-1), will be modeled and validated. Therefore, a brief discussion on basic battery concepts is included.

A battery is a device that converts the chemical energy contained in its active materials directly into electric energy by means of an electrochemical oxidation-reduction (redox) reaction. This type of reaction involves the transfer of electrons from one material to another through an electric circuit. In a non-electrochemical redox reaction, such as rusting or burning, the transfer of electrons occurs directly and only heat is involved.

While the term battery is often used, the basic electrochemical unit being referred to is the cell. A battery consists of one or more cells, connected in series or parallel, or both, depending on the desired output voltage or capacity.

The cell consists of three major components.

1. The anode or negative electrode – which gives up electrons to the external circuit and is oxidized during the electrochemical reaction.
2. The cathode or positive electrode – which accepts electrons from the external circuit and is reduced during the electrochemical reaction.
3. The electrolyte – the ionic conductor – which provides the medium for transfer of electrons, as ions, inside the cell between the anode and the cathode. The electrolyte is typically a liquid, such as water or other solvent, with dissolved salts, acids, or alkalis to impart ionic conductivity.

The lead-acid battery, as will be used in the AAAV, uses lead dioxide as the active material for the positive electrode and metallic lead, in a high surface area porous structure, as the negative active material. The electrolyte is a sulfuric acid solution [Ref. 9].

THIS PAGE INTENTIONALLY LEFT BLANK

V. COMPONENT MODELING AND VALIDATION

A. Introduction

This chapter contains a discussion of the modeling efforts applied to the NBC fan drive, ultra capacitor, and battery unit. It also provides results and conclusions for each model.

B. NBC Fan Drive Model

The circuit diagram of the NBC fan motor and its associated three-phase inverter drive is shown in Figure 5-1. The resistance and the inductance of the cable connecting the motor drive to the high power 28-volt bus are included in the diagram as r_{line} and L_{line}. The input capacitance of the inverter is given by C_{dc}.

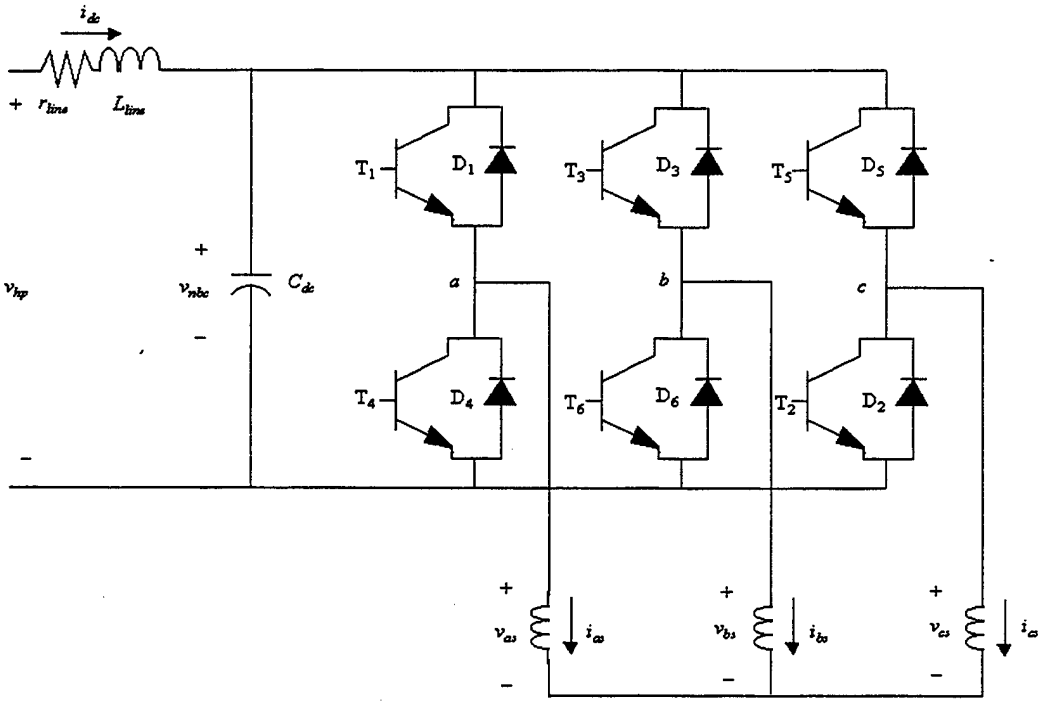

Figure 5-1, NBC Motor Drive System Circuit Diagram.

As discussed in Chapter 4, the equations describing the brushless dc motor are expressed as:

$$v_{qs}^{r} = (r_s + \rho L_s) i_{qs}^{r} + \omega_r L_s i_{ds}^{r} + \omega_r \lambda_m' \tag{5.1}$$

$$v_{ds}^{r} = (r_s + \rho L_s) i_{ds}^{r} - \omega_r L_s i_{qs}^{r} \tag{5.2}$$

$$T_e = \left(\frac{3}{2}\right)\left(\frac{P}{2}\right)\lambda_m' i_{qs}^{r} \tag{5.3}$$

where

$$\omega_r = \frac{P}{2}\omega_{rm} \tag{5.4}$$

and P is the number of poles. These equations together with the transformation of the phase voltages into the rotor reference frame and the inverse transformation of the rotor reference frame currents back to machine variables are coded in ACSL in a straightforward manner.

The mechanical speed is established by integrating

$$\rho\omega_{rm} = (T_e - T_L)/J_L \tag{5.5}$$

where T_e is the electromagnetic torque, T_L is the load torque, and J_L is the inertia of the motor and the connected fan load. It is assumed that the load torque is proportional to the square of the rotor speed. In particular,

$$T_L = K_m \omega_{rm}^2 \tag{5.6}$$

The actual inverter is a 120° discontinuous-current inverter based on sensorless control. The current model being exercised by PCK&A is that of the NBC fan motor with a 180° continuous–current inverter using Hall-effect sensors to detect rotor position. The first step in developing an accurate model was to build a model similar to that being currently exercised. This model would allow for a better understanding of the inverter and motor assembly.

The 180° inverter model was developed and exercised. The transistor gating signals are derived based on the waveforms illustrated in Figure 4-4. The phase voltages are then determined from (4.22) – (4.24). The current drawn by the inverter is established by summing the phase currents corresponding to the gated transistors connected to the top rail. The parameters used are shown in Table 5.1. The parameters were derived using manufacturer provided data. The complete ACSL model can be found in Appendix A. For convenience, a fixed 28-volt ideal source was used as the input to the inverter.

Symbol	Value	Description	Origin
L_s	0.005 mH	Stator self Inductance	Calculated from manufacturer supplied data (average of upper and lower values)
r_s	0.003 Ω	Stator resistance	Calculated from manufacturer Supplied data (average of upper and lower values)
λ'_m	0.00344 V-s/rad	Back emf constant	Calculated from manufacturer supplied data
P	4	Number of poles	Communication from manufacturer
C_{dc}	0.036 F	Filter capacitance	Communication from manufacturer
L_{line}	1 μH	Cable inductance	Estimated
r_{line}	0.01 Ω	Cable resistance	Estimated
J_m	$1.171X10^{-4}$ kg·m^2	Inertia	Estimated
K_m	$1.128X10^{-6}$N·m·s	Load constant	Estimated from manufacturer supplied data

Table 5.1, NBC Fan Motor Drive Parameters.

Figure 5-2 shows the first few cycles of the stator currents, i_{as}, i_{bs}, and i_{cs}, upon startup of the 180° inverter model using the data derived from communication with the manufacturer. With the low value of stator resistance, these currents illustrate a large startup transient, on the order of 4000A for i_{as}. Since rated current for the drive is approximately 125A, this current draw represents a significant transient load on the high-power bus.

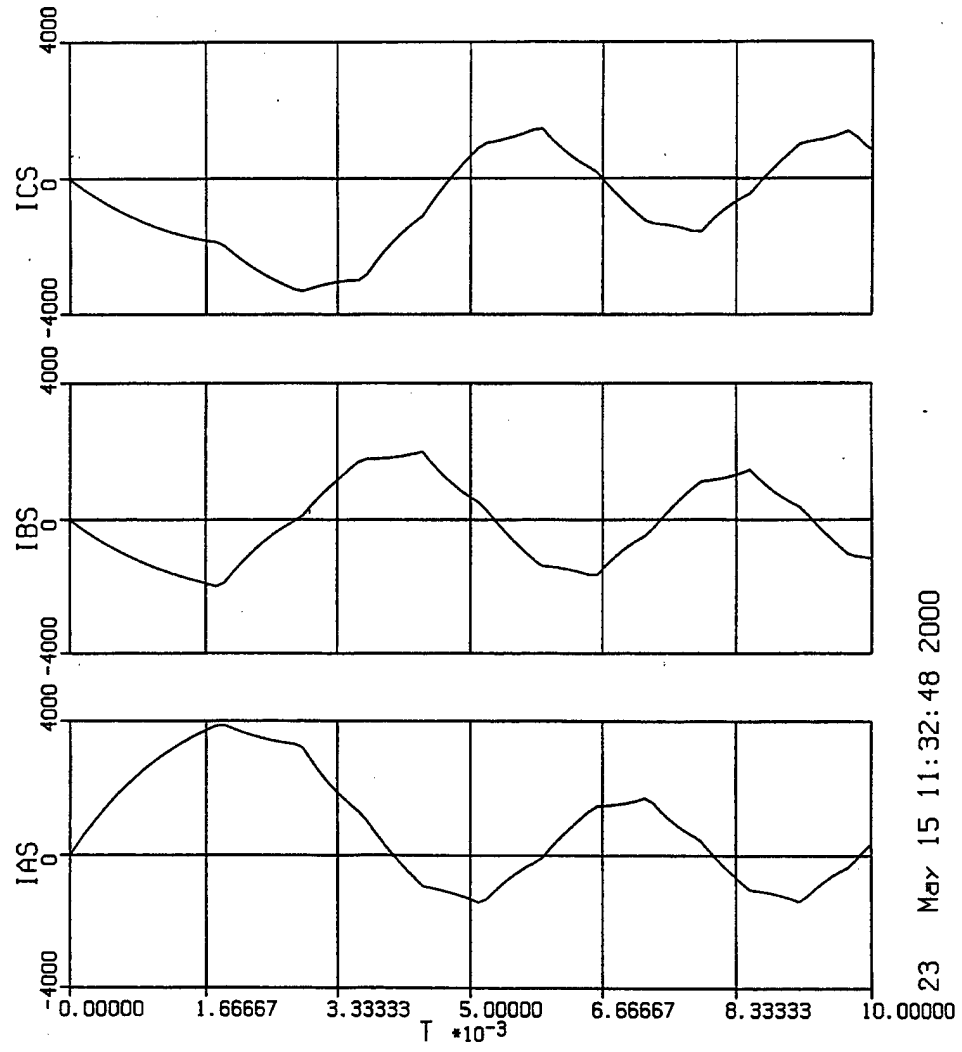

Figure 5-2, Initial Stator Currents of NBC Fan Model
with 180° Continuous-Current Inverter Upon Startup.

Figure 5-3 shows simulation results for the drive extending from startup to steady state. The variables plotted include ω_{rm} – rotor speed in rads/s, T_e – electromagnetic torque in Newton-meters, i_{as} - stator current in Amps, and i_{ii} – inverter input current in Amps. The large spike in inverter input current is readily apparent as are the considerable

current harmonics resulting from the applied six-step voltage waveforms. The motor speed settles out at a final value of about 1250 rad/sec.

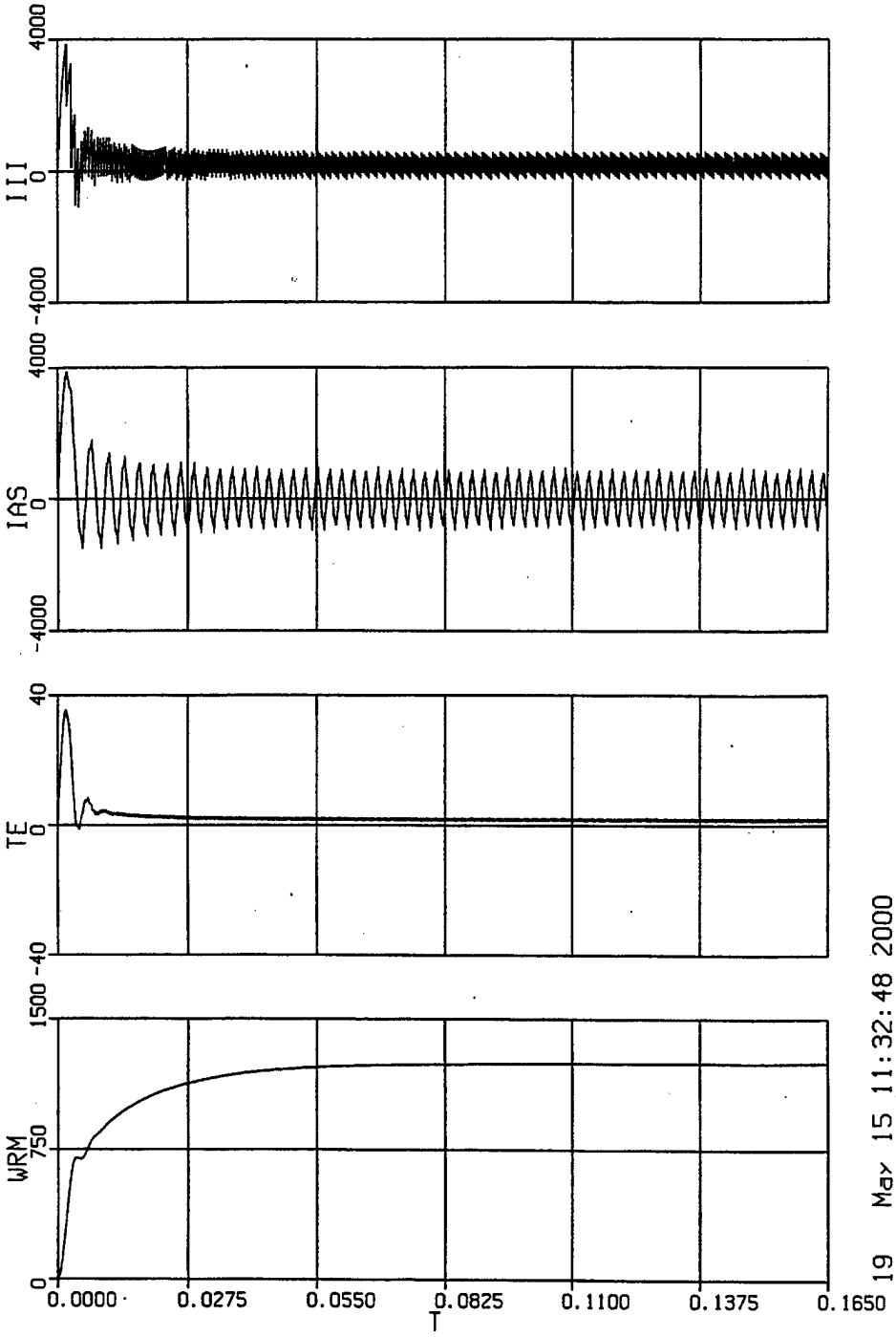

Figure 5-3, Plot of Start-up of NBC Fan Model with 180° Continuous-Current Inverter.

Figure 5-4 illustrates steady-state waveforms for the 180^o inverter drive. In particular, the figure shows variables v_{as} - stator voltage in Volts, i_{as} - stator current in Amps, and i_{ii} – inverter current in Amps, T_e – electromagnetic torque in Newton-meters, and ω_{rm} – rotor speed in rads/s. The $6\omega_r$ dominant harmonic in i_{ii} is apparent and the peak value of i_{as} appears to be on the order of 800A. This 800A amplitude is much larger than the anticipated 125A, though the final speed of the device is rather close to the anticipated rated speed (1310 rad/sec). The difference may be due to the drive actually being a 120^o inverter drive or to an inaccurate assumption on the motor parameters.

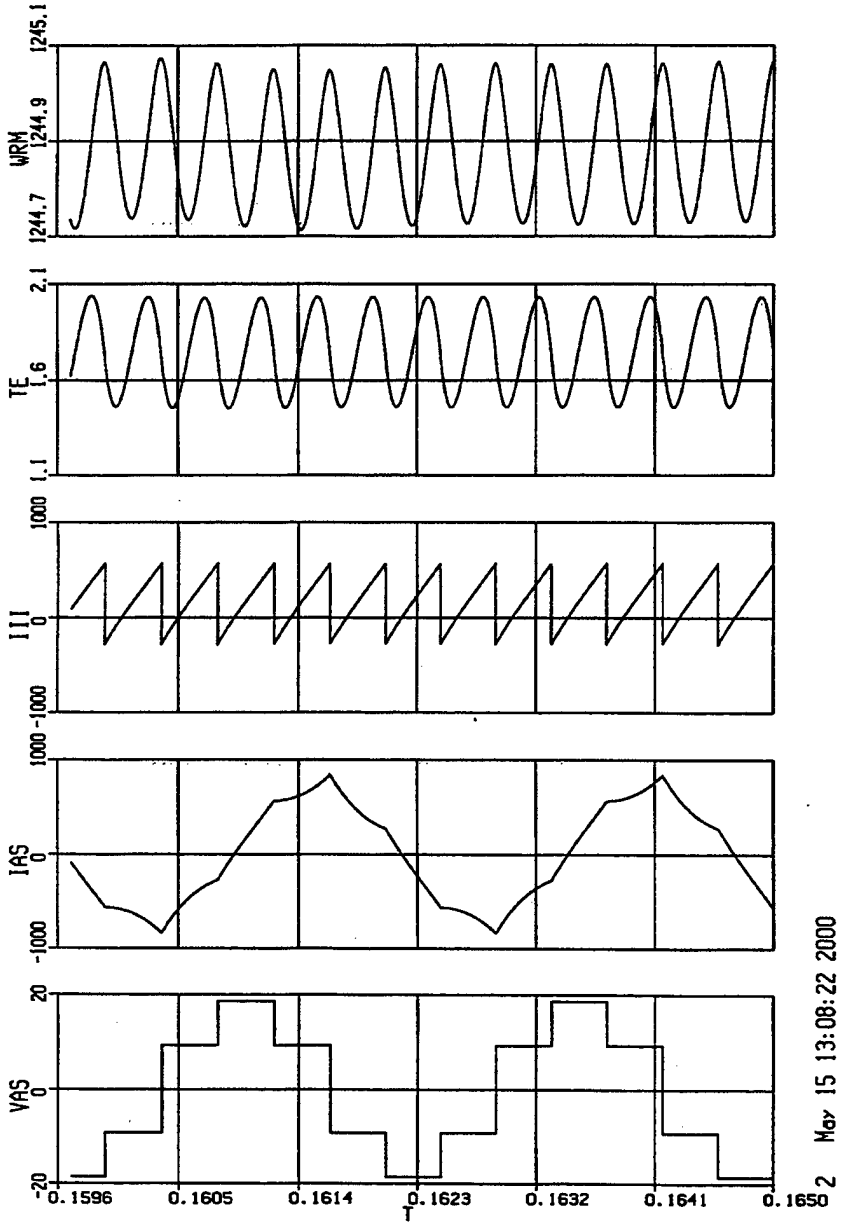

Figure 5-4, Plot of Steady State of NBC Fan Model with 180° Continuous-Current Inverter.

Research then began on implementation of a 120° discontinuous-current inverter using a sensorless control scheme. As discussed in Chapter IV, paragraph C, subsection 3.b, sensorless control can be initiated by indirectly assessing the rotor position using the back emf of the motor. The back emf can be monitored to detect the instant at which the back emf in the unexcited phase crosses zero or reaches a predetermined level. The instant at which this happens is then used to establish a switching sequence for commutation of the transistors in the inverter.

The main nuance between the simulation of the 120° and the 180° inverter is establishing which devices are conducting. In particular, when neither transistor in the inverter leg is gated, then one of the diodes may be conducting or the phase could be open-circuited. In addition depending on the back emf, the open-circuited phase voltage may change and cause one of the diodes to turn on. The logic used in the simulation for establishing the status of D_1 and D_4 is illustrated below.

```
IF ((T1) .OR. (T4)) THEN

        D1 = .false.
        D4 = .false.

ELSEIF (ias .GT. hold) THEN

        D4 = .true.
        D1 = .false.

ELSEIF (ibs .LT. -hold) THEN

        D1 = .true.
        D4 = .false.

ELSEIF ((Vagoc .LT. (Vdc + eps)) .OR. (Vagoc .GT. -eps)) THEN

        D1 = .false.
        D4 = .false.
```

```
ELSEIF (Vagoc .GT. (Vdc + eps)) THEN
        D1 = .true.
ELSE
        D4 = .true.
ENDIF
```

Note, if neither transistor is gated and the phase current is positive, then D_4 must conduct. Conversely, if the current is negative, the D_1 must conduct. Otherwise, the back emf must be assessed. If it is greater than the input voltage (V_{dc}), then the upper diode is turned on. If it is less than zero volts, then D_4 is turned on. If the open-circuit voltage remains between zero volts and V_{dc}, then the phase remains open circuited.

The complete ACSL code for the NBC Fan with the 120° discontinuous-current inverter can be found in Appendix B. The 120° inverter model was developed and exercised. The λ'_m parameter was adjusted through simulation to yield steady-state stator current waveforms consistent with manufacturer data. The complete set of parameters is documented in Table 5.2. Once again a fixed 28-volt source was used as the input to the inverter.

Symbol	Value	Description	Origin
L_s	0.005 mH	Stator self Inductance	Calculated from manufacturer supplied data (average of upper and lower values)
r_s	0.003 Ω	Stator resistance	Calculated from manufacturer Supplied data (average of upper and lower values)
λ'_m	0.006 V-s/rad	Back emf constant	Adjusted by simulation
P	4	Number of poles	Communication from manufacturer
C_{dc}	0.036 F	Filter capacitance	Communication from manufacturer
L_{line}	1 μH	Cable inductance	Estimated
r_{line}	0.01 Ω	Cable resistance	Estimated
J_m	$1.171X10^{-4}$ kg·m^2	Inertia	Estimated
K_m	$1.128X10^{-6}$N·m·s	Load constant	Estimated from manufacturer supplied data

Table 5.2, NBC Fan Motor Drive Parameters.

Figure 5-5 shows the first few cycles of the stator currents, i_{as}, i_{bs}, and i_{cs}, upon startup of the 120° inverter model assuming that rotor position is available. Similar to the 180° model, the currents illustrate a large starting transient, reaching levels of approximately 2600A. Also, following the initial swing, the currents assume the classical 120° waveform, where the open-circuit waveform is apparent.

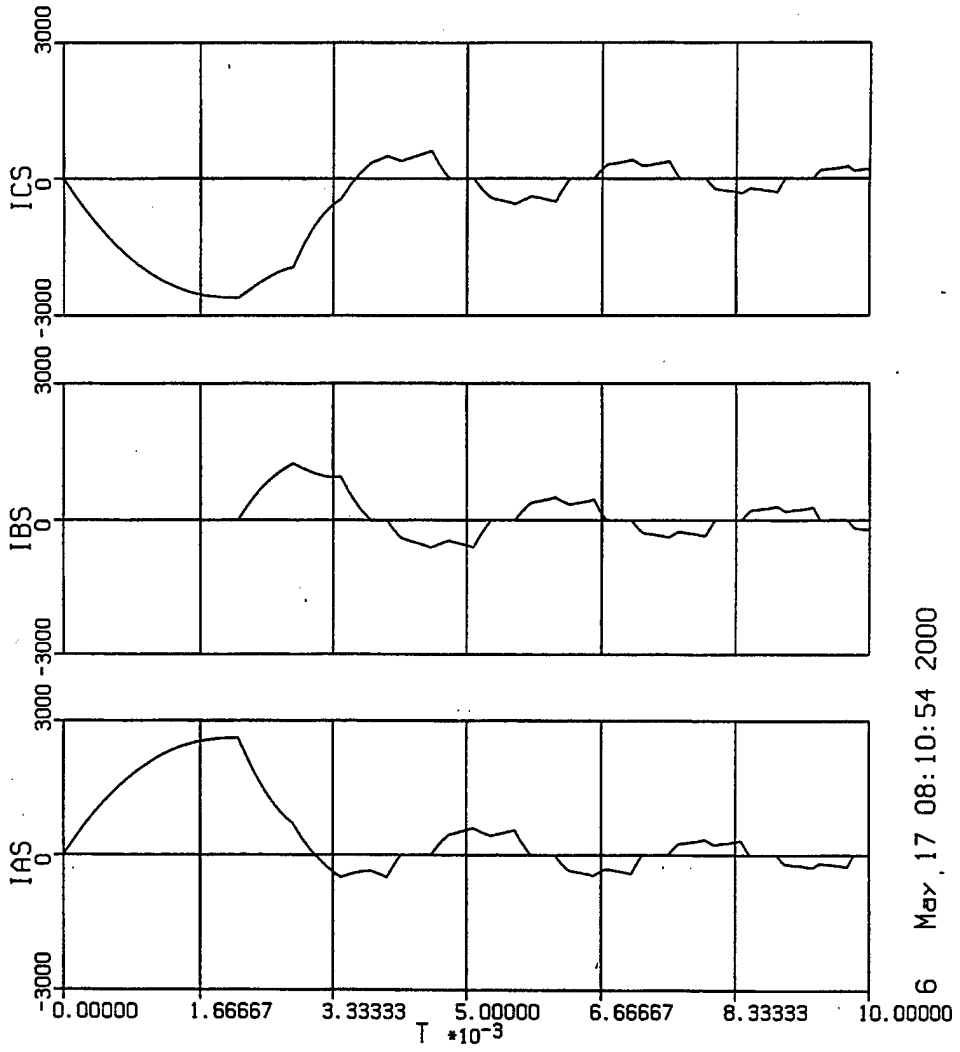

Figure 5-5, NBC Fan Model Plot with 120°
Discontinuous-Current Inverter.

Figure 5-6 illustrates a complete startup to steady state and documents ω_{rm} – rotor speed in rads/s, T_e – electromagnetic torque in Newton-meters, i_{as} - stator current in Amps, and i_{ii} – inverter current in Amps.

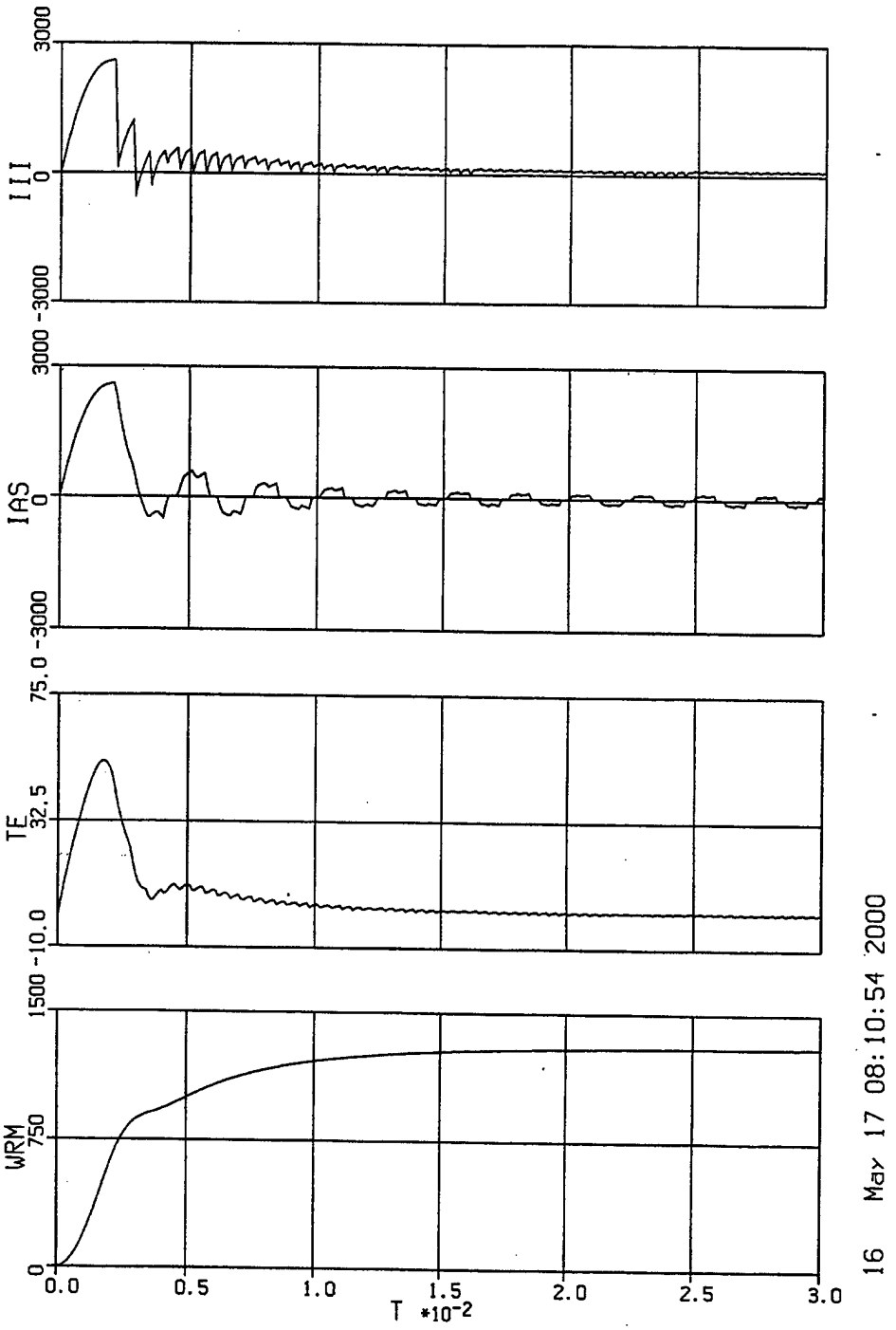

Figure 5-6, Plot of Start-up of NBC Fan Model with 120° Discontinuous-Current Inverter.

Figure 5-7 shows two cycles of the steady-state variables: v_{as} - stator voltage in Volts, i_{as} - stator current in Amps, and i_{ii} – inverter current in Amps, T_e – electromagnetic torque in Newton-meters, and ω_{rm} – rotor speed in rads/s. The inverter current once again exhibits a $6\omega_r$ fundamental variation, but it clearly has a different harmonic content than in the 180^o model. The a-phase terminal voltage closely resembles the back emf as it should with the quasi-rectangular phase current waveforms. The a-phase stator current has a peak value of about 120A, inline with what the manufacturer data predicted.

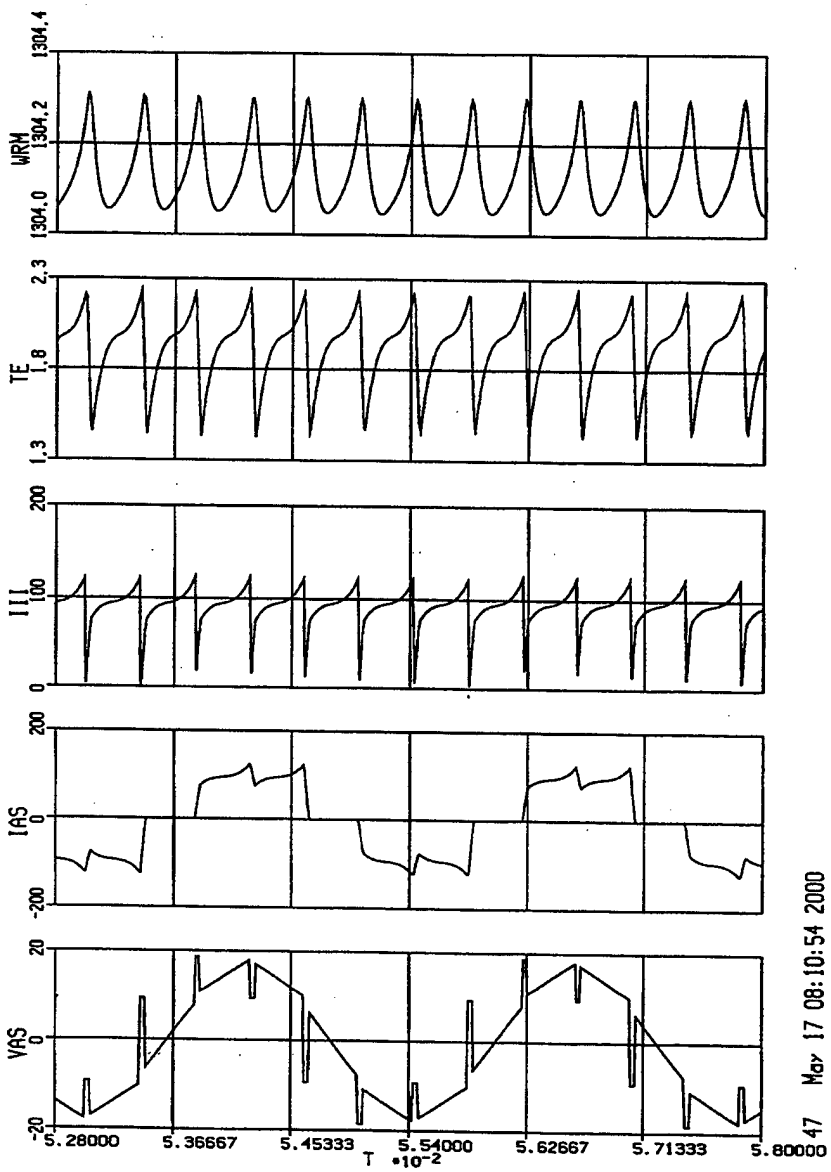

Figure 5-7, Plot of the Steady State of NBC Fan Model with 120° Discontinuous-Current Inverter.

The simulation of the NBC fan model with 180° continuous-current inverter was run again using the parameters in Table 5.2 to illustrate the effect of varying λ'_m. The

results can be found in Appendix C. Also, the simulation of the NBC fan model with 120° discontinuous-current inverter was run again using the parameters in Table 5.1 to illustrate the effect of changing λ_m'. The results can be found in Appendix D.

After successful implementation of the NBC fan model with 120° discontinuous-current inverter with a known rotor position, work began on implementing sensorless control of the motor. In order to accomplish this the open-circuit voltage signal would need to be processed into a signal that could be utilized to gate transistors T_1 through T_6 as discussed in Chapter IV, paragraph C, subsection 3d. Figure 5-8 depicts the signal processing block diagram that was implemented in order to process the open-circuit voltage.

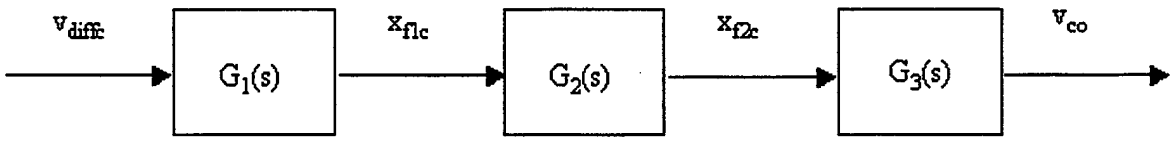

Figure 5-8, Open-Circuit Voltage Signal Processing Block Diagram.

$$G_1(s) = \frac{\omega_c}{s + \omega_c} \tag{5-7}$$

$$G_2(s) = \frac{\alpha}{s} \tag{5-8}$$

$$G_3(s) = \frac{\tau s}{\tau s + 1} \tag{5-9}$$

where $\omega_c = 10{,}000$, $\alpha = 2500$, $\tau = 0.004$.

G_1, a low-pass filter, smoothes out the choppy terminal voltage waveform (v_{diffc}). G_2, an integrator, introduces a 90° phase shift. G_3 serves to block any dc component that may be introduced when the integrator starts. The zero-crossings of v_{co} (together with analogous v_{ao} and v_{bo} signals from phase A and B) may be used for gating $T_1 - T_6$. Figure 5-9 documents the start-up to steady-state waveforms from the block diagram with the machine operating with rotor position feedback. In Figure 5-9 the integrator is disabled until near the first peak of v_{diffc}. This ensures that x_{f2c} does not have a large dc offset that would then need to settle out. Figure 5-10 documents the steady-state waveforms from the block diagram with the machine operating with rotor position feedback. The 90° phase shift between v_{diffc} (and x_{f1c}) and x_{f2c} (and v_{co}) is readily apparent.

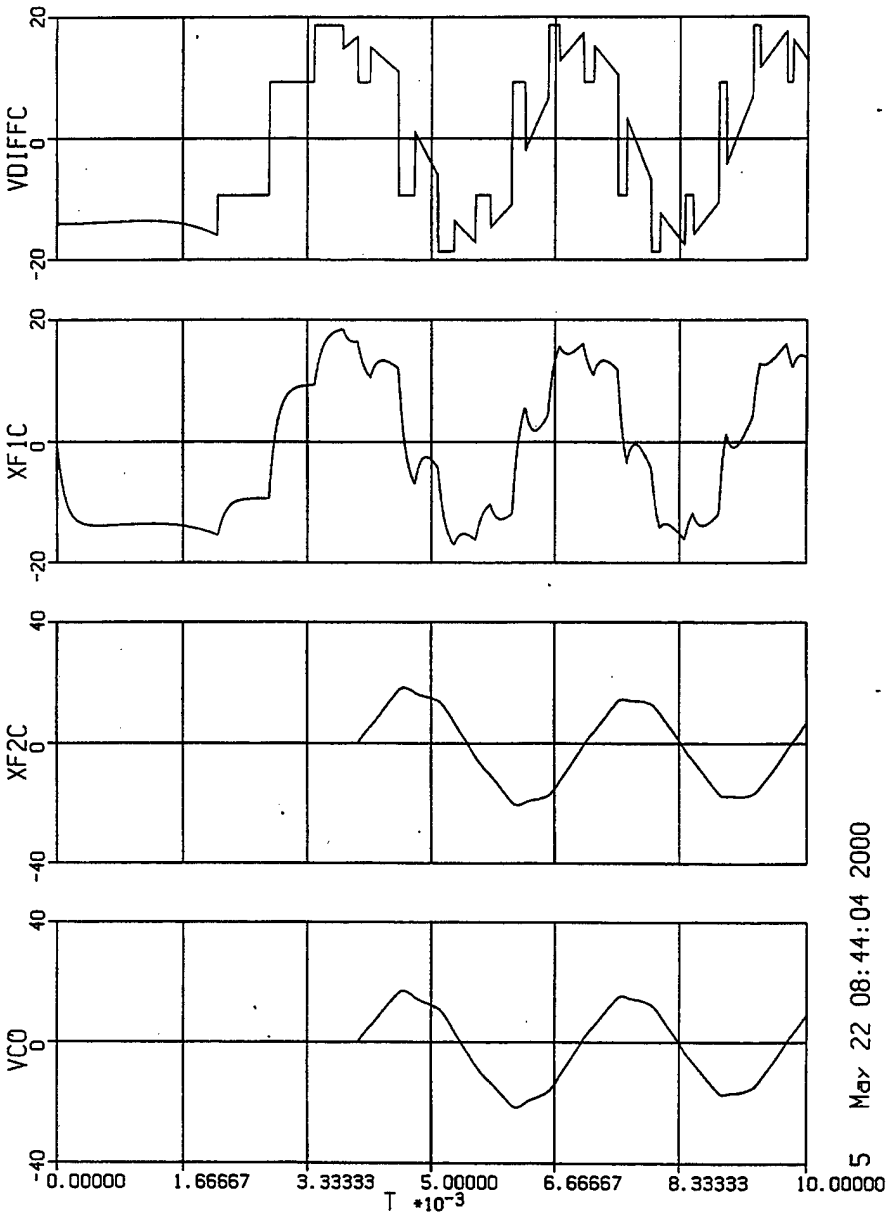

Figure 5-9, Plot of the Start-Up of NBC Fan Model with 120° Discontinuous-Current Inverter.

The logical statements required to transition to sensorless operation are illustrated below.

```
IF ((vco .LT. 0.0) .AND. (vbo .LT. 0.0)) THEN
        T1a = .FALSE.
        T2a = .TRUE.
        T3a = .TRUE.
        T4a = .FALSE.
        T5a = .FALSE.
        T6a = .FALSE.
ELSEIF ((vbo .GT. 0.0) .AND. (vao .GT. 0.0)) THEN
        T1a = .FALSE.
        T2a = .FALSE.
        T3a = .TRUE.
        T4a = .TRUE.
        T5a = .FALSE.
        T6a = .FALSE.
ELSEIF ((vao .LT. 0.0) .AND. (vco .LT. 0.0)) THEN
        T1a = .FALSE.
        T2a = .FALSE.
        T3a = .FALSE.
        T4a = .TRUE.
        T5a = .TRUE.
        T6a = .FALSE.
ELSEIF ((vco .GT. 0.0) .AND. (vbo .GT. 0.0)) THEN
        T1a = .FALSE.
        T2a = .FALSE.
        T3a = .FALSE.
        T4a = .FALSE.
        T5a = .TRUE.
        T6a = .TRUE.
ELSEIF ((vbo .LT. 0.0) .AND. (vao .LT. 0.0)) THEN
        T1a = .TRUE.
        T2a = .FALSE.
        T3a = .FALSE.
        T4a = .FALSE.
        T5a = .FALSE.
        T6a = .TRUE.
ELSEIF ((vao .GT. 0.0) .AND. (vco .GT. 0.0)) THEN
        T1a = .TRUE.
        T2a = .TRUE.
        T3a = .FALSE.
        T4a = .FALSE.
        T5a = .FALSE.
        T6a = .FALSE.
ENDIF
```

Details for the entire simulation are documented in Appendix B.

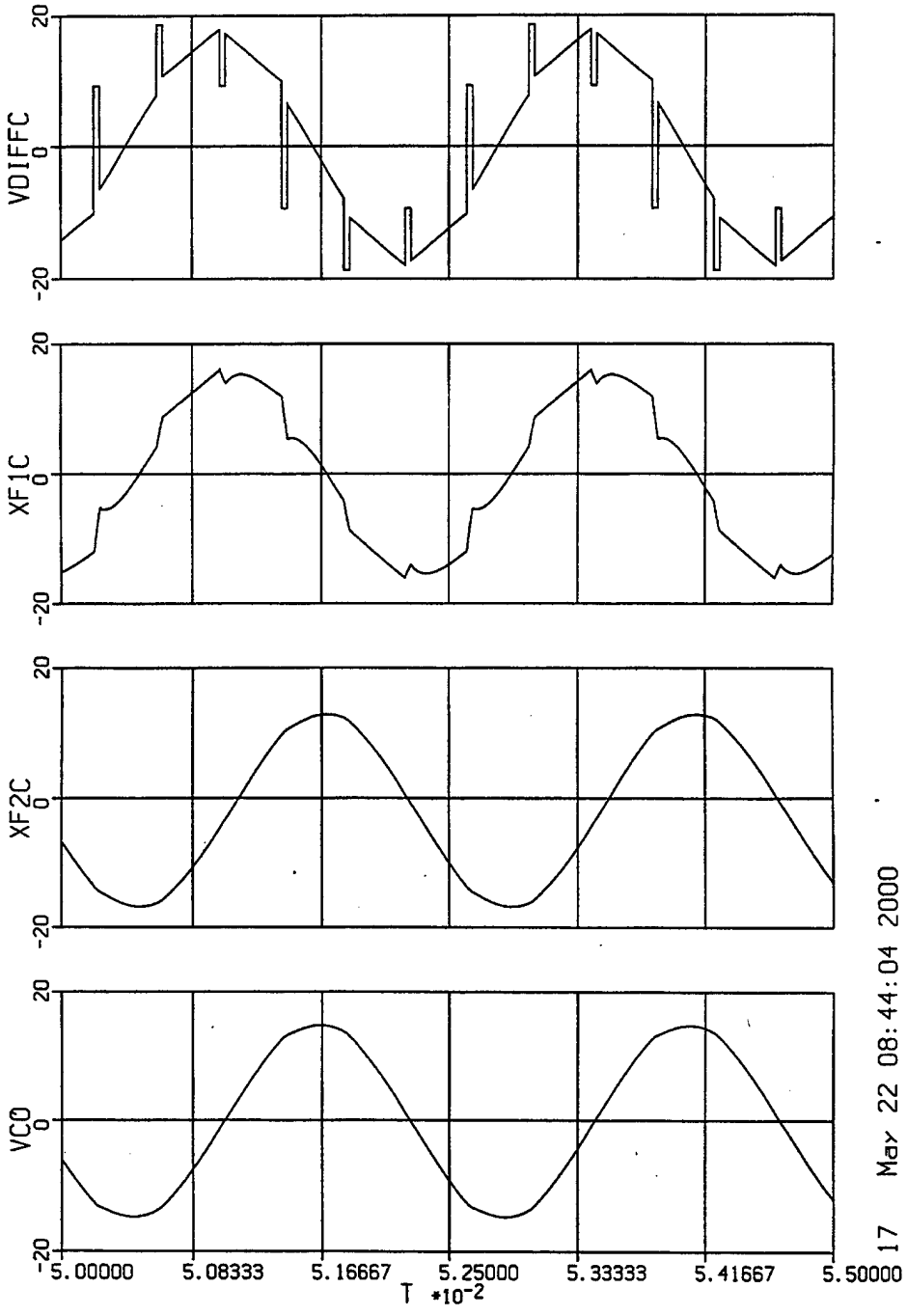

Figure 5-10, Steady-State Waveforms From Block Diagram with the Machine Operating with Rotor Position Feedback.

The following simulation study was conducted to verify the feasibility of sensorless operation. Rotor position information was used to start the machine (no back-emf voltages are initially available). At t=0.05, Figures 5-11 through 5-12 illustrate the signals derived from the actual rotor position information (T_{1a} through T_{6a}). Clearly the signals T_{1a} through T_{6a} are very nearly in phase with T_1 through T_6, respectively, and can be used to gate the transistors. Figure 5-14 depicts transitioning from using the rotor feedback signals to using the sensorless derived signals. The rotor maintains synchronism, with only a small drop in speed.

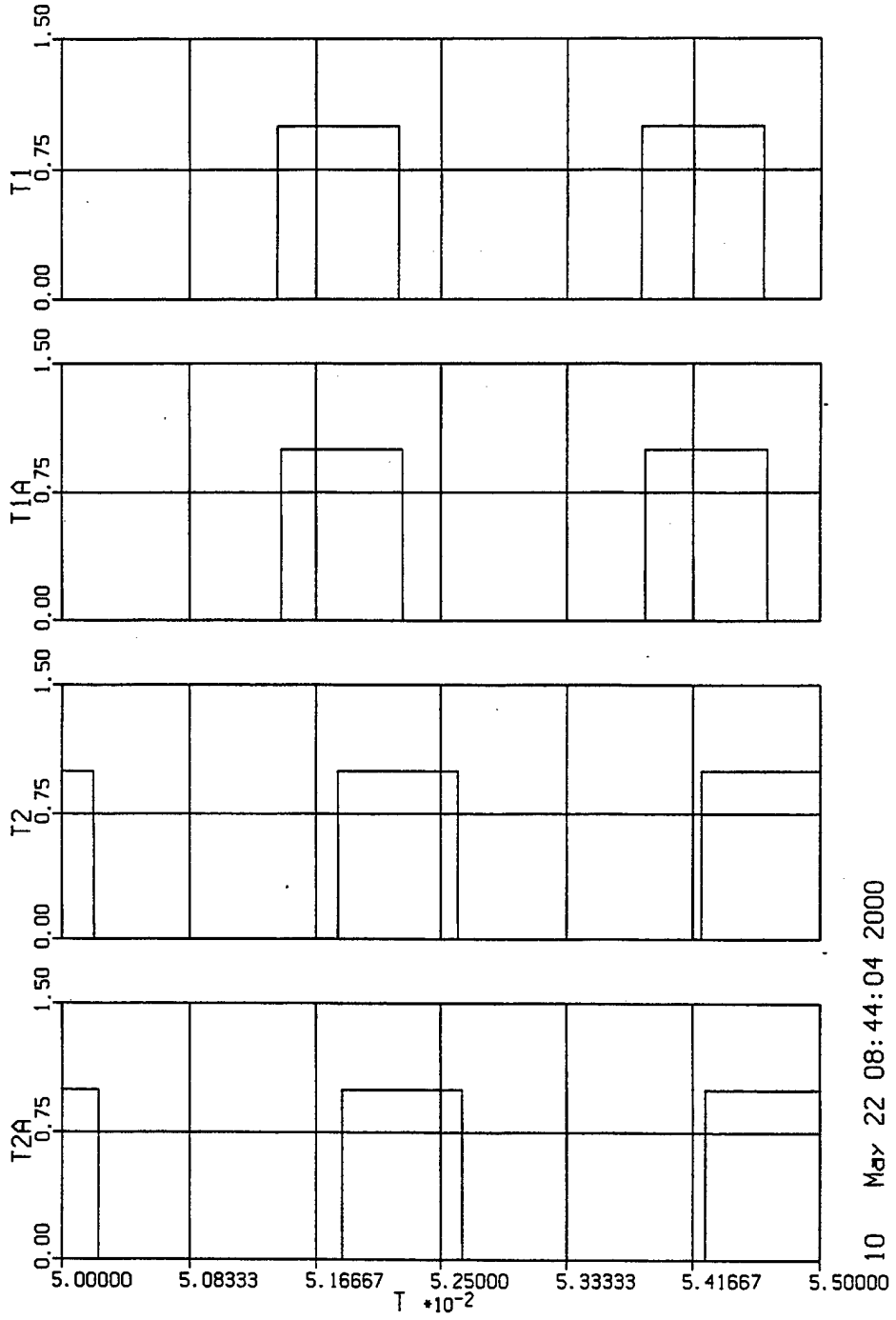

Figure 5-11, Plot of the Switching Signals of NBC Fan Model with 120° Discontinuous-Current Inverter.

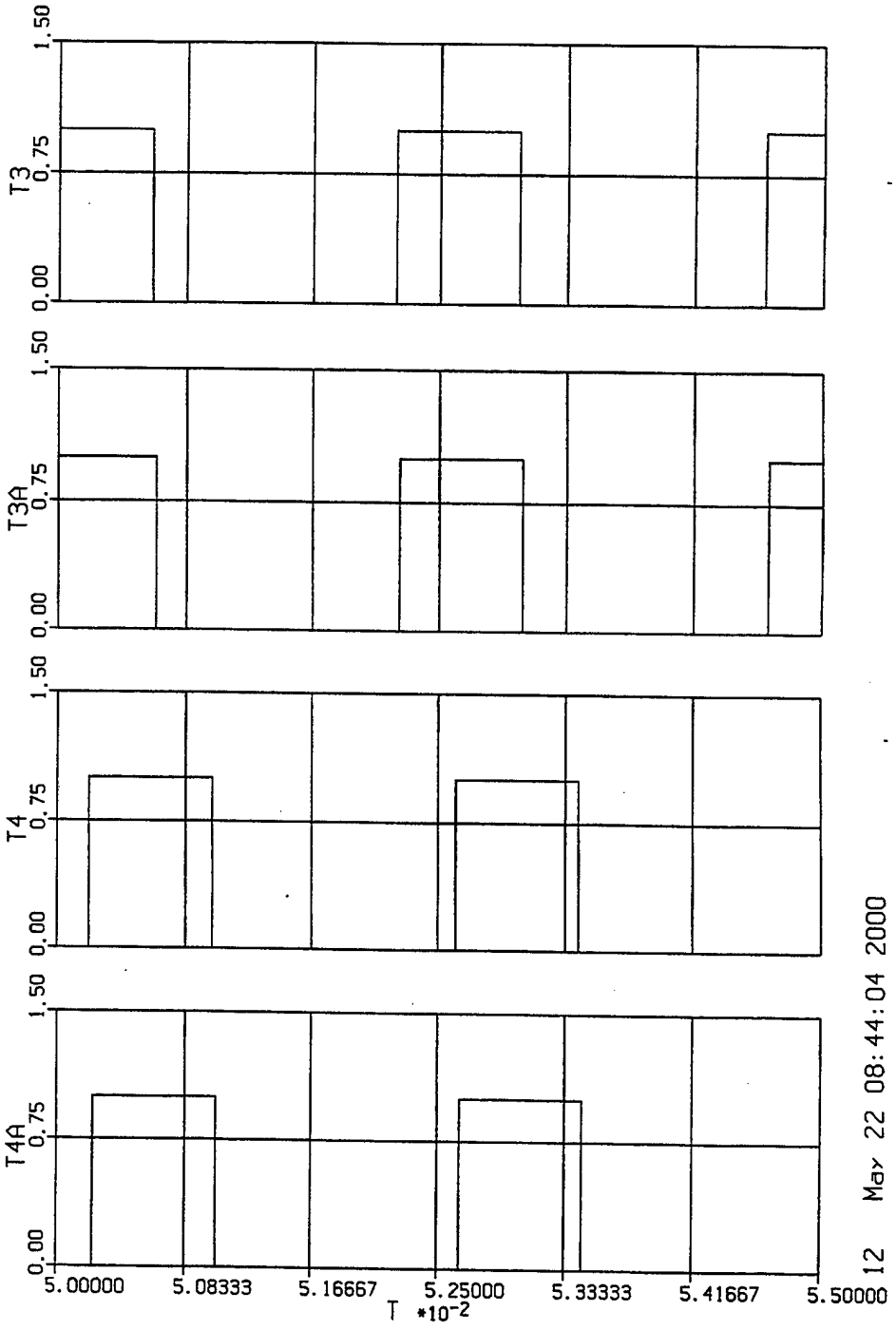

Figure 5-12, Plot of the Switching Signals of NBC Fan Model with 120° Discontinuous-Current Inverter.

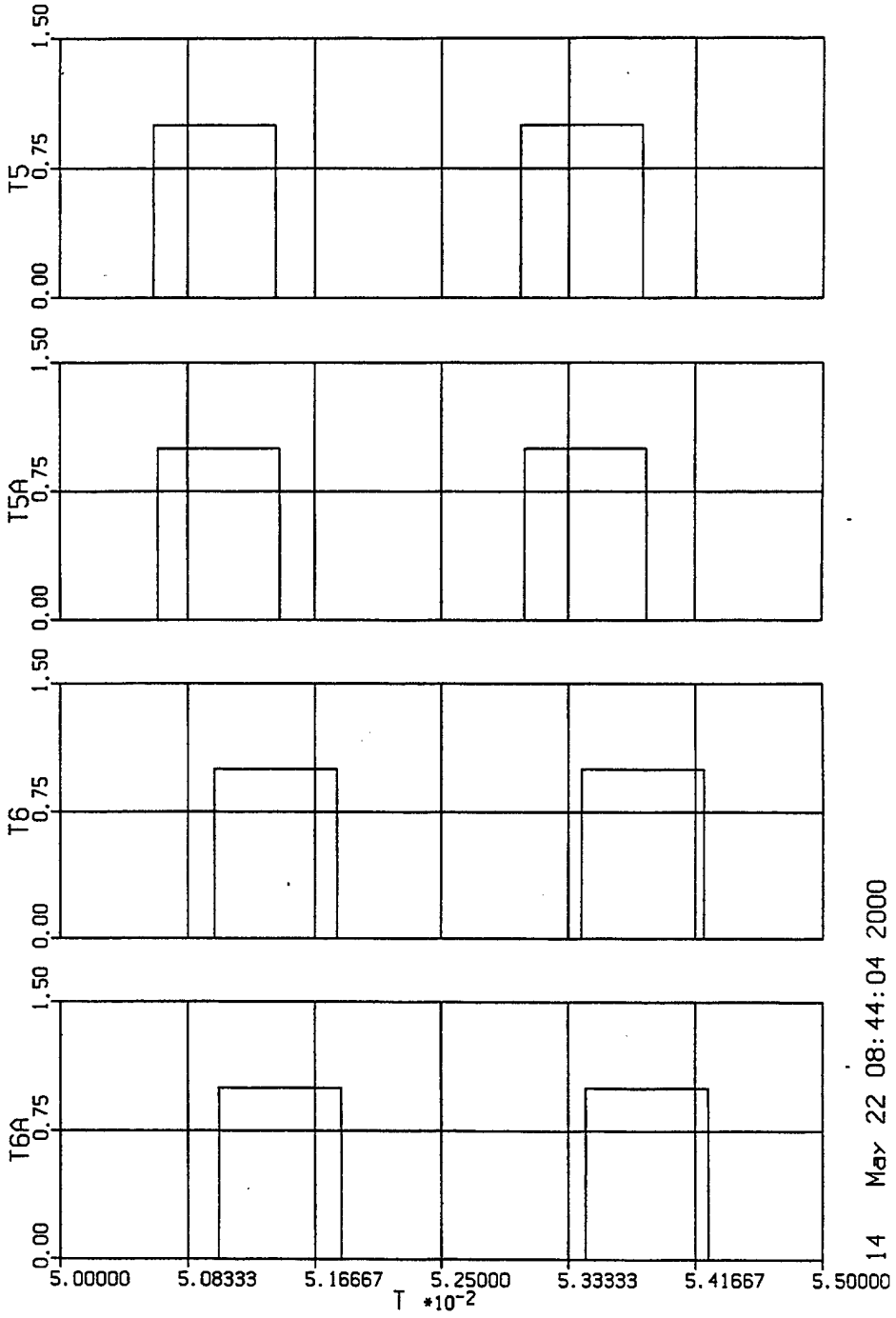

Figure 5-13, Plot of the Switching Signals of NBC Fan Model with 120° Discontinuous-Current Inverter.

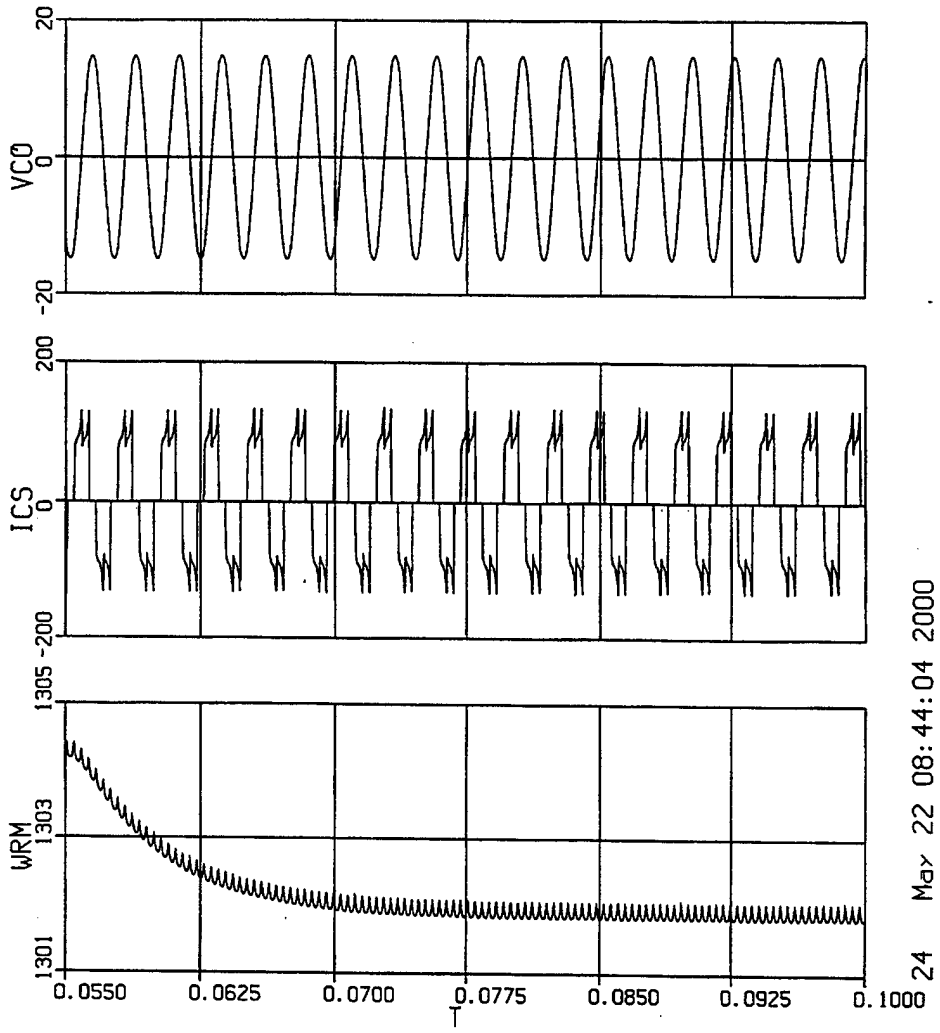

Figure 5-14, Plot of the Rotor Feedback Signals and the Sensorless Derived Signals.

While the model introduced does implement sensorless control with good results, the problem of transitioning to sensorless control from rotor position feedback must still be resolved. This transition is an area that can be addressed in future wok.

C. Ultra Capacitor Model

Pinnacle Research Institute, Inc. provided tabular data on their 100V, 1F, 5000J Ultra-Capacitor. The manufacturer's measured data was entered into a MATLAB file, ultracap.m. This file is included as Appendix C. The following plot illustrates the manufacturer's measured impedance versus frequency data.

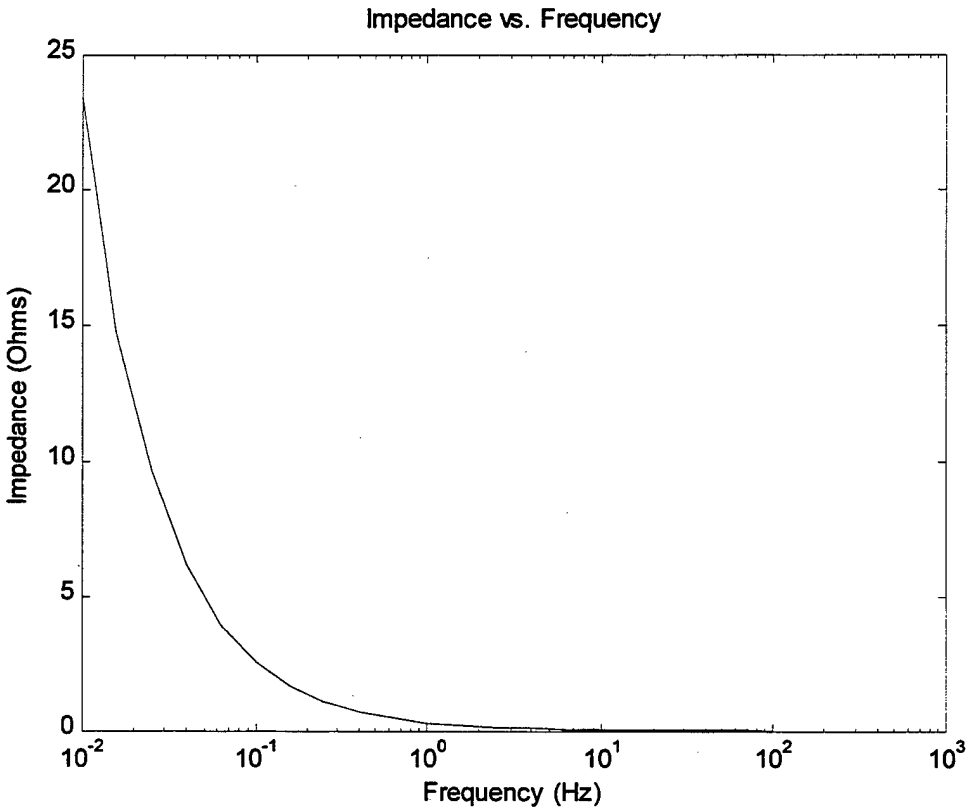

Figure 5-15, Ultra Capacitor Impedance vs. Frequency
(Manufacturer's Measured Data).

A computer model of the ultra capacitor would need to produce comparable results when exercised over the same frequency range. An attempt to duplicate the actual results would be initiated using an equivalent series resistance (ESR) as in Figure 5-16.

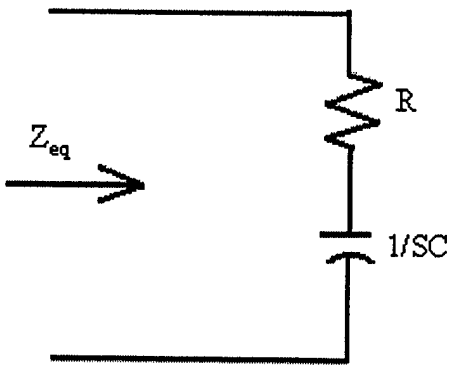

Figure 5-16, ESR Circuit Diagram.

The input impedance of the circuit is found by inspection to be

$$Z_{eq} = \left(R + \frac{1}{SC} \right) \tag{5.10}$$

which can be rewritten as

$$Z_{eq} = \left(\frac{R\left(S + \frac{1}{RC} \right)}{S} \right) \tag{5.11}$$

An initial guess for the constants R and 1/RC was formulated using the PRI, Inc. frequency response data. After many iterations of manipulating these constants the following plot of impedance vs. frequency was achieved.

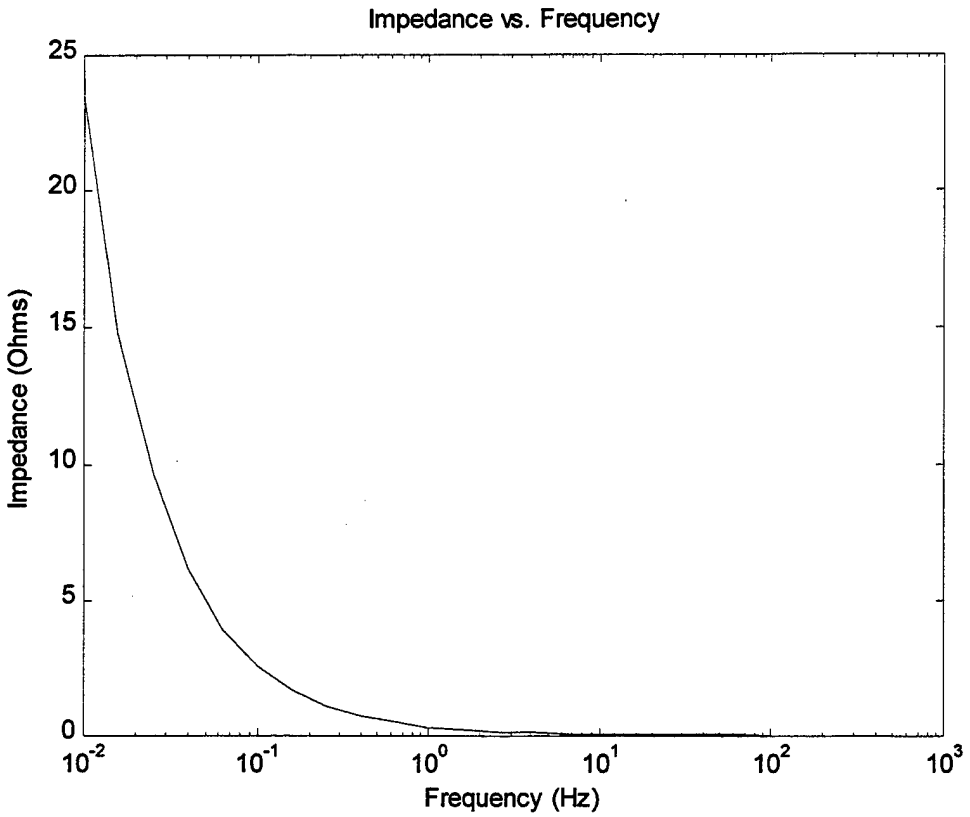

Figure 5-17, Ultra Capacitor Impedance vs. Frequency (Model).

Figure 5-18 illustrates both actual data points and model generated data and confirms that the model is valid as a reasonable representation of the actual ultra capacitor.

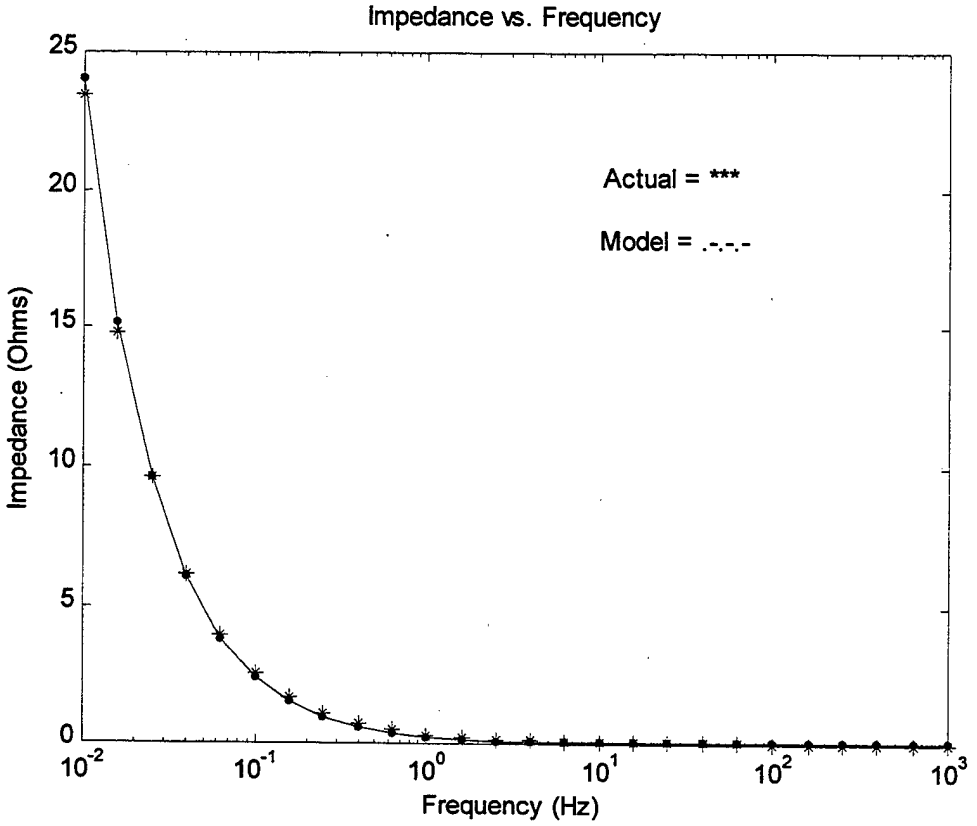

Figure 5-18, Ultra Capacitor Impedance vs. Frequency (Actual and Model).

The constants R and $\frac{1}{RC}$ were found to be:

$$R = 0.045 \text{ ohms} \tag{5.12}$$

$$\frac{1}{RC} = 5.35 \text{ s}^{-1} \tag{5.13}$$

and the transfer function representation for the ultra capacitor would be characterized as

$$Z_{eq} = \frac{0.045(S + 5.35)}{S} \tag{5.14}$$

D. Battery Model

The AAAV electrical system consists of two battery banks, one connected to the Vetronics bus and the other to the Auxiliary bus. The bank connected to the Vetronics bus consists of two series connected 12-Volt (nominal) batteries. The bank connected to the auxiliary bus consists of three parallel branches with two series-connected 12-Volt batteries per branch. In the current Purdue Distributed Computing AAAV system representation, the batteries are modeled as a Thevenin equivalent circuit, where the open-circuit voltage and the Thevenin resistance can be adjusted to correspond to the chemical and thermodynamic state of the battery. The resulting circuit diagram is shown in Figure 5-19. The associated parameters are summarized in Table 5.3. In Figure 5-19, S_1, S_2, and S_3 are closed for starting. After start-up S_2 and S_3 are opened, and S_1 is left closed during operation.

When no battery is connected to the Vetronics bus, a bus voltage oscillation was observed. The stiffening action of the battery seems to mitigate this instability. It is hypothesized that the oscillation is due to a limit cycle imposed by the generator voltage regulator, particularly at low power.

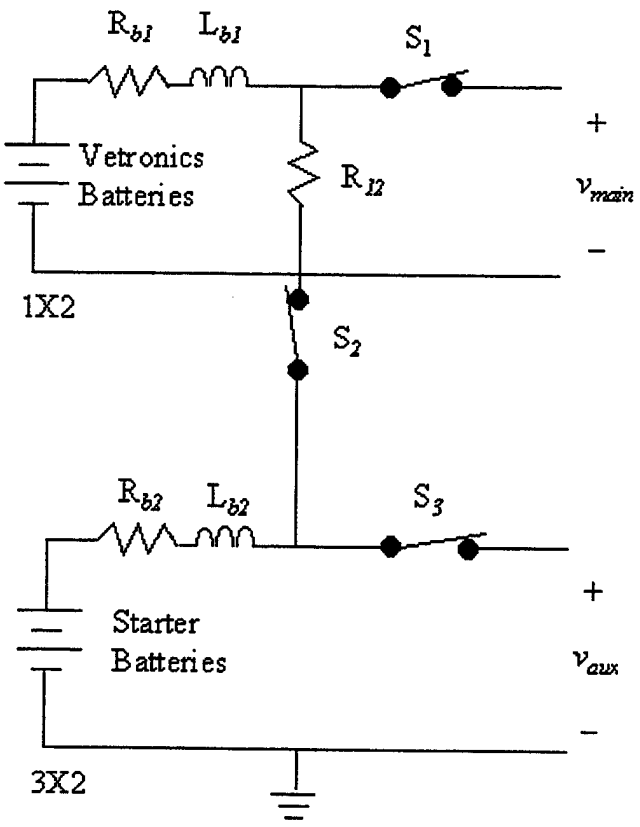

Figure 5-19, Circuit Diagram of Battery Banks.

Symbol	Description	Value	Origin
R_{b1}	Vetronics bus battery series resistance	0.007648 Ω	Calculated using charge/discharge data
R_{b2}	Auxiliary bus battery series resistance	0.00255 Ω	Calculated using charge/discharge data
R_{12}	Resistance of cable between main and auxiliary buses	0.0002 Ω	Estimated
L_{b1}	Vetronics bus battery series inductance	1.0 μH	Estimated
L_{b2}	Auxiliary bus battery series inductance	1.0 μH	Estimated

Table 5.3, Battery Parameters.

The model of Figure 5.19 is preliminary and further laboratory testing has been conducted on the 800U Optima battery. Of particular interest was the battery's frequency response at various levels of charge. The circuit shown in Figure 5.20 was constructed and the parameters for the test circuit are summarized in Table 5.4. The purpose of R_1 is to establish a quiescent load condition on the battery. Transistor Q_1 is gated at the user-specified frequency, with a 50% duty cycle. With R_2 larger than R_1, switching Q_1 results in a smaller rectangular sink of current from the battery. Therefore, i_{term} consists of a steady-state dc level with a small rectangular ripple. This AC component of current flows through the battery resulting in an AC component of voltage across the battery (v_{term}). Therefore, if the assumed internal battery model is that given by Figure 5-21, the AC component of the measured voltage will facilitate the calculation of the impedance given by r_{batt} and L_{batt}. The current was monitored with a Tektronix, 8-Amp, clamp-on, current probe, while the terminal voltage was monitored with a direct connection to the oscilloscope and with a digital handheld multi-meter. Both signals were displayed on a Tektronix, 60 MHz, digital storage oscilloscope. The ratio of the amplitudes of the ripples in v_{term} and i_{term} provides a measure of the impedance magnitude, while the phase angle (θ) between those signals relates how the impedance divides between real and reactive components. Figure 5-21 reflects the assumed internal battery representation.

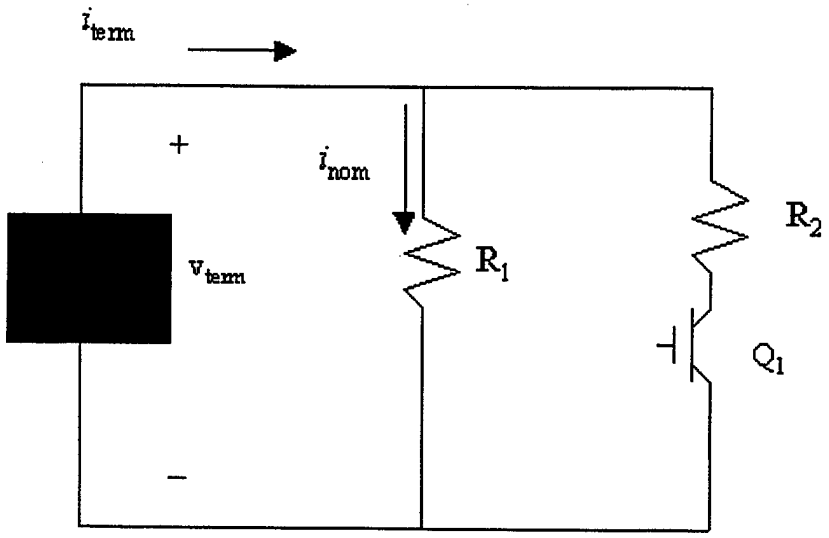

Figure 5.20, Circuit Diagram for Optima Battery Frequency Response Test.

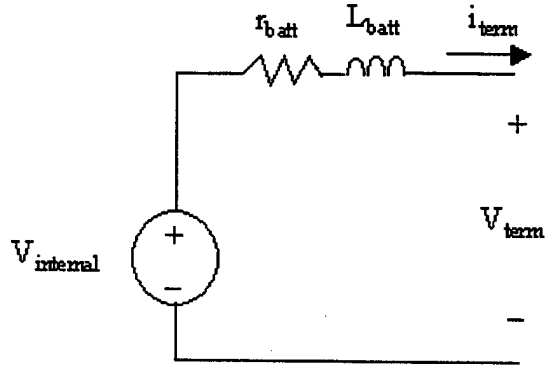

Figure 5-21, Assumed Internal Battery Representation.

Symbol	Description	Measured Value	General Information
R_1	Ceramic Resistor	4.0 Ω	4 X 16 Ω resistors in parallel, 10 W each
R_2	Carbon Resistor	40.1 Ω	(1) 39 Ω
Q_1	Power MOSFET (2N6796)		8.0 A, 100 V
	Optima 800U Battery	12.8	56 A-hr

Table 5.4, Test Circuit Parameters.

Testing was conducted at frequencies of 20 Hz to 20 kHz. The upper end of 20kHz was deemed sufficient since the ripple frequency out of the 12-pulse generator/rectifier is less than 20 kHz. The testing was conducted at three different charge states, (100%, 75%, and 50%). The charge state of the battery is determined using the manufacturer supplied capacity of 56 A-hr. Full battery specifications are provided in the Manufacturer Data Sheet listed in Appendix F. Given that

$$1\,A-hr = 1\frac{C}{s} X\ 3600\ s = 3600\,C, \tag{5.15}$$

the stored charge (q_{stored}) is determined as

$$q_{stored} = 56\,A-hr\ X\ 3600\frac{C}{A-hr} = 201{,}600\,C\ . \tag{5.16}$$

Since charge is related to current by

$$q = \int_0^t i\, dt\ , \tag{5-17}$$

then for constant current (I), equation (5-17) becomes

$$q = I\ \Delta t \tag{5.18}$$

By drawing a fixed current (I) over a specific time interval (Δt), the amount of charge left in the battery can be estimated.

Initial test results of the battery at full charge, V = 12.8 Volts, I =3.5A, and f = 2kHz are depicted in Figure 5-22.

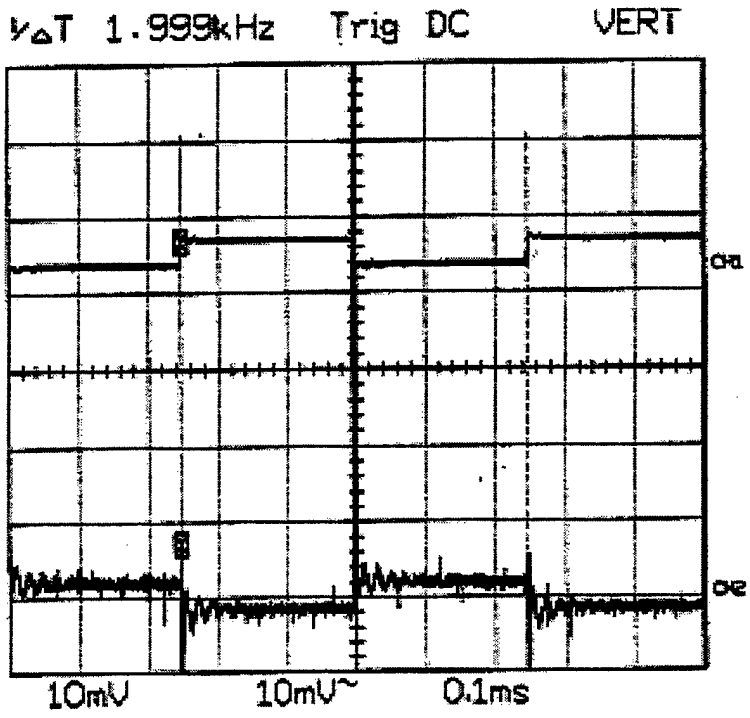

Figure 5-22, Test Results with Battery at Full Charge,
V = 12.8 Volts, I =3.5A, and f = 2kHz
CH1 = current (1Amp/div), CH2 = voltage (1Volt/div).

The plot reveals $\tilde{V}$ (mV_{pp}) = 3.0, $\tilde{I}$ (mA_{pp}) = 310, θ (rads), = π, giving an internal resistance, R (mΩ) = 9.67, and internal inductance, L (mH) = 0.0.

The battery was then drained at a current level of approximately 15.5A for 52 minutes to arrive at a charge state of about 75% rated. At 75% charge test results of the battery with V = 11.9 Volts, I =3.3A, and f = 2kHz are depicted in Figure 5-23.

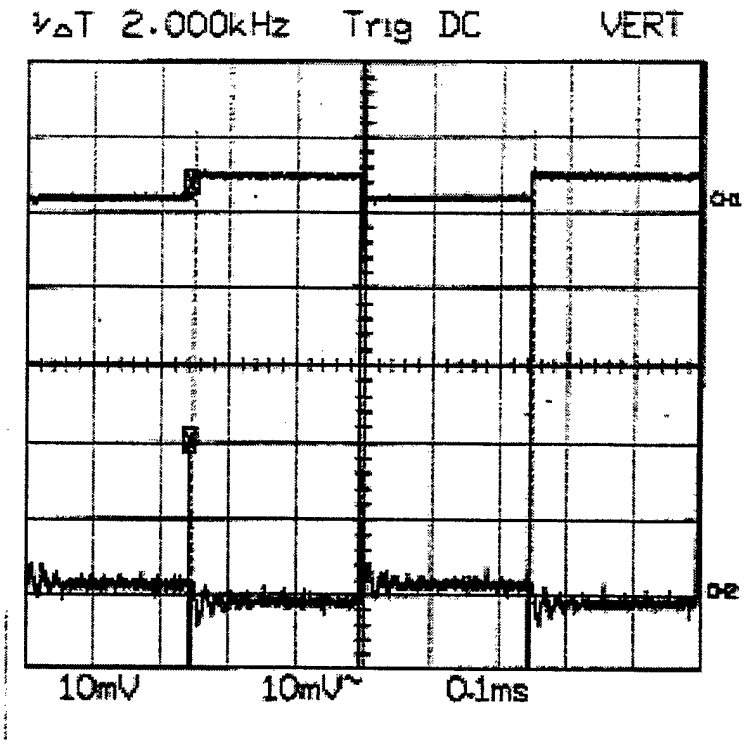

Figure 5-23, Test Results with Battery at 75% Charge,
V = 11.9 Volts, I =3.3A, and f = 2kHz
CH1 = current (1Amp/div), CH2 = voltage (1Volt/div).

The plot reveals $\tilde{V}$ (mV_{pp}) = 2.5, $\tilde{I}$ (mA_{pp}) = 300, θ (rads), = π, giving an internal resistance, R (mΩ) = 8.33, and internal inductance, L (mH) = 0.0.

The battery was then drained at a current level of approximately 15A for 55 minutes to arrive at a charge state of about 50% rated. At 50% charge test results of the battery with, V = 11.8 Volts, I =3.25A, and f = 2kHz are depicted in Figure 5-24.

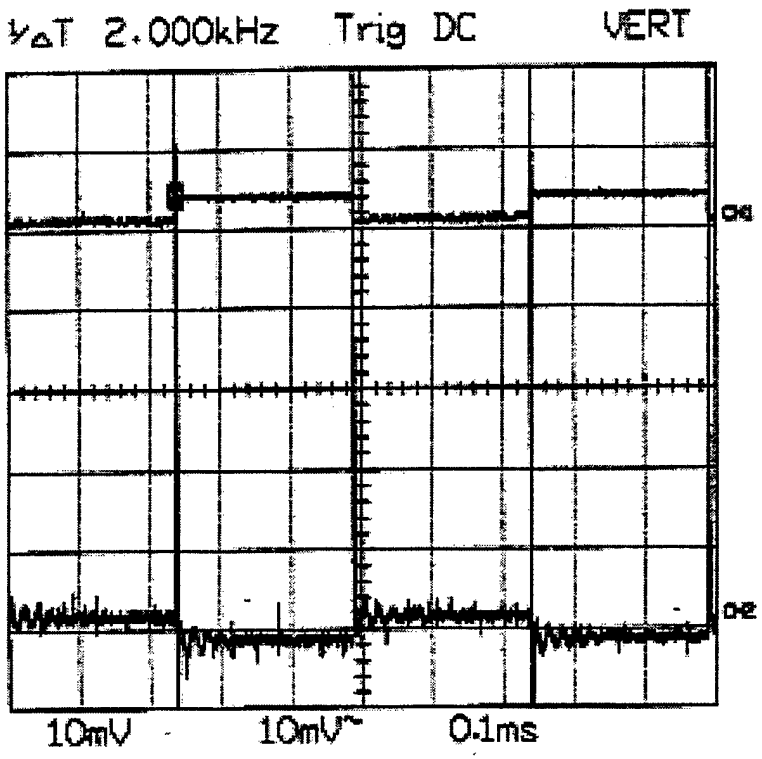

Figure 5-24, Test Results with Battery at 50% Charge,
V = 11.8 Volts, I =3.25A, and f = 2kHz
CH1 = current (1Amp/div), CH2 = voltage (1Volt/div).

The plot reveals $\tilde{V}$ (mV_{pp}) = 2.7, $\tilde{I}$ (mA_{pp}) = 290, θ (rads), = π, giving an internal resistance, R (mΩ) = 9.31, and internal inductance, L (mH) = 0.0.

Complete laboratory test results for all frequencies are summarized in Table 5.5.

	100% Charge					75% Charge					50% Charge				
f	$\tilde{V}$ mV_{pp}	$\tilde{I}$ mA_{pp}	θ rad	**R** mΩ	**L** mH	$\tilde{V}$ mV_{pp}	$\tilde{I}$ mA_{pp}	θ rad	**R** mΩ	**L** mH	$\tilde{V}$ mV_{pp}	$\tilde{I}$ mA_{pp}	θ rad	**R** mΩ	**L** mH
20 Hz	3.1	310	π	10.0	0.0	2.5	260	π	9.62	0.0	2.8	280	π	10.0	0.0
200 Hz	2.9	300	π	9.67	0.0	2.5	300	π	8.33	0.0	2.7	280	π	9.64	0.0
2 kHz	3.0	310	π	9.67	0.0	2.5	300	π	8.33	0.0	2.7	290	π	9.31	0.0
20 kHz	3.5	370	π	9.46	0.0	2.8	320	π	8.75	0.0	2.9	310	π	9.35	0.0

Table 5.5, Laboratory Test Results.

Test results conclude that the internal resistance of the battery does exhibit a small change as a result of frequency and charge-state of the battery. Further, tests conclude that the internal inductance of the battery is negligibly small. It appears reasonable that the battery can be adequately represented by an equation of the form

$$v_{term} = v_{\text{int}} - r_{batt} i_{term} \tag{5-19}$$

If v_{term} is the same as the bus voltage and it is a state variable then

$$i_{term} = \frac{v_{\text{int}} - v_{bus}}{r_{batt}} \tag{5-20}$$

where i_{term} is then available to evaluate the derivative of the bus voltage.

VI. CONCLUSION

A. Synopsis of Work Completed

1. Introduction

The Advanced Amphibious Assault Vehicle (AAAV) was introduced and a general system description was set forth. The introduction and description are critical to understanding where and how the AAAV fits into the Marine Corps amphibious triad (AAAV, V-22, LCAC) to execute the concepts of Operational Maneuver from the Sea and Ship to Objective Maneuver. The AAAV's operating modes and associated mode characteristics were also documented and developed.

2. Electrical System Architecture

The entire electrical system architecture is introduced in block diagram form and the system's primary components are listed and discussed. A discussion on the theory behind distributed computing techniques through networking is included. This technique is the foundation of P. C. Krause and Associates' troubleshooting tool that can be used by the Marine Corps in addressing current electrical system issues that must be resolved. An Advanced Continuous Simulation Language (ACSL) background is included. This software is used in this research to model and simulate various components of the electrical system.

3. Candidate Electrical System Architecture

From the entire electrical system architecture, a scaled down candidate system architecture is developed. Components from the candidate system are tested, modeled, simulated, and validated. The Nuclear, Biological, and Chemical (NBC) fan/filter motor drive, an ultra capacitor, and a battery unit are the components selected for research in this document.

4. NBC Fan/Filter Motor Drive

A simulation of the NBC fan motor drive with a 180° continuous-current inverter using Hall-effect sensors to detect rotor position was modeled in ACSL. The simulation allowed for a thorough understanding of the inverter and motor assembly, and also served as a tool for gaining an understanding of ACSL simulations and representative signal waveforms.

Efforts then shifted to implementing a NBC fan motor drive model with the 120° discontinuous-current inverter based on sensorless control. This model was achieved in two stages. First, the 120° discontinuous-current inverter model was developed assuming the availability of rotor position. The second step was to incorporate sensorless control into the simulation. This was achieved by indirectly sensing the rotor position using the back emf of the motor. The switching sequence for commutation of the transistors in the inverter was established using this back emf. The results were consistent with theoretical expectations ensuring this model was a valid representation of the NBC fan motor and inverter assembly.

5. Ultra Capacitor

Tabular data was collected from Pinnacle Research Institute Inc., on the 100V, 1F, 5000J, ultra capacitor. This data was analyzed and plotted using MATLAB and an impedance vs. frequency plot was developed. An attempt to duplicate this plot using a model with an equivalent series resistance (ESR) was initiated. A transfer function was developed and an initial guess was made for constants. By manipulating the transfer function constants, an impedance vs. frequency plot matching that plot from the manufacturer's data was achieved.

6. Battery Unit

The area of concern for the battery unit was its frequency response characteristics at different charge states. A test circuit was constructed that would load the battery drawing a constant DC level of current and an AC component of current. The current and the voltage levels were displayed on an oscilloscope and monitored. From the steady-state and ripple current and voltage waveforms, an internal impedance was calculated. These tests were conducted at three charge states (100%, 75%, and 50%) of the battery over a frequency range of 20 Hz to 20 kHz. The upper frequency level of 20 kHz was based on the ripple frequency of the 12-pulse generator/rectifier. Test results concluded that the internal impedance of the battery was almost purely resistive with a negligibly small internal inductance. Further, tests concluded that the internal resistance of the battery did fluctuate as a result of charge state and frequency.

B. DOD Relevance

The AAAV will join the Marine Corps inventory to complete the amphibious triad which also includes the V-22 Osprey, tilt-rotor aircraft, and the Landing Craft, Air Cushion (LCAC). The AAAV will provide the principal means of water mobility, land mobility, and direct fire support to Marine Corps infantry units.

As the AAAV travels through its prototyping stage in an effort to successfully pass its operational testing, electrical system issues and problems have arisen which must be addressed before entering into full-scale production. Computer simulation of the electrical system will facilitate the analysis and evaluation of hardware design prior to and in concert with actual production. Accurate simulation will provide invaluable insight into design flaws or system limitations before extensive capital investments are made on hardware.

C. Further Work

Complete simulation for the AAAV's entire electrical system is the next step in providing the Marine Corps with a tool where by it can successfully analyze and evaluate the system. Once a complete and accurate representative model exists, a distributed computing network must be established in order to exercise the entire model. Funding for such a network at NPS has not yet been obtained and a future researcher may be able to pursue possible avenues for funding.

Other research that can begin now includes a paralleling strategy for the auxiliary generator. The current auxiliary generator is incapable of supporting predicted power

requirements. Finally, research could be initiated in an attempt to resolve instability problems in the electrical system during low power operation. General Dynamic's engineers recently discovered low power instability problems during prototype testing.

THIS PAGE INTENTIONALLY LEFT BLANK

APPENDIX A. [ACSL CODE FOR NBC FAN MODEL WITH 180° INVERTER]

```
PROGRAM  NBC Fan Model w/ 180 Degree Inverter

INITIAL

        MAXTERVAL maxt = 1.0e-6

        MINTERVAL mint = 1.0e-7

        CINTERVAL cint = 1.0e-4

        ALGORITHM ialg = 5

        CONSTANT tstop = 0.165


        "---initial circuit constants---"


        CONSTANT rL=0.01
        CONSTANT LL=.000001
        CONSTANT Cdc=.036
        CONSTANT Vdc=28.0

        LOGICAL SA
        LOGICAL SB
        LOGICAL SC

        "----switch initial conditions----"

        SA = .false.
        SB = .false.
        SC = .false.

        END  ! "of initial"

DYNAMIC

        TERMT (t .GE. tstop)

  DERIVATIVE

        !"Switch Status Generation"

        CONSTANT pi=3.14159265
        twopi = 2.0*pi
```

```
PROCEDURAL(thetar = thetarm)

  thetar = (Poles/2.) * thetarm

  SCHEDULE reset .XP. (thetar-twopi)
  SCHEDULE reset2 .XN. (thetar)

END ! End of Procedural


  !"Firing of Switches"


  IF ((thetar .GE. 0.0) .AND. (thetar .LT. pi/6.)) THEN
          SA = .true.
          SB = .false.
          SC = .false.

 ELSEIF ((thetar .GE. pi/6.) .AND. (thetar .LT. pi/2.)) THEN
          SA = .true.
          SB = .true.
          SC = .false.

 ELSEIF ((thetar .GE. (pi/2.)) .AND. (thetar .LT. (5.*pi/6.))) THEN
          SA = .false.
          SB = .true.
          SC = .false.

 ELSEIF ((thetar .GE. (5.*pi/6.)) .AND. (thetar .LT. (7.*pi/6.))) THEN
          SA = .false.
          SB = .true.
          SC = .true.

 ELSEIF ((thetar .GE. (7.*pi/6.)) .AND. (thetar .LT. (3.*pi/2.))) THEN
          SA = .false.
          SB = .false.
          SC = .true.

 ELSEIF ((thetar .GE. (3.*pi/2.)) .AND. (thetar .LT. (11.*pi/6.))) THEN
          SA = .true.
          SB = .false.
          SC = .true.

 ELSEIF ((thetar .GE. (11.*pi/6.)) .AND. (thetar .LT. (2.*pi))) THEN
          SA = .true.
          SB = .false.
          SC = .false.
 ENDIF


 !"Assume lower switches are conducting"
```

```
PROCEDURAL(Vas, Vbs, Vcs, iii = SA, SB, SC, Vdc, ias, ibs, ics)

      Vap = 0.0

      iia = 0.0

      Vbp = 0.0

      iib = 0.0

      Vcp = 0.0

      iic = 0.0

      !" Check if top switch is closed"

      IF (SA) THEN
            Vap = Vdc
            iia = ias
      ENDIF

      IF (SB) THEN
            Vbp = Vdc
            iib = ibs
      ENDIF

      IF (SC) THEN
            Vcp = Vdc
            iic = ics
      ENDIF

      !" Establish the phase voltages"

      Vnp = (Vap + Vbp + Vcp)/3.0

      Vas = Vap - Vnp
      Vbs = Vbp - Vnp
      Vcs = Vcp - Vnp

      !" Find the inverter input current"

      iii = iia + iib + iic

END   ! End of Procedural


      !" Link Dynamic Equations"

      Vcap = 28.0


      !"Brushless DC Motor Constants"

      Ls = .000005
```

```
rs = 0.003
lamref = 0.006
Poles = 4.0
Jm = 0.00011711
Km = 0.000001128

!"Brushless DC Motor Equations"

!"Rotor Ref Frame Voltages"

Vqsr = 2.*cos(thetar)*Vas/3. + 2.*cos(thetar-2.*pi/3.)*Vbs/3. &
        + 2.*cos(thetar + 2.*pi/3.)*Vcs/3.

Vdsr = 2.*sin(thetar)*Vas/3. + 2.*sin(thetar-2.*pi/3.)*Vbs/3. &
        + 2.*sin(thetar + 2.*pi/3.)*Vcs/3.



!"Inverter Currents"

ias = cos(thetar)*iqsr + sin(thetar)*idsr

ibs = cos(thetar - 2.*pi/3.)*iqsr + sin(thetar - 2.*pi/3.)*idsr

ics= -ias-ibs


!" Rotor Ref Frame Currents"

piqsr = (-rs*iqsr - wr*Ls*idsr - wr*lamref + vqsr)/Ls

iqsr = INTEG(piqsr , 0.0)

pidsr = (-rs*idsr + wr*Ls*iqsr + vdsr)/Ls

idsr = INTEG(pidsr , 0.0)

!"Rotor Ref Frame Angle Thetar  and wr"

pwrm = (Te - Tl)/ Jm

wrm = INTEG(pwrm, 0.0)

wr = (Poles/2.) * wrm

pthetarm = wrm

thetarm = INTEG(pthetarm , 0.0)

!" Torque Equations"
```

```
        Te = (Poles/2.) * ((3./2.) * lamref) * iqsr

        Tl = Km * (wrm*wrm)

    END  ! " End of derivative"

        DISCRETE reset
                thetarm = 0.0
        END

        DISCRETE reset2
                thetarm = thetarm + twopi
        END

END  ! "End of dynamic section"

END  ! "End of program"
```

THIS PAGE INTENTIONALLY LEFT BLANK

APPENDIX B. [ACSL CODE FOR NBC FAN MODEL WITH 120° INVERTER]

```
PROGRAM  NCB FAN MODEL (AAAV)

INITIAL

      !"Preliminary stuff"
      MAXTERVAL maxt = 1.0e-7          !"max time step"
      MINTERVAL mint = 1.0e-7          !"min time step"
      CINTERVAL cint = 1.0e-5          !"communication interval"
      ALGORITHM ialg = 5               !"4th order Runge-Kutta"
      CONSTANT tstop = 0.007           !"adjustable stop time"

      "---initial circuit constants---"
      CONSTANT rL=0.01                 !"input line series R"
      CONSTANT LL=.000001              !"input line series L"
      CONSTANT Cdc=.036                !"input capacitance"
      CONSTANT Vdc=28.0                !"input voltage"

      !"---parameters for determining circuit status"
      CONSTANT hold = 1.e-1            !"holding current for diodes"
      CONSTANT eps = 0.7               !"diode drop"

      !"Brushless DC Motor Constants"
      CONSTANT Ls = .000005            !"self inductance"
      CONSTANT rs = 0.003              !"stator resistance"
      CONSTANT lamref = 0.006          !"magnet parameter"
      CONSTANT Poles = 4.0             !"number of poles"
      CONSTANT Jm = 0.00011711         !"motor+load inertia"
      CONSTANT Km = 0.000001128        !"TL=Km*wrm*wrm"

      "---logical variables for transistor conduction status"
      LOGICAL T1, T2, T3, T4, T5, T6
      "---logical variables for diode conduction status"
      LOGICAL D1, D2, D3, D4, D5, D6

      "---logical variables derived from sensorless signals"
      LOGICAL T1a, T2a, T3a, T4a, T5a, T6a

      "----switch initial conditions----"
      "-------all devices off"
      T1 = .false.
      T2 = .false.
      T3 = .false.
      T4 = .false.
      T5 = .false.
      T6 = .false.
      D1 = .false.
      D2 = .false.
      D3 = .false.
      D4 = .false.
      D5 = .false.
      D6 = .false.
```

```
            "---all sensorless signals initially false"
            T1a = .false.
            T2a = .false.
            T3a = .false.
            T4a = .false.
            T5a = .false.
            T6a = .false.

            "---logical signals initiate integration of phase voltages"
            LOGICAL flaga, flagb, flagc
            flaga = .TRUE.
            flagb = .TRUE.
            flagc = .TRUE.


            "---logical symbol to switch over to sensorless signals"
            LOGICAL NOSENSE
            NOSENSE = .TRUE.

    END  ! "of initial"

  DYNAMIC

            "----simulation termination condition"
            TERMT (t .GE. tstop)

     DERIVATIVE

            !"constants needed for manipulating angles"
            CONSTANT pi=3.14159265
            twopi = 2.0*pi
            CONSTANT alpha = 1.047198        !"60 degrees"

       PROCEDURAL(thetar = thetarm)
            !"--shift rotor electrical angle by alpha"
            thetarx= (Poles/2.) * thetarm + alpha

            !"keep angle between 0 and twopi"
            IF (thetarx .GE. twopi) THEN
                    thetarx= thetarx - twopi
            ELSEIF (thetarx .LT. 0.0) THEN
                    thetarx = thetarx + twopi
            ENDIF
            thetarx= MOD(thetarx, twopi)
            !"recover thetar"
            thetar = thetarx - alpha
       END  !" End of Procedural"


           !"Firing of Switches"
           !"if NOSENSE is TRUE, use rotor position signals for T1-T6"
           !"if NOSENSE is FALSE, use open-circuit-derived signals"
IF (NOSENSE) THEN
IF ((thetarx .GE. 0.0) .AND. (thetarx .LT. pi/3.)) THEN
                    T1 = .true.
                    T2 = .false.
                    T3 = .false.
```

```
                T4 = .false.
                T5 = .false.
                T6 = .true.
 ELSEIF ((thetarx .GE. pi/3.) .AND. (thetarx .LT. (2.*pi/3.))) THEN
                T1 = .true.
                T2 = .true.
                T3 = .false.
                T4 = .false.
                T5 = .false.
                T6 = .false.
 ELSEIF ((thetarx .GE. (2.*pi/3.)) .AND. (thetarx .LT. pi)) THEN
                T1 = .false.
                T2 = .true.
                T3 = .true.
                T4 = .false.
                T5 = .false.
                T6 = .false.
 ELSEIF ((thetarx .GE. pi) .AND. (thetarx .LT. (4.*pi/3.))) THEN
                T1 = .false.
                T2 = .false.
                T3 = .true.
                T4 = .true.
                T5 = .false.
                T6 = .false.


 ELSEIF ((thetarx .GE. (4.*pi/3.)) .AND. (thetarx .LT. (5.*pi/3.))) THEN
                T1 = .false.
                T2 = .false.
                T3 = .false.
                T4 = .true.
                T5 = .true.
                T6 = .false.
 ELSEIF ((thetarx .GE. (5.*pi/3.)) .AND. (thetarx .LT. (2.*pi))) THEN
                T1 = .false.
                T2 = .false.
                T3 = .false.
                T4 = .false.
                T5 = .true.
                T6 = .true.
ENDIF
ELSE
        T1 = T1a
        T2 = T2a
        T3 = T3a
        T4 = T4a
        T5 = T5a
        T6 = T6a
ENDIF

        !"---Determine diode conduction status"

        !"---establish the open-circuit voltage"
        Vagoc = ((Vdc/2.) + ((3.*lamref*wr*cos(thetar))/2.))
        Vbgoc = ((Vdc/2.) + ((3.*lamref*wr*cos(thetar - (2.*pi/3.)))/2.))
        Vcgoc = ((Vdc/2.) + ((3.*lamref*wr*cos(thetar + (2.*pi/3.)))/2.))
```

```
!"diode logic for PHASE LEG A"
!"if either transistor is gated, then either the transistor "
"  or diode will be conducting"
IF ((T1) .OR. (T4)) THEN
        D1 = .false.
        D4 = .false.

!"if the leg transistors are not gated:"
!"if ias>hold, then the lower diode is on, upper is off"
ELSEIF (ias .GT. hold) THEN
        D4 = .true.
        D1 = .false.

!"if ias<-hold, then the upper diode is on, lower is off"
ELSEIF (ias .LT. -hold) THEN
        D1 = .true.
        D4 = .false.

!"if open circuit voltages are between Vdc + eps and -eps"
!"then both diodes are off"
ELSEIF ((Vagoc .LT. (Vdc + eps)) .OR. (Vagoc .GT. -eps)) THEN
        D1 = .false.
        D4 = .false.

!"if open circuit voltage is above vdc + eps, upper diode is made"
!"to turn on"
ELSEIF (Vagoc .GT. (Vdc + eps)) THEN
        D1 = .true.

!"otherwise the lower diode turns on"
ELSE
        D4 = .true.

ENDIF


!"diode logic for PHASE LEG B"
IF ((T3) .OR. (T6)) THEN
        D3 = .false.
        D6 = .false.

ELSEIF (ibs .GT. hold) THEN
        D3 = .false.
        D6 = .true.

ELSEIF (ibs .LT. -hold) THEN
        D3 = .true.
        D6 = .false.

ELSEIF ((Vbgoc .LT. (Vdc + eps)) .OR. (Vbgoc .GT. -eps)) THEN
        D3 = .false.
        D6 = .false.

ELSEIF (Vbgoc .GT. (Vdc + eps)) THEN
        D3 = .true.
```

```
      ELSE
              D6 = .true.

      ENDIF


      !"diode logic for PHASE LEG C"
      IF ((T5) .OR. (T2)) THEN
              D5 = .false.
              D2 = .false.

      ELSEIF (ics .GT. hold) THEN
              D5 = .false.
              D2 = .true.

      ELSEIF (ics .LT. -hold) THEN
              D2 = .false.
              D5 = .true.

      ELSEIF ((Vcgoc .LT. (Vdc + eps)) .OR. (Vcgoc .GT. -eps)) THEN
              D5 = .false.
              D2 = .false.

      ELSEIF (Vcgoc .GT. (Vdc + eps)) THEN
              D5 = .true.

      ELSE
              D2 = .true.

      ENDIF



      !"Procedural for finding stator voltages"

PROCEDURAL(Vas, Vbs, Vcs, iii = T1, T2, T3, T4, T5, T6, D1, D2, D3, D4, &
              D5, D6, ias, ibs, ics)


      ! " Finding pole voltages and currents for A-phase"
      !"upper device is on"
      IF ((T1) .OR. (D1)) THEN
              Vag = Vdc
              iia = ias


      !"lower device is on"
      ELSEIF ((T4) .OR. (D4)) THEN
              Vag = 0.0
              iia = 0.0

      !"leg is open circuited"
      ELSE
              Vag = ((Vdc/2.) + ((3.*lamref*wr*cos(thetar))/2.))
              iia = 0.0
      ENDIF
```

```
      ! " Finding pole voltages and currents for B-phase"
      IF ((T3) .OR. (D3)) THEN
              Vbg = Vdc
              iib = ibs

      ELSEIF ((T6) .OR. (D6)) THEN
              Vbg = 0.0
              iib = 0.0
      ELSE
              Vbg = ((Vdc/2.) + ((3.*lamref*wr*cos(thetar - (2.*pi/3.)))/2.))
              iib = 0.0
      ENDIF


      ! " Finding pole voltages and currents for C-phase"
      IF ((T5) .OR. (D5)) THEN
              Vcg = Vdc
              iic = ics

      ELSEIF ((T2) .OR. (D2)) THEN
              Vcg = 0.0
              iic = 0.0
      ELSE
              Vcg = ((Vdc/2.) + ((3.*lamref*wr*cos(thetar + (2.*pi/3.)))/2.))
              iic = 0.0
      ENDIF



      !" Establish the phase voltages"
      Vas = ((2.*Vag/3.) - (Vbg/3.) - (Vcg/3.))
      Vbs = ((2.*Vbg/3.) - (Vag/3.) - (Vcg/3.))
      Vcs = ((2.*Vcg/3.) - (Vag/3.) - (Vbg/3.))

      !" Find the inverter input current"

      iii = iia + iib + iic

END !" End of Procedural"

      !"evaluate the neutral voltage"
      vng = (vag + vbg + vcg)/3.0


      !"C-Phase Sensorless Signal derivation"
      CONSTANT wc = 10000.0              !"low-pass filter frequency"
      CONSTANT tau2 = 0.004
      !"calculate the terminal voltage: should be Vcs"
      vdiffc = vcg - vng

      !"lowpass filter to eliminate abrupt transitions"
      CONSTANT xf1cic = 0.0
      pxf1c = -wc*xf1c + wc*vdiffc
      xf1c = INTEG(pxf1c, xf1cic)
```

```
!"activate integrator following first peak"
SCHEDULE intonc .XP. (16.0 - xf1c)
IF (flagc) then
        pxf2c = 0.0
ELSE
        pxf2c = 2500.0*xf1c
ENDIF
xf2c = INTEG(pxf2c, 0.0)

!"apply result to third filter to eliminate dc component"
pvcx = (xf2c - vcx)/tau2
vcx = INTEG(pvcx, 0.0)
vco = -vcx + xf2c

!"do same for the A-Phase"
vdiffa = vag - vng
CONSTANT xf1aic = 0.0
pxf1a = -wc*xf1a + wc*vdiffa
xf1a = INTEG(pxf1a, xf1aic)
SCHEDULE intona .XP. (16.0 - xf1a)
IF (flaga) then
        pxf2a = 0.0
ELSE
        pxf2a = 2500.0*xf1a
ENDIF
xf2a = INTEG(pxf2a, 0.0)
pvax = (xf2a - vax)/tau2
vax = INTEG(pvax, 0.0)
vao = -vax + xf2a

!"do same for the B-Phase"
vdiffb = vbg - vng
CONSTANT xf1bic = 0.0
pxf1b = -wc*xf1b + wc*vdiffb
xf1b = INTEG(pxf1b, xf1bic)
SCHEDULE intonb .XP. (16.0 - xf1b)
IF (flagb) then
        pxf2b = 0.0
ELSE
        pxf2b = 2500.0*xf1b
ENDIF
xf2b = INTEG(pxf2b, 0.0)
pvbx = (xf2b - vbx)/tau2
vbx = INTEG(pvbx, 0.0)
vbo = -vbx + xf2b


vcsoc = lamref*wr*cos(thetar + 2.*pi/3.)


!" Link Dynamic Equations"
!"removed for simulation development convenience"
!piL = (Vdc - rL*iL - Vcap)/LL
!iL = INTEG(piL , 0.0)
!pVcap = (iL - iii)/Cdc
!Vcap = INTEG(pVcap , 28.0)
Vcap = 28.0             !"assume hard input voltage"
```

```
!"Brushless DC Motor Equations"

!"Rotor Ref Frame Voltages"
Vqsr = 2.*cos(thetar)*Vas/3. + 2.*cos(thetar-2.*pi/3.)*Vbs/3. &
       + 2.*cos(thetar + 2.*pi/3.)*Vcs/3.

Vdsr = 2.*sin(thetar)*Vas/3. + 2.*sin(thetar-2.*pi/3.)*Vbs/3. &
       + 2.*sin(thetar + 2.*pi/3.)*Vcs/3.

!"Phase Currents"
ias = cos(thetar)*iqsr + sin(thetar)*idsr
ibs = cos(thetar - 2.*pi/3.)*iqsr + sin(thetar - 2.*pi/3.)*idsr
ics= -ias-ibs


!"Differential equation for the machine"
piqsr =(-rs*iqsr - wr*Ls*idsr - wr*lamref + vqsr)/Ls
iqsr = INTEG(piqsr , 0.0)

pidsr = (-rs*idsr + wr*Ls*iqsr + vdsr)/Ls
idsr = INTEG(pidsr , 0.0)

!" Torque and mechanical dynamics"
Te = (Poles/2.) * ((3./2.) * lamref) * iqsr
Tl = Km * (wrm*wrm)

pwrm = (Te - Tl)/ Jm
wrm = INTEG(pwrm, 0.0)
wr = (Poles/2.) * wrm

pthetarm = wrm
thetarm = INTEG(pthetarm , 0.0)

!"use sensorless signals to derive switching signals"
IF ((vco .LT. 0.0) .AND. (vbo .LT. 0.0)) THEN
        T1a = .FALSE.
        T2a = .TRUE.
        T3a = .TRUE.
        T4a = .FALSE.
        T5a = .FALSE.
        T6a = .FALSE.
ELSEIF ((vbo .GT. 0.0) .AND. (vao .GT. 0.0)) THEN
        T1a = .FALSE.
        T2a = .FALSE.
        T3a = .TRUE.
        T4a = .TRUE.
        T5a = .FALSE.
        T6a = .FALSE.
ELSEIF ((vao .LT. 0.0) .AND. (vco .LT. 0.0)) THEN
        T1a = .FALSE.
        T2a = .FALSE.
        T3a = .FALSE.
        T4a = .TRUE.
        T5a = .TRUE.
        T6a = .FALSE.
```

```
        ELSEIF ((vco .GT. 0.0) .AND. (vbo .GT. 0.0)) THEN
                T1a = .FALSE.
                T2a = .FALSE.
                T3a = .FALSE.
                T4a = .FALSE.
                T5a = .TRUE.
                T6a = .TRUE.
        ELSEIF ((vbo .LT. 0.0) .AND. (vao .LT. 0.0)) THEN
                T1a = .TRUE.
                T2a = .FALSE.
                T3a = .FALSE.
                T4a = .FALSE.
                T5a = .FALSE.
                T6a = .TRUE.
        ELSEIF ((vao .GT. 0.0) .AND. (vco .GT. 0.0)) THEN
                T1a = .TRUE.
                T2a = .TRUE.
                T3a = .FALSE.
                T4a = .FALSE.
                T5a = .FALSE.
                T6a = .FALSE.
        ENDIF


        END  ! " End of derivative"


        DISCRETE intona
                flaga = .FALSE.
        END     !"of discrete inton"
        DISCRETE intonb
                flagb = .FALSE.
        END     !"of discrete inton"
        DISCRETE intonc
                flagc = .FALSE.
        END     !"of discrete inton"

    END  ! "End of dynamic section"

END  ! "End of program"
```

THIS PAGE INTENTIONALLY LEFT BLANK

APPENDIX C. [ACSL PLOTS FOR NBC FAN MODEL WITH 180° INVERTER]

Machine parameters are those from Table 5.2.

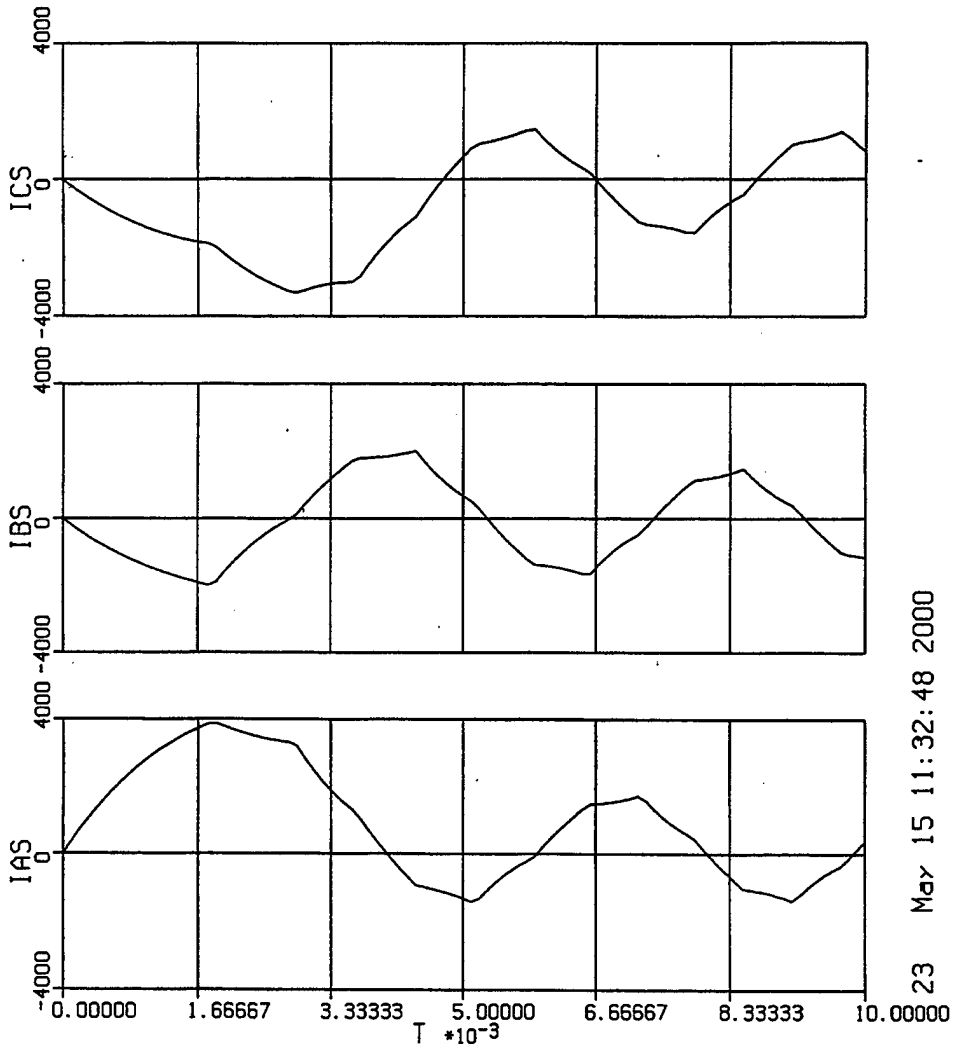

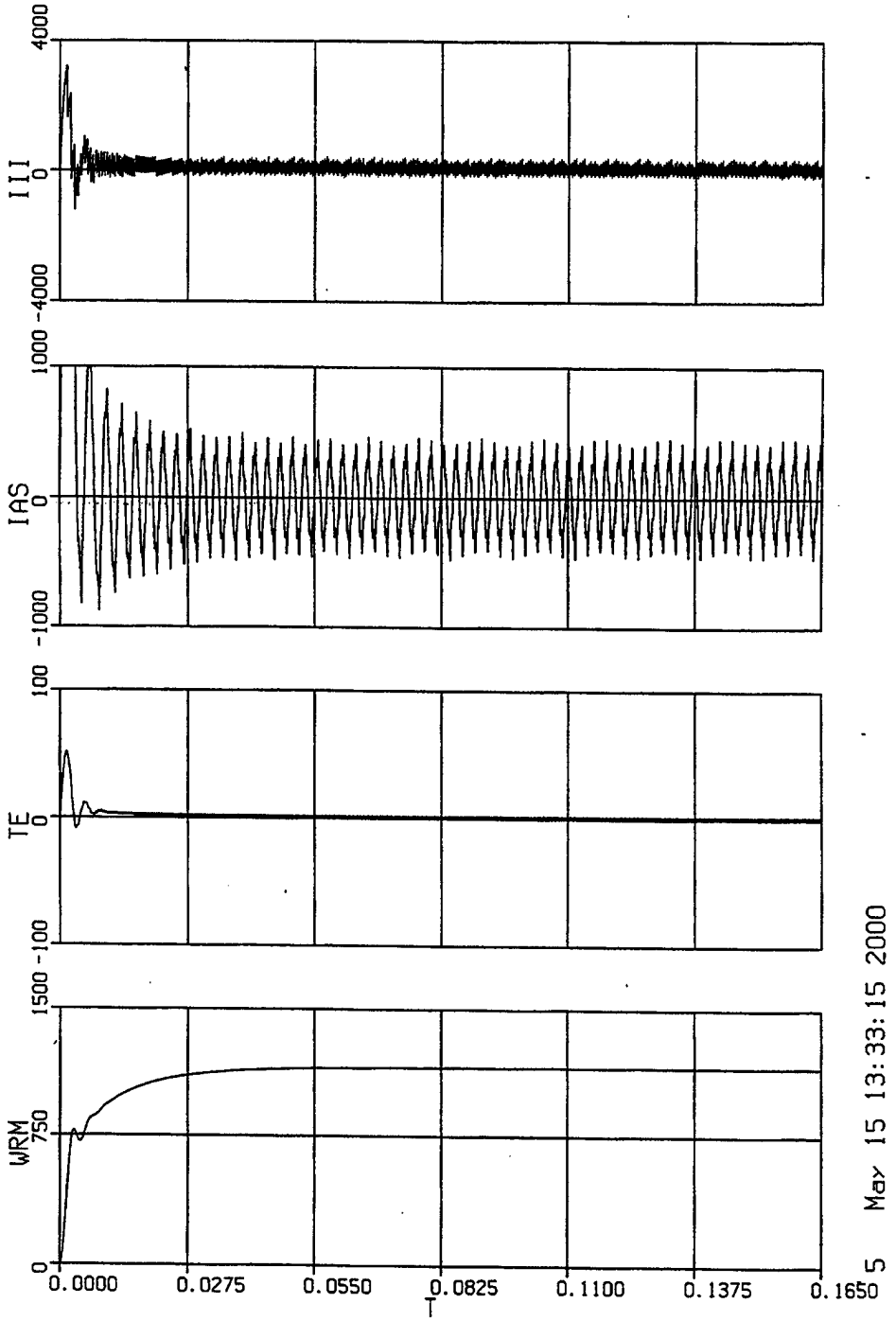
4000
III
0
-4000
1000
IAS
0
-1000
100
TE
0
-100
1500
WRM
750
0
0.0000
0.0275
0.0550
0.0825
0.1100
0.1375
0.1650
T
May 15 13:33:15 2000

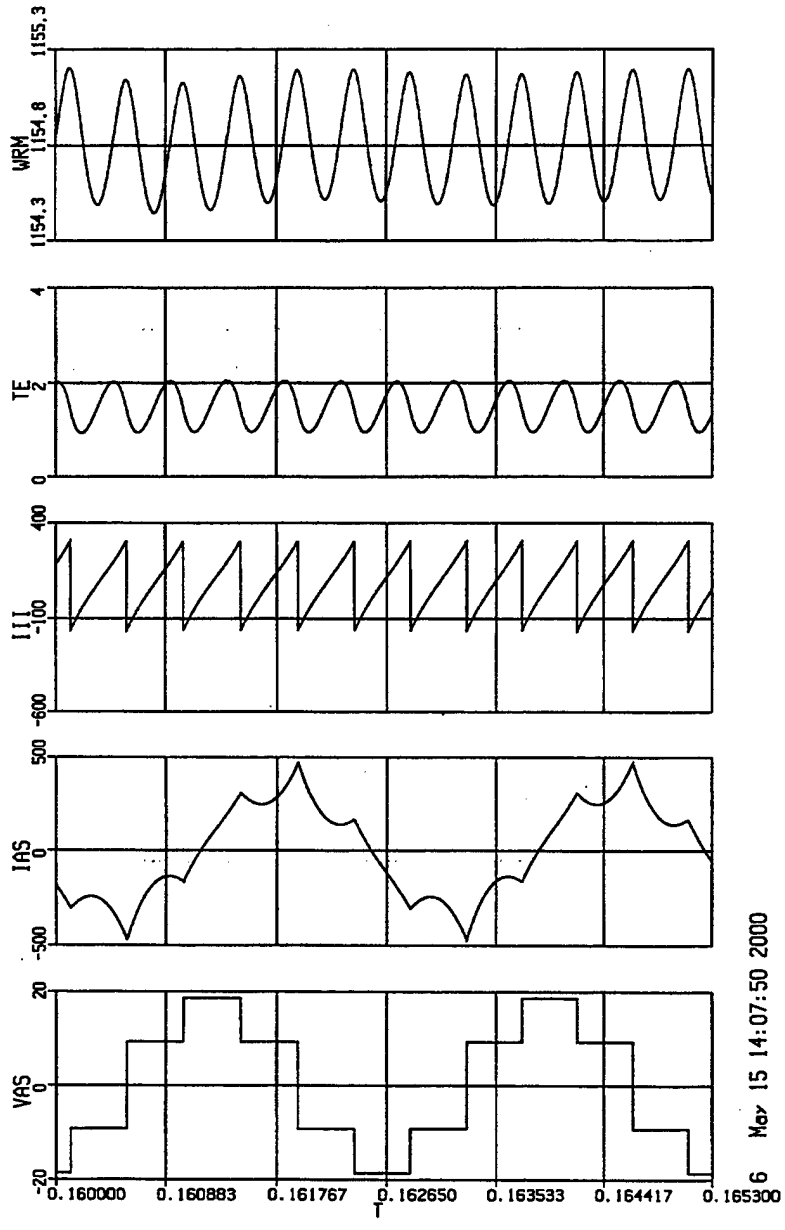
WRM
1155.3
1154.8
1154.3
TE
4
2
0
III
400
-100
-600
IAS
500
0
-500
VAS
20
0
-20
0.160000
0.160883
0.161767
0.162650
0.163533
0.164417
0.165300
T
6 Mar 15 14:07:50 2000

THIS PAGE INTENTIONALLY LEFT BLANK

APPENDIX D. [ACSL PLOTS FOR NBC FAN MODEL WITH 120° INVERTER]

Machine parameters are those from Table 5.1.

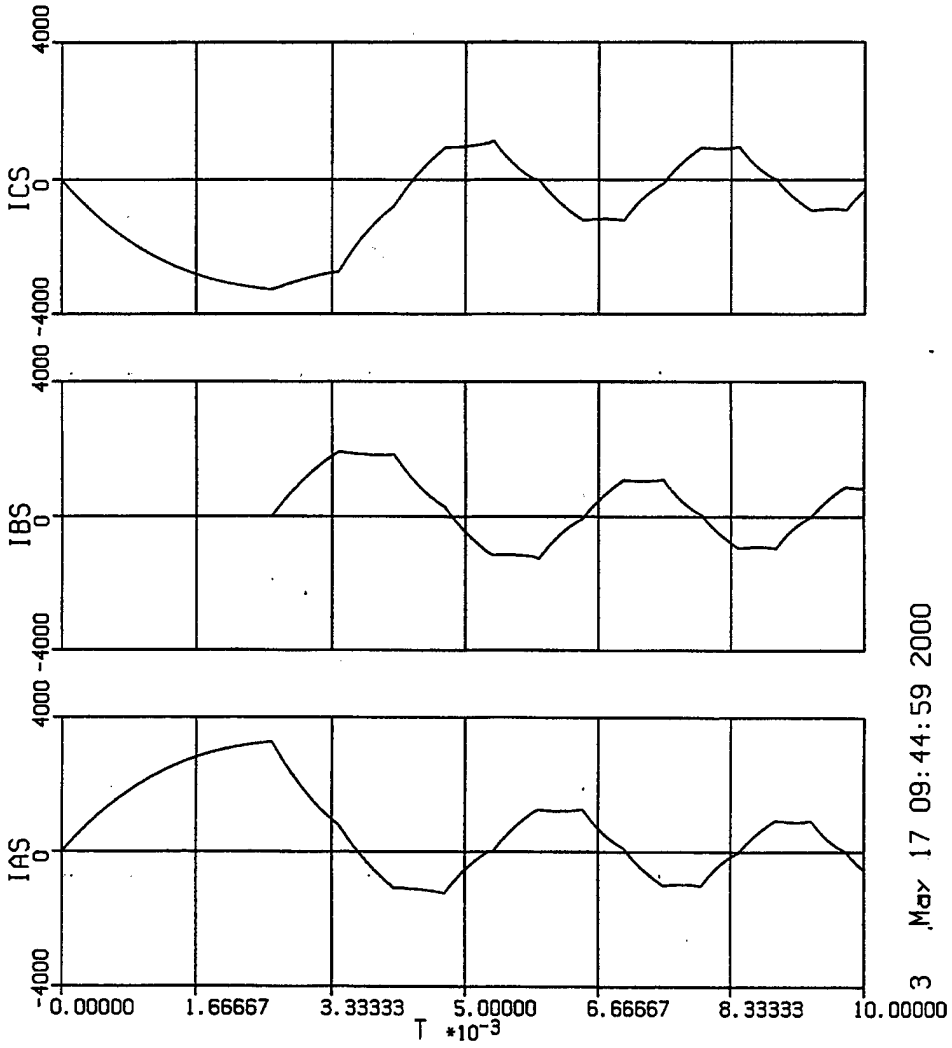

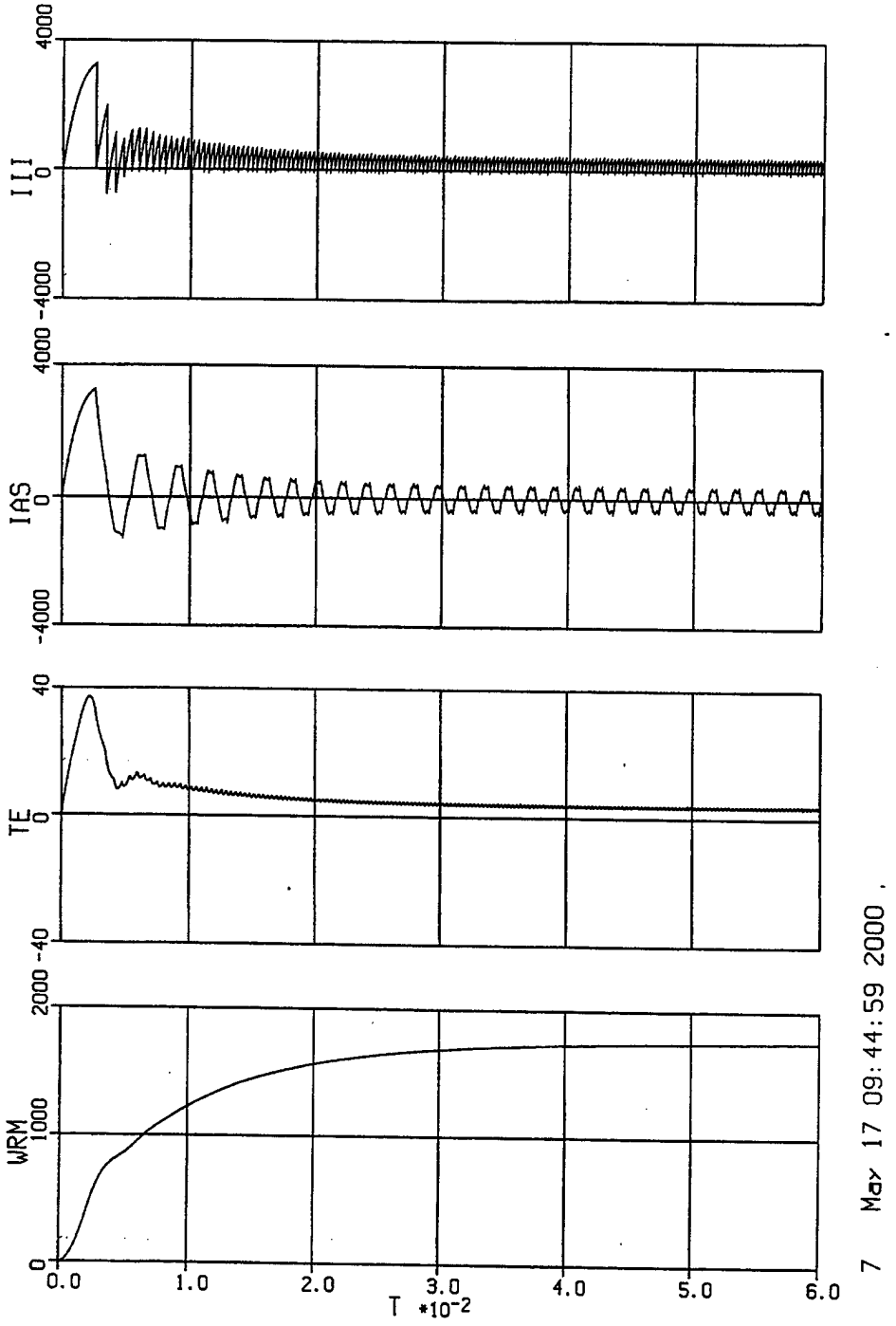
4000
III
0
-4000
4000
IAS
0
-4000
40
TE
0
-40
2000
WRM
1000
0
0.0
1.0
2.0
3.0
4.0
5.0
6.0
T *10-2
7 May 17 09:44:59 2000

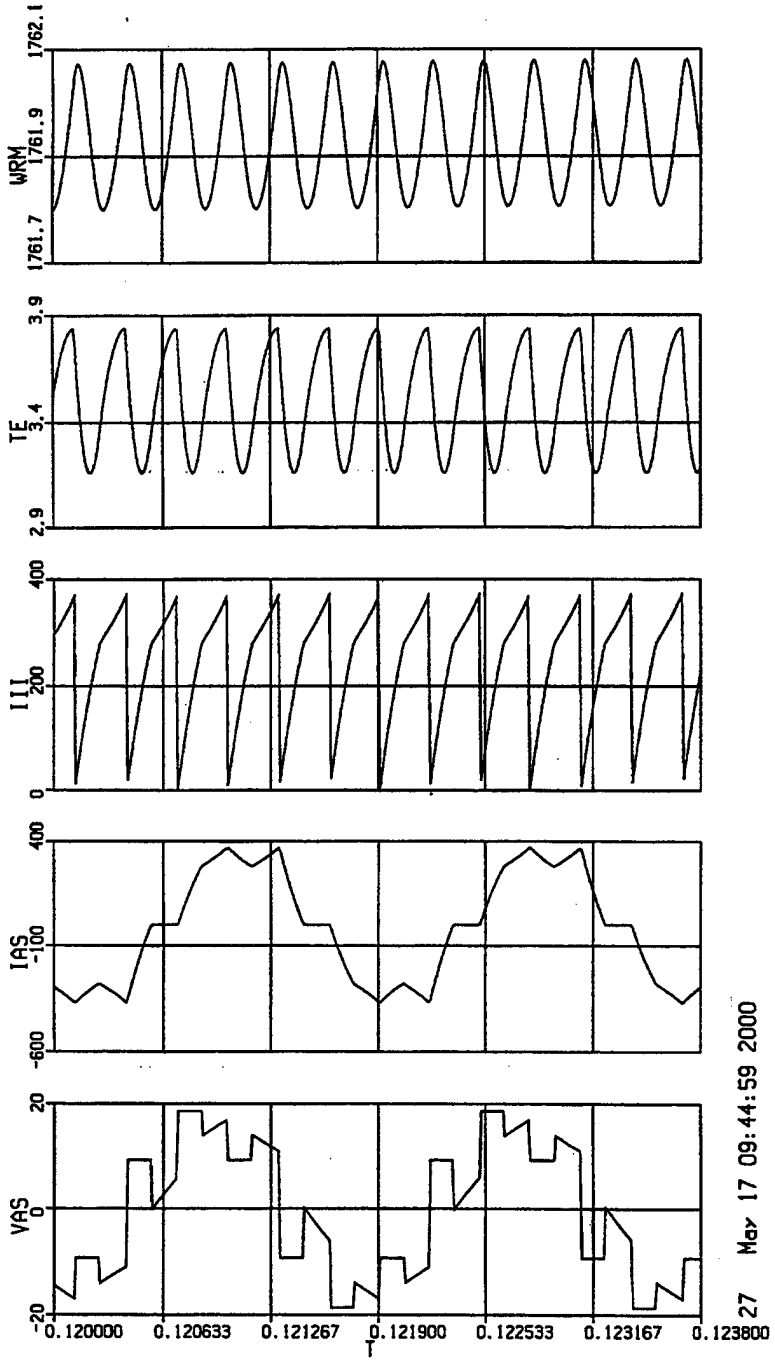
WRM
1762.1
1761.9
1761.7
TE
3.9
3.4
2.9
III
400
200
0
IAS
400
-100
-600
VAS
20
0
-20
0.120000
0.120633
0.121267
0.121900
0.122533
0.123167
0.123800
T
27 May 17 09:44:59 2000

THIS PAGE INTENTIONALLY LEFT BLANK

APPENDIX E. [MATLAB CODE FOR ULTRA CAPACITOR MODEL]

```
%%%%%%%%%%%%%%%%%%%%%%%%%%%%%%%%%%%%%%%%%%%%%%%%%%%%%%%%%%%%%%%%%%%%%%%%%%%%%%%%
%Capt Gabriel Beltran                                                            %
%18 Jan 00                                                                       %
%Ultra Capacitor Model                                                           %
%%%%%%%%%%%%%%%%%%%%%%%%%%%%%%%%%%%%%%%%%%%%%%%%%%%%%%%%%%%%%%%%%%%%%%%%%%%%%%%%

% Vendor Data

figure(1)
freq = [.01,.0159,.0251,.0398,.0631,.1,.1585,.2512,.3981,.6310,1.0,1.5849...
       2.5119,3.9811,6.3096,     10.0,15.8489,25.1189,39.8107,63.0957...
       100.0,158.4893,251.1887,398.1072,630.9574,1000.0];

mag = [23.4411,14.8375,9.6032,6.1331,3.9368,2.5595,1.6641,1.0782,0.7172...
      0.4805,0.3291,0.2325,0.1692,0.1275,0.0991,0.0787,0.0639,0.0528...
      0.0446,0.0384,0.0337,0.0300,0.0270,0.0246,0.0226,0.0210];

% Plot
semilogx(freq,mag)

title('Impedance vs. Frequency')
xlabel('Frequency (Hz)')
ylabel('Impedance (Ohms)')

% Transfer Function Simulation

figure(2)
a = 5.350;

b=input('input b')

num = [b, b*a];

den = [1.0, 0.0];

magus = abs(freqs(num,den,freq));

% Plot
semilogx(freq,magus)
title('Impedance vs. Frequency')
xlabel('Frequency (Hz)')
ylabel('Impedance (Ohms)')

% Overlay Plots

figure(3)
semilogx(freq,mag,'*',freq,magus,'.-')
title('Impedance vs. Frequency')
xlabel('Frequency (Hz)')
ylabel('Impedance (Ohms)')
gtext('Actual = ***')
gtext('Model = .-.-.-')
```

THIS PAGE INTENTIONALLY LEFT BLANK

APPENDIX F. [MANUFACTURER DATA SHEET FOR OPTIMA 800U]

Battery Model: 800U

Partnumber: 8004-003

Nominal Voltage: 12 volts

NSN: 6140-01-374-2243

Description: High power, sealed, lead acid, engine starting battery.

Physical Characteristics:

Plate Design:	High purity lead-tin alloy. Wound cell configuration using utilizing proprietary SPIRALCELL technology.
Electrolyte:	Sulfuric acid, H2SO4. Specific gravity: 1.286
Case:	Polypropylene
Color:	Case: Dark Gray Cover: "Optima" Red
Group Size:	BCI: 34/78

	Standard	Metric
Length:	10"	254 mm
Width:	6.8"	172.2 mm
Height:	7.8"	198.1 mm(height at the top of the terminals)
Minimum Weight:	38.8lb.	17.6 kg

Terminal Configuration: SAE / BCI automotive and GM style side terminal (3/8 - 16 UNC - 2B, threaded nut).

Performance Data:

Open Circuit Voltage (full charged):	12.8 volts
Internal resistance (fully charged):	.0032 ohms
Capacity:	56 Ah (C/20) 50 Ah (C/2)
Reserve Capacity:	BCI:120 minutes (25 amp discharge, 80°F (26.7°C), to 10.5 volts cut-off)

Power:

CCA (BCI 0°F):	800 amps
MCA (BCI 32°F):	1000 amps
Battery Power (C/2)	10.2 kW 569.8 W/Kg 1159 W/L
Battery Energy (C/2)	600 Wh 33.5 Wh/kg 68.18 Wh/L

Cycle life:

Cycle Life - deep cycle (BCI):	~ 50 cycles
40% Life Cycle (BCI):	10,000 - 12,000 cycles

Recommended Charging:

The following charging methods are recommended to ensure a long battery life: (Always use a voltage regulated charger, with voltage limits set as described below.)

Model: 800U

These batteries are designed for engine starting applications. They are <u>not</u> recommended or warranted for use in deep cycle applications.

Recommended charging information:

Alternator	13.8 to 15.0 volts no amperage limit
Battery charger	13.8 to 15.0 volts, 10 amps maximum, 8 hours maximum
Boost Recharge	Maximum voltage: 15.6 volts (regulated). Maximum current: 60 amps. Maximum recharge time: 2 hours. **All limits must be strictly adhered to**
Float charge	13.2 to 13.8 volts, 1 amp maximum current, time indefinite (at lower voltage levels).

ays wear safety glasses when working with batteries.

ays use a voltage regulated battery charger with limits set to the above ratings. Overcharging an cause the safety valves to open and battery gasses to escape, causing premature failure. These asses are flammable! You cannot replace water in sealed batteries that have been overcharged. battery that becomes very hot while charging should be disconnected immediately.

ally charging a battery can result in poor performance and a reduction in capacity.

ping and Transportation information:

ma batteries can be shipped by AIR. The battery is non-spillable and is tested according to AO Technical Instructions DOC. 9284-AN/905 to meet the requirements of Packing Instructions 806 and is classified as non-regulated by IATA Special Provision A-48 and A-67 for UN2800. minals must be protected from short circuit.

facturing Location:

ma Batteries, Inc.
500 East 22nd Avenue
ora, CO 80011
ited States of America
one: 303-340-7400
303-340-7474

= Battery Council International
= European Norm

charge versus temperature (800 amps):
charge versus temperature (400 amps):
Discharge:
neering Drawing:

ma Batteries, Inc.
duct Specifications: Model 800U
/08/97

THIS PAGE INTENTIONALLY LEFT BLANK

LIST OF REFERENCES

1. Direct Reporting Program Manager, Advanced Amphibious Assault Vehicle, www.aaav.usmc.mil, MARCORSYSCOM, Quantico, VA, 2000.

2. Krause, P.C., "Multilevel Heterogeneous Modeling of AAAV," 2000.

3. Ciezki, J.G., "An Introduction to the Dynamic Simulation of Power Systems," Course Notes, Naval Postgraduate School, Monterey, CA, 1997.

4. Wasynczuk, O.; Sudhoff, S.D., "Automated State Model Generation Algorithm," Purdue University, West Lafayette, IN, 1996.

5. Krause, P.C.; Wasynczuk, O., *Electromechanical Motion Devices*, McGraw-Hill Book Co., New York, NY, 1989.

6. Krause, P.C.; Wasynczuk, O., Sudhoff, S.D., *Analysis of Electric Machinery*, IEEE Press, Piscataway, NJ, 1995.

7. Sudhoff, S.D., *Theory and Simulation of the Brushless DC 120° Inverter System*, Master's Thesis, School of Electrical Engineering, Purdue University, West Lafayette, IN, 1989.

8. Iizuka, K.; Uzuhashi, H., "Microcomputer Control of Sensorless Brushless Motors," *IEEE Transactions on Industrial Applications*, 1985.

9. Linden, D., *Handbook of Batteries*, McGraw-Hill Inc., New York, NY, 1995.

THIS PAGE INTENTIONALLY LEFT BLANK

INITIAL DISTRIBUTION LIST

1. Defense Technical Information Center 2
   8725 John J. Kingman Rd., STE 0944
   Ft. Belvoir, VA 22060-6218

2. Dudley Knox Library 2
   Naval Postgraduate School
   411 Dyer Road
   Monterey, CA 93943-5101

3. Director, Training and Education 1
   MCCDC, Code C46
   1019 Elliot Road
   Quantico, VA 22134-5107

4. Director, Marine Corps Research Center 2
   MCCDC, Code C40RC
   2040 Broadway Street
   Quantico, VA 22134-5107

5. Marine Corps Representative 1
   Naval Postgraduate School
   Code 037, Bldg. 330, Ingersoll Hall, Room 116
   555 Dyer Road
   Monterey, CA 39343

6. Marine Corps Tactical Systems Support Activity 1
   Technical Advisory Branch
   Attn: Librarian
   Box 555171
   Camp Pendleton, CA 92055-5080

7. Chairman, Code EC 1
   Department of Electrical and Computer Engineering
   Naval Postgraduate School
   Monterey, CA 93943-5121

8. John G. Ciezki, Code EC/Cy 2
   Department of Electrical and Computer Engineering
   Naval Postgraduate School
   Monterey, CA 93943-5121

9. Robert W. Ashton, Code EC/Ah 1
   Department of Electrical and Computer Engineering
   Naval Postgraduate School
   Monterey, CA 93943-5121

10. Engineering and Technology Curricular Office (Code 34).....1
    Naval Postgraduate School
    Monterey, CA 93943-5109

11. Gabriel Beltran 2
    6503 Willow Pond Dr.
    Fredricksburg, VA 22407